Probing Deformable Oil-Water Interfaces by Atomic Force Microscopy and Cascade Partial Coalescence Measurements

by

Natalie Paige Kuznicki

A thesis submitted in partial fulfillment of the requirements for the degree of

Doctor of Philosophy

in

Chemical Engineering

Department of Chemical and Materials Engineering

University of Alberta

ABSTRACT

Phase separation of stable oil-in-water and water-in-oil emulsions poses major challenges for a variety of industries, including the petroleum industry. The stability and destabilizing of petroleum emulsions highly depend on interfacial properties such as surface/interfacial charges, interfacial rheology, etc. Contrarily, for surfactant-free systems, determining the charge of liquid-liquid interface is very challenging due to inherent droplet deformations and large distribution of emulsified droplet sizes. Limited understanding is available on "clean" and "contaminated" droplets. Coated substrates, often used to study interfacially active materials, behave very differently from curved deformable interfaces. This thesis focuses on understanding the stability and characteristics of both charge-stabilized "clean" and surfactant-stabilized "contaminated" industrial systems.

For "clean" oil-in-water systems, the occurrence of cascade partial coalescence was studied to link the observed partial oil droplet coalescence in surfactant-free electrolyte solutions to charged interfaces and determine the ζ-potential (linked to surface potential) of liquid-liquid interfaces. For a variety of fluids, it has been observed that a small droplet of organic liquid 1, slowly approaching through an immiscible liquid 2 a liquid 2- liquid 1 interface, underwent partial coalescence upon reaching the interface. During this process, only a part of the initial "mother" droplet passed through the interface and a smaller **"**daughter**"** droplet was left behind. We successfully linked the sizes of the last "mother" and "daughter" droplets to the surface potential bounds for a given set of liquids using

the balance of van der Waals and electrostatic double layer forces, together with viscous resistance and apparent weight of the drop.

Multiple emulsions are very difficult to remove from the water-crude oil system due to their special physical and interfacial properties, such as intermediate density and viscosity. Indigenous surface-active species, such as asphaltenes, form rigid skins at oil-water interfaces and alter surface properties of fine particles present in the system, causing further separation difficulties. In our study of "contaminated" systems using atomic force microscopy (AFM), we focus on interactions between a silica sphere and interfacial materials stabilizing water-in-diluted bitumen emulsions. The rapid dynamic aging of the interface results in formation of a rigid "skin" around water droplets, which changes the rheological properties of the interface, with the interface becoming non-Laplacian. To accurately describe the deformation of the oil-water interface, a viscoelasticity factor is successfully incorporated into the high force formula of the augmented Stokes-Reynolds-Young-Laplace (SRYL) equation to account for interfacial elasticity arising from the aging of the system. Incorporation of elasticity significantly improved predictions of droplet deformation in asphaltene-in-solvent solutions by SRYL equation for aged droplets. The AFM results show the droplet becoming less deformable and a rapid increase in adhesion force over time. After the addition of a demulsifier (ethyl cellulose, EC), droplets immediately become more deformable and unstable, with the interface becoming Laplacian again. Within minutes of EC addition, immersion of the probe into the droplet is observed. These changes at the interface, measured with AFM, provide insights

on the effectiveness of demulsification by different chemicals, such as EC, at a fundamental level, showing the promise to ultimately reduce the cost of commercial operations in the petroleum industry.

The major contributions to science of this thesis are developing a novel model describing the stability of “clean” surfactant-free systems using cascade partial coalescence measurements, and quantifying the forces present in “contaminated” water-in-oil emulsion systems by AFM colloidal probe force measurements. Introducing a novel viscoelasticity parameter in the high force SRYL equation to account for surface elasticity makes the SRYL model more accurate and versatile for predicting droplet deformation in non-Laplacian systems.

PREFACE

This thesis is composed of a series of papers that have either been published or submitted for publication. The following is a statement of contributions made to the jointly authored papers contained in this thesis:

- Chapter 1: Introduction: Original work by N. P. Kuznicki.
- Chapter 2: Literature Review: Original work by N. P. Kuznicki.
- Chapter 3: A version of this chapter has been published as "Cascade partial coalescence phenomena at electrolyte-oil interfaces and determination of bounds for the surface potential", co-authored by N. P. Kuznicki, M. Krasowska, P. M. F. Sellaperumage, Z. Xu, J. Masliyah, J. Ralston and M. N. Popescu in: *Soft Matter* **2013** *9*, 4516-4523. Kuznicki was responsible for the droplet-interface collision tests and data processing. Krasowska supervised the project and conducted refractive index measurements. Sellaperumage and Krasowska were responsible for the electrophoretic mobility measurements. Popescu was responsible for the theoretical analysis and model development. Popescu, Krasowska and Kuznicki were responsible for manuscript preparation. Xu and Masliyah supervised the project, provided insights into data interpretation and proofread the manuscript prior to submission.
- Chapter 4: A version of this chapter has been published as "Dynamic interactions between a silica sphere and deformable interfaces in organic solvents studied by atomic force microscopy", co-authored by N. P. Kuznicki, D. Harbottle, J. Masliyah and Z. Xu in: *Langmuir* **2016**, DOI:

10.1021/acs.langmuir.6b02306. Kuznicki performed all of the experiments and data analysis, and was responsible for manuscript preparation. Xu and Masliyah supervised the project, made suggestions and provided insights into data interpretation. Harbottle was greatly involved in manuscript corrections and made adjustments to the rheology data analysis. Xu, Masliyah and Harbottle proofread the manuscript before submission.

- Chapter 5: A version of this chapter has been submitted to *Energy & Fuels* as "Probing mechanical properties of water-crude oil emulsion interfaces using atomic force microscopy" co-authored by N. P. Kuznicki, D. Harbottle, J. Masliyah and Z. Xu. This paper was presented at Petro Phase 2016 in 06.2016 and has been submitted to the special issue of *Energy & Fuels* for the Petro Phase conference. Kuznicki performed all of the experiments and data analysis, and was responsible for manuscript preparation. Xu and Masliyah supervised the project and assisted with the concept formation. Harbottle made suggestions on data interpretation and restructuring of the manuscript. Xu, Masliyah and Harbottle proofread the manuscript before submission.
- Chapter 6: Conclusions: Original work by N. P. Kuznicki.

Other co-authored publications not listed as Thesis Chapters include:

- Wang, S.; Segin, N.; Wang, K.; Masliyah, J. H.; Xu, Z. *J. Phys. Chem. C* **2011**, 115, 10576-10587.
- Natarajan, A.; Kuznicki, N.; Harbottle, D.; Masliyah, J.; Zeng, H.; Xu, Z. *Langmuir* **2014**, 30 (31), 9370-9377.

- Natarajan, A.; Kuznicki, N.; Harbottle, D., Masliyah, J.; Zeng, H.; Xu, Z. **2016** Submitted to *Energy & Fuels.*

In these second author publications, Kuznicki was responsible for the AFM imaging and force measurements, as well as contact angle experiments. Kuznicki also assisted with manuscript preparation and submission.

ACKNOWLEDGEMENTS

I would like to express my sincere gratitude and appreciation to:

- My supervisors, Professor Zhenghe Xu and Distinguished University Professor Emeritus Jacob Masliyah for their guidance, support, patience and helpful discussions during the course of this study.
- Emeritus Laureate Professor John Ralston for inviting me to the Ian Wark Research Institute (now Future Industries Research Institute) and giving me an opportunity to experience a new work environment and Australia.
- Dr. David Harbottle, Dr. Plamen Tchoukov, Dr. Shengqun Wang and Dr. Zifu Li for the great discussions, help and suggestions.
- Dr. Marta Krasowska for teaching me about overcoming the difficulties of using a "clean" setup, always encouraging and supporting me.
- Dr. Mihail Popescu for all the help on the "clean" system and many great discussions.
- Dr. Derek Chan, Dr. Rogerio Manica and Dr. Ray Dagastine for their insight and discussions on deformable droplet systems and the helpful suggestions on the AFM project.
- The technicians in our lab, Mr. James Skwarok, Ms. Jie Ru and Ms. Ni Yang for their help in locating supplies and troubleshooting skills.
- Ms. Lisa Carreiro, Ms. Patricia Siferd, Mr. Carl Corbett and Ms. Lily Laser, as well as Ms. Louise Jennings at the Ian Wark (now Future Industries Research Institute) for administrative and technical assistance and optimism even in the most stressful situations.

- Ms. Andrée Koenig, Mr. Kevin Heidebrecht and all the members of the machine shop for all of their help.
- My amazing friends, in particular Dr. Meijiao Deng, Ms. Meghan Curran, Dr. Teresa Bisson, Dr. Erin Bobicki, Dr. Dominik Kosior, Dr. Anton Majmutov, Ms. Veronica Ramirez, Ms. Urška Žbogar, Ms. Iliana Delcheva, Ms. Rajni Garg, Mr. Pasindu Sellaperumage, Ms. Jamila Joseph, Dr. Nida Khan, Ms. Xurui Zhang, Ms. Yin Liang, Ms. Jiebin Bi, Ms. Adriana Briones and Dr. Xue Zhai. I've greatly enjoyed our coffees, drinks, the serious and not-so-serious discussions, laughter and adventures.
- All of the fellow members of the Oil Sands Research Group.
- NSERC Industrial Chair Program in Oil Sands Engineering and Alberta Innovates- Energy and Environmental Solutions (AI-EES) for financial support of the program.

A special thank you goes to my boyfriend, Dr. Benjamin Ireland, for all of the support and patience, and for keeping me happy in the highly stressful time of thesis finalization.

An enormous thank you goes to my family, especially to my younger brother Steven, as well as Dan and Jenn, for always being there and reminding me not to take myself too seriously.

Finally, my deepest gratitude goes to my parents, Dr. Tanya Kuznicki and Prof. Steven Kuznicki, as well as grandparents, Prof. Mariya Orynchak and Dr. Mykola Orynchak. Thank you for inspiring me to aim higher and be better. I couldn't have done it without you. It is to you that I dedicate this work.

TABLE OF CONTENTS

TABLE OF FIGURES

CHAPTER 1 INTRODUCTION

1.1 "CLEAN" AND "CONTAMINATED" EMULSION SYSTEMS

Emulsions surround us in everyday life and are defined as a fine dispersion of minute droplets of one liquid in another, where the dispersed phase is not miscible or only sparingly soluble in the continuous phase. They are widely used in a variety of industries including food, cosmetic, pharmaceutical and petroleum processing. For some applications, stable emulsions are desirable. For instance, well-dispersed oil-in-water (milk) and water-in-oil (facial creams) emulsions are necessary to extend the shelf life of everyday consumables. However, in other industries, such as the petroleum industry, phase separation is required in order to improve product quality, while emulsification may be beneficial in reservoir production phase.

The presence/absence of charge at oil-water interfaces, leading to stability/instability of "clean" emulsions has been a great debate in research. Cascade partial coalescence phenomenon has been observed for various fluids/ interfaces over the last 50 years. However, only recently, detailed studies on the mechanism of this process were conducted, with the help of high speed imaging. For a variety of fluids, cascade partial coalescence occurs when a droplet of liquid 1 through liquid 2 approaches a liquid 2- liquid 1 interface, during which a part of the initial "mother" drop passes through the interface and a small "daughter" droplet of liquid 1 is left behind.[1-3] A "cascade" of these steps may occur and result in either complete coalescence or a stable "daughter" droplet left behind.

The occurrence and dynamics of cascade partial coalescence depend on a multitude of factors, including the initial droplet diameter, density, viscosity and interfacial tension of the two liquids.[1,4] However, the final state of the drop (stable droplet at the interface or complete coalescence) depends on interactions between the interfaces in close proximity. Even through the mechanics of this process have been well described through modelling, limited measurements of this process are available since "clean" systems as a whole are very difficult to study due to the significant effect of trace contaminants on system properties.

When surface active species are present at the interface, steric repulsive effects are dominant, since the two droplets or droplet-interface cannot come into close proximity for other forces to have any effect. To improve understanding of molecular interactions at the interfaces, the molecules to be studied are typically coated on a substrate, and interaction forces between these substrates are measured via atomic force microscopy (AFM) or surface force apparatus (SFA).[5,6] However, direct comparison between "model" planar surfaces and emulsion interfaces cannot be made from such studies, since the droplet curvature of emulsified droplets affects the adsorption/displacement of various surface-active materials.

Over the last two decades, AFM has been extensively used to measure forces between rigid surfaces, and expanded to study interactions involving at least one deformable surface. Surface forces and surface deformations for particle-droplet, particle-bubble, droplet-droplet and bubble-bubble systems in various solutions have been successfully measured in recent studies.[7] However, these

measurements are typically performed on oil droplets in water due to evaporation of solvent and provide limited applications.

Formation of water in oil emulsions poses a great challenge to the oil sands industry. Small water droplets (on the order of μm) are stabilized by asphaltenes and other interfacially active species, which are extremely difficult to remove from the interface. These water droplets travel downstream to upgrading facilities, causing corrosion and equipment malfunctions. Therefore, reducing the amount of emulsified water in bitumen froth is highly desirable, as it would decrease plant operating and capital replacement costs. Asphaltene accumulation at the oil-water interface prevents coalescence of water droplets by steric hindrance and formation of rigid networks that resist the rupture of the intervening liquid film.[8-10] In order to break the water-in-oil emulsions, demulsifiers are typically added to the diluted bitumen froth. Their presence at oil-water interfaces provides an opportunity for water droplet flocculation and/or coalescence.[11] However, limited understanding is available on the aging effect of asphaltene-covered droplets or their interactions with demulsifiers. In order to separate the phases and "break" the emulsions, fundamental understanding of the governing forces for emulsion stabilization and deformations at the interface is essential.

1.2 OBJECTIVES AND SCOPE OF THE THESIS

The major objective of this work is to understand the emulsification process and its characteristics for both "clean" charge-stabilized and "contaminated" asphaltene-stabilized industrial systems. The first part of the thesis focuses on the "clean" system. In this part, a microfluidics device and a high-speed camera were

used to study small (D ≈ 300 μm) oil droplets in aqueous solutions. The objective of this part is to link the occurrence of cascade partial coalescence to charges of the interfaces. In this work, a novel approach was formulated to estimate the surface potential for a given set of fluids, which can be used to differentiate between different models describing the charging state of the interface.

The second part of this work utilizes Atomic Force Microscopy (AFM) to investigate the interactions between clays and "contaminated" interfaces stabilized by asphaltenes, which are the most problematic fraction of crude oil. This micron-scale AFM study focused on interactions between a small silica sphere (representing clays) and the interfacial materials stabilizing water-in-crude oil emulsions. The system described here is of extremely high industrial relevance. This original AFM application provides a unique way of measuring the forces present within a multiphase system during bitumen froth flotation and bitumen froth treatment.

The major contributions of this thesis research to science are developing a new method to predict charge bounds for clean interfaces by investigating the cascade partial coalescence process, and probing the dynamic interfacial properties of a "contaminated" deformable water-crude oil systems using AFM. Incorporating experimentally-measured interfacial properties (elasticity) of the aged interfaces with the results of AFM force measurements allowed more accurate predictions of droplet deformation. As a whole, this work provides insights into emulsion stability and forces present in deformable emulsion systems.

It should be noted that the systems described in this study, particularly the asphaltene and bitumen with demulsifier addition, were investigated from a fundamental perspective to provide scientific directions for optimized performance of industrial processes.

1.3 THESIS STRUCTURE

This thesis has been structured as a compilation of papers. Chapters 3-5 are research papers published in or submitted to scientific journals for publication. The key content of each chapter is given below as an outline of the thesis.

Chapter 1 provides the overall introduction to the thesis, which includes some background information, and describes the objectives with major approaches and structure of the thesis.

Chapter 2 provides a comprehensive literature review on the cascade partial coalescence process and challenges in emulsion "breaking" and water removal in the oil sands industry. The effect of different bitumen fractions and demulsifier addition on emulsion stability is also discussed.

Chapter 3 describes a novel method to predict charges of "clean" interfaces by investigating the cascade partial coalescence process at "clean" oil-water interfaces. The link between fundamental properties such as the isoelectric point and Debye length on charge distribution of a given salt and effect of specific adsorption of ions on structure of the "clean" oil-water interface is investigated. Surface charge appears to be the predominant stabilizing mechanism for "clean" emulsions. A version of this paper has been published in:

Kuznicki, N. P.; Krasowska, M.; Sellaperumage, P. M. F.; Xu, Z.; Masliyah, J.; Ralston, J.; Popescu, M. N. *Soft Matter* **2013**, 9, 4516-4523.

Chapter 4 discusses a "contaminated" asphaltene (natural polyaromatic molecule, NPAM)- stabilized water-in-oil emulsion system, where water droplets are aged in asphaltene (NPAM)- in solvent solutions. Here a "stiffening" of a water droplet and "skin" development is observed due to asphaltene adsorption and molecular assembly at the oil-water interface. This mechanical barrier is investigated through crumpling, dilatational rheology and interfacial tension measurements. Deviation in the droplet shape from Laplacian, observed through crumpling upon droplet volume reduction, occurs upon aging. The interfacial rheological properties are linked with measured AFM forces over time, and a new experimentally-measured viscoelasticity term is introduced into the Stokes-Reynolds Young-Laplace (SRYL) droplet deformation equation, also referred to as the high force equation. Adding this key parameter allows incorporation of interfacial rheology into the original equation set, developed for purely viscous interfaces and to correct the under prediction of droplet deformation by the SRYL model. A version of this chapter has been published in:

Kuznicki, N. P.; Harbottle, D.; Masliyah, J. H.; Xu, Z *Langmuir* **2016**, DOI: 10.1021/acs.langmuir.6b02306.

Chapter 5 illustrates the effect of asphaltene and bitumen concentration, as well as demulsifier addition to the aged interfaces, on droplet deformation and forces measured with AFM. Water droplets aged in asphaltene and bitumen solutions exhibited strong "skins" (non-Laplacian behavior) and a significant adhesion of

the interface to the probe during retraction from the interface. After a demulsifier, ethyl cellulose, EC, was added to the system, droplets became more deformable and unstable over time, resulting in immersion of the probe into the droplet upon approach (after 10 minutes of EC addition) and coalescence of the neighboring droplets. Following EC addition, the interface reverted back to Laplacian and droplet deformations could be well predicted by the high force SRYL equation using the interfacial tension of the system. The colloidal probe technique was shown to provide a convenient way to quantify forces at deformable oil/water interfaces and characterize the *in-situ* effectiveness of competing surface active species. A version of this chapter has been submitted for publication in a special issue of *Energy & Fuels* dedicated to the Petrophase 2016 conference:

Kuznicki, N.P.; Harbottle, D.; Masliyah, J.; Xu, Z. **2016**.

Chapter 6 is the summary of the thesis, conclusions, major contributions and recommendations for future work.

1.3 REFERENCES

1. Gilet, T.; Mulleners, K.; Lecomte, J. P.; Vandewalle, N.; and Dorbolo, S. *Phys. Rev. E* **2007**, 75 (3), 036303-1-036303-14.

2. Chen, X.; Mandre, S.; Feng, J. J. *Phys. Fluids* **2006**, 18 (9), 092103-1-092103-14.

3. Ray, B.; Biswas, G.; Sharma, A. *J. Fluid Mech.* **2010**, 655, 72-104.

4. Blanchette, F.; and Bigioni, T. P. *Nat. Phys.* **2006**, 2 (4), 254-257.

5. Wang, S.; Liu, J.; Zhang, L.; Masliyah, J.; Xu, Z. *Langmuir* **2010**, 26 (1), 183-190.

6. Natarajan, A.; Xie, J.; Wang, S.; Masliyah, J.; Zeng, H.; Xu, Z. *J. Phys. Chem. C* **2011**, 115 (32), 16043-16051.

7. Chan, D. Y. C.; Klaseboer, E.; Manica, R. *Soft Matter* **2011**, 7 (6), 2235-2264.

8. Masliyah, J.; Zhou, Z.; Xu, Z.; Czarnecki, J.; Hamza, H. *Can. J. Chem. Eng.* **2004**, 82 (4), 628-654.

9. McLean, J. D.; Kilpatrick, P. K. *J. Colloid Interface Sci.* **1997**, 196 (1), 23-34.

10. Yarranton, H. W.; Sztukowski, D. M.; Urrutia, P. *J. Colloid Interface Sci.* **2007**, 310 (1), 246-252.

11. Feng, X.; Xu, Z.; Masliyah, J. *Energy & Fuels* **2009**, 23 (1), 451-456.

CHAPTER 2 LITERATURE REVIEW

2.1 CASCADE PARTIAL COALESCENCE PROCESS

Stability and coalescence of drops and bubbles is important for a number of industrial processes involving emulsions. Droplet coalescence plays a significant role in industrial mixing and separation.[1] Partial coalescence, where only a part of a droplet/bubble merges with the interface, leaving a smaller droplet behind, can significantly slow down gravity-driven phase separation of immiscible liquids.[2] Moreover, separation of emulsions becomes increasingly difficult as droplet size decreases.[3] The following sections will focus on describing the partial coalescence process, its dynamics and importance for "clean" systems as well as systems where surface-active species are present along with interfacial charge.

2.1.1 Cascade Partial Coalescence Process and its Dynamics

An illustration of a partial versus complete coalescence process is shown in Figure 2.1.1. Here, a droplet of fluid 1 moves through an ambient fluid 3 under gravity, and approaches a fluid 2- fluid 3 interface (fluid 2 may or may not be the same as fluid 1).[4] As the droplet gets closer to the interface, fluid 3 beneath it is squeezed out and forms a thin film.[4,5] The droplet may remain stable at the interface, however, if the film drains sufficiently and ruptures, the droplet would come into contact with the reservoir and undergo partial or complete coalescence.[5,6] It should be noted that interfacial curvature plays a significant role in this process and can influence the outcome.[7]

For partial/complete coalescence process, residence time is defined as the time it takes the fluid between the droplet and interface to drain until film ruptures. After this period, the film thickness becomes sufficiently small, typically 10-100 nm, and van der Waals forces become important and generate a hole, resulting in film rupture.[8] The rupture point typically occurs off center due to an overpressure at the center of the film from the surrounding fluid as it is drained outward.[2]

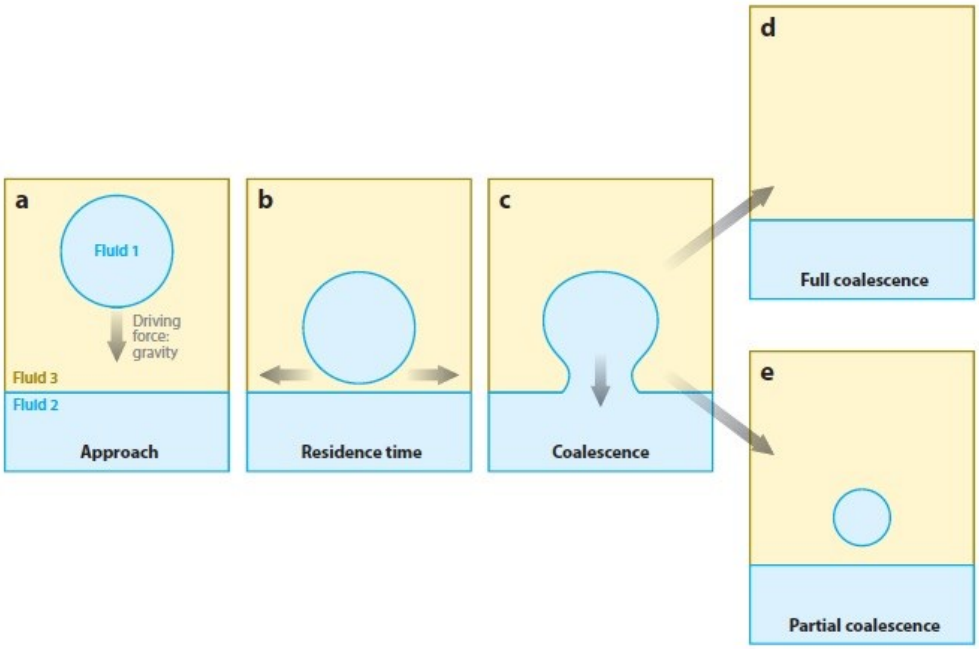

Figure 2.1.1 A schematic of the classic droplet-interface problem.[4]

The resulting fluid neck joining fluid 1 and fluid 3 rapidly opens up. As surface tension acts to minimize the surface energy of the interface, the neck progressively widens. The fluid within the droplet is accelerated towards the bulk fluid by the surface tension pulling on top of the droplet.[8] Two outcomes may occur at this point: complete coalescence, where the droplet merges entirely with the reservoir, or only a fraction of the drop merges with the reservoir, leaving a

daughter droplet behind.[9] In the event of partial coalescence, the daughter droplet is projected downward, bounces on the reservoir surface, and eventually comes to rest before undergoing a similar process, resulting in a cascade.[9] Depending on whether or not the viscous effects are present, this cascade may or may not proceed to completion.[10]

Partial coalescence process has been of interest to researchers for decades. Charles and Mason attributed this occurrence to a Rayleigh-Plateau instability, which causes a thin column of fluid to break up into a sequence of droplets under the influence of surface tension.[11] Eggers[12] gives a comprehensive review of both theoretical and experimental work related to the pinch-off of droplets from a nozzle. However, with recent advances in high-speed cameras, the partial coalescence process has been examined in greater detail, shedding light on dynamics of the cascade partial coalescence process.[13]

Partial coalescence occurs for an intermediate range of droplet sizes, and proceeds in two stages: capillary waves propagating along the droplet and transforming it into a fluid column, and neck formation on the column and pinch-off of the secondary droplet. In the first stage, interfacial energy turns into kinetic energy following film rupture. In the second stage, kinetic energy overcomes an energy barrier due to the increase in interfacial area during neck formation.[5]

The vast majority of studies focusing on partial coalescence utilize four dimensionless numbers: the Ohnesorge number (*Oh*; viscosity of both fluids versus surface tension), the Bond number (*Bo*; gravity versus surface tension**),** the density ratio and viscosity ratio.[5] These dimensionless numbers are calculated for

the case of fluid 1 (droplet) being the same as reservoir in Figure 2.1.1, and fluid 2 representing the matrix phase (instead of the reservoir in Figure 2.1.1).

$$Oh = \frac{\mu_1}{\sqrt{\rho_1 \sigma D}} \quad (1)$$

$$Bo = \frac{|\rho_1 - \rho_2| g D^2}{\sigma} \quad (2)$$

$$\rho^* = \frac{\rho_1}{\rho_2} \quad (3)$$

$$\mu^* = \frac{\mu_1}{\mu_2} \quad (4)$$

Where D is the droplet diameter, g is the acceleration of gravity, μ is the viscosity, ρ is the density of the two fluids and σ is the interfacial tension. *Bo* indicates the tendency of gravity to inhibit partial coalescence, while *Oh* signifies tendency of viscosity in both phases to dampen capillary waves and suppress partial coalescence.[5]

To further understand the mechanism of partial coalescence, the Navier-Stokes equations have been numerically solved, while including surface forces along with pressure and velocity fields inside the droplet.[7] Blanchette and Bigioni's work[7,8] focused on depositing an ethanol droplet on an air/ethanol interface. By examining the velocity fields, they showed that pinch-off depends on the inward momentum of the collapsing neck. When gravitational effects are negligible, the coalescence process is controlled by competition between the vertical and horizontal rates of collapse, which depend on the ability of capillary waves to stretch the droplet. These waves travel up the side of the drop, and carry enough momentum to significantly distort the droplet as they converge at its summit. If

the waves can stretch the droplet enough vertically, the horizontal collapse would reach completion, leading to partial coalescence.[7]

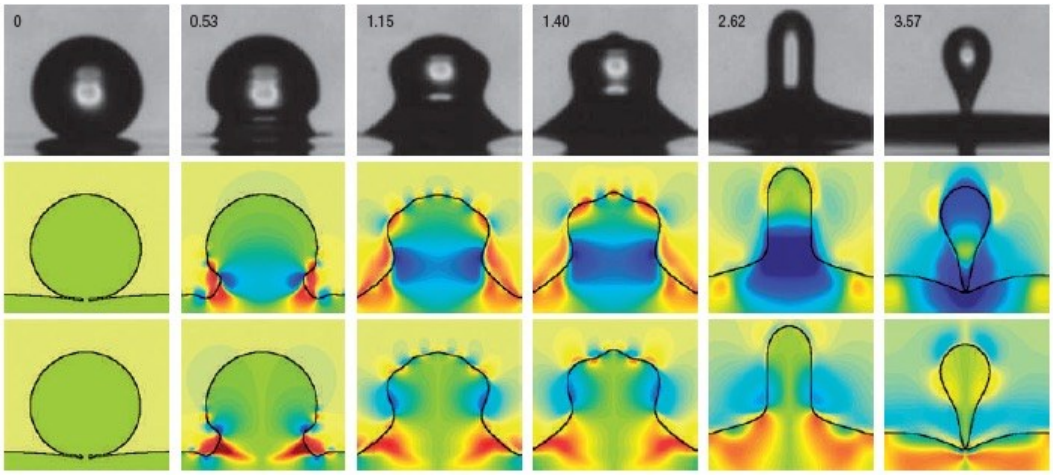

Figure 2.1.2 Partial coalescence of an ethanol droplet on an ethanol reservoir. Top row shows experimental results, while numerical simulations are shown in the middle and bottom rows. Vertical velocity is represented by red (upward) and blue (downward motion) colors in the middle row. The horizontal velocity is represented with red (away from) and blue (towards the center) colors in the bottom row.[7]

Simulations also revealed that droplet viscosity determines the extent to which capillary waves can stretch the droplet. For sufficiently viscous liquids, capillary waves are strongly damped before converging on the summit, resulting in complete coalescence with the underlying fluid.[2,7] However, for the case of a viscous matrix phase (fluid 2), partial coalescence could still be observed.[2]

Using the flow parameters that resulted in pinch-off in Figure 2.1.2, the authors[7] then interrupted evolution of the interface at the maximally stretched state, set all

velocities to zero, and restarted simulations (Figure 2.1.3). This process never led to formation of a daughter droplet, as the geometry of the drop was not sufficiently elongated. Therefore, the Rayleigh-Plateau instability could not be the cause of daughter droplet formation, suggesting that pinch off mechanism depends on the early dynamics of coalescence.

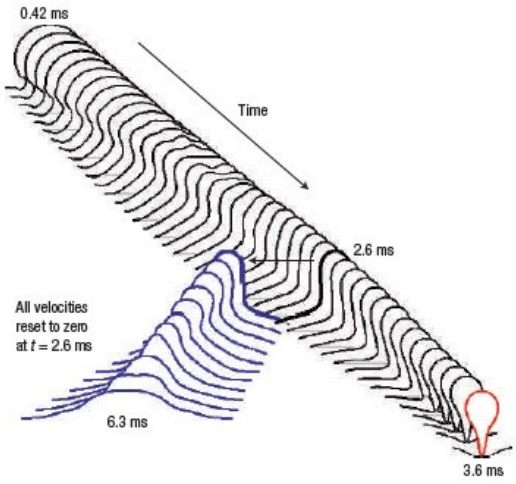

Figure 2.1.3 Time evolution of the interface using the same parameters as in Fig. 2.1.2. Resetting the fluid velocity to zero at the maximally stretched state resulted in complete coalescence.[7]

Gilet and coauthors[2] studied the partial coalescence process for silicon oil droplets travelling through water and alcohol mixtures before arriving at the same interface, evaluating the importance of various dimensionless parameters. In this work, initial droplet sizes, viscosities and densities of both fluids were varied. For negligible Bo, Oh_1, and Oh_2 surface tension is the only dominant force, and dynamics is governed entirely by capillary and inertia forces. Therefore, the convergence of capillary waves cannot be the only mechanism responsible for the

process. Different mechanisms depending on Oh_1 and Oh_2 are responsible for aiding the horizontal collapse or enhancing the emptying of the droplet.[2] A hypothetic schematic of fluid motion is shown in Figure 2.1.4.

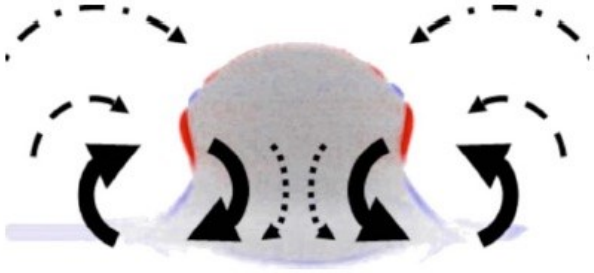

Figure 2.1.4 A schematic of observed trends during the coalescence process. Solid arrows correspond to the nominal movement, dotted arrows- to the movement induced by a high viscosity of fluid 1, dashed arrows- to the movement induced by an intermediate viscosity of fluid 2, and dash-dotted arrows- to the movement induced by a high viscosity of fluid 2. The blue interface is progressing toward fluid 2, while the red interface is receding.[2]

This work was further elaborated on by Ray,[14] who used a coupled level set and volume of fluid method to simulate dynamics of partial coalescence. They numerically established that the competition between the horizontal and vertical momentum of the droplet determines the transition between partial and complete coalescence. Pinch-off occurs for systems where the horizontal momentum exceeds the vertical momentum.

It should be noted that most numerical simulations have difficulties processing the initial film rupture and droplet pinch-off due to the three length scales that have to be accommodated, and droplet size >> draining film thickness >> interface

thickness (of the droplets).[5] The impact velocity of the drop may also affect coalescence dynamics. Marangoni effects due to composition, temperature, surfactant concentration differences between a drop and reservoir further alter the outcome of this merging process.[8] These factors will be discussed in more detail in the following sections.

A less numerically challenging approach has been taken by many authors to predict the occurrence of partial versus complete coalescence as a function of system properties. Earlier studies varied *Bo* and *Oh* numbers by changing the droplet size, density, viscosity and surface tension.[8] Pinch-off was observed only for small *Oh* and *Bo* values. For low *Bo* values, the transition between partial and complete coalescence has been shown to occur at a critical Ohnesorge value Oh^* ≈0.026.[7] Therefore, for a wide range of fluid densities and viscosities, as long as *Bo* is small, a criterion for partial coalescence in terms of a maximum Ohnesorge number can be established.[5] Larger *Bo* numbers are not favorable to pinch off, as they correspond to larger influence of gravity and accelerate vertical collapse. Figure 2.1.5 shows the partial to complete coalescence transition for various *Oh* and *Bo*.

An approximate criterion for systems with low viscosity based on *Oh* and *Bo* has been proposed to predict whether the pinch off would occur:[2]

$$\frac{Oh\left(1+\frac{0.53}{\mu^*}\right)}{\sqrt{1+\frac{2.22}{\rho^*}}} < 0.026 - 0.013Bo \qquad (5)$$

However, while the data fit using Eqn. 5 was successful for small *Bo* numbers, the critical *Oh* number was under predicted for systems where $\mu_2 > \mu_1$.

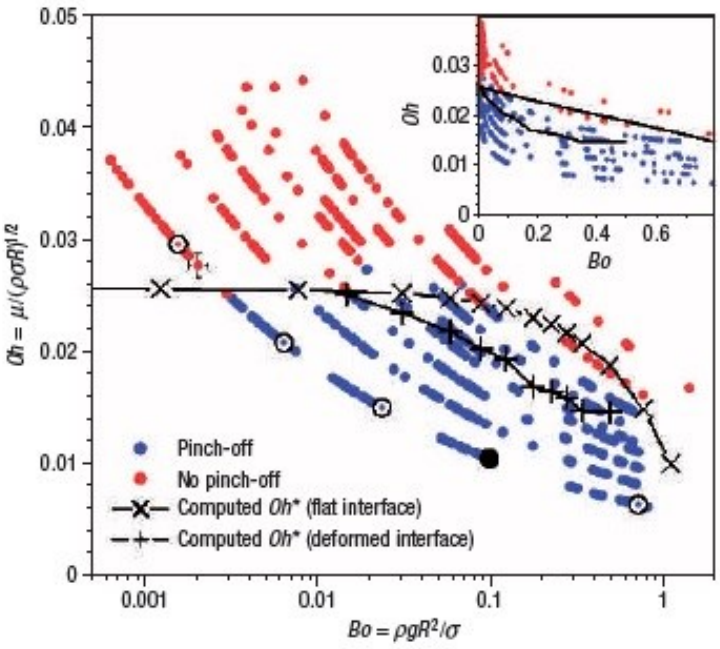

Figure 2.1.5 Experimental results for partial and complete coalescence events, plotted in terms of *Bo* and *Oh*. The blue dots represent drops that underwent partial coalescence process, while the red dots indicate complete coalescence. Numerically computed values of the critical Oh^* are also shown for a spherical drop on planar surface and a drop at equilibrium on an interface.[7]

The dimensionless numbers, described in Eqns. 1-4, have also been used to predict the ratio between the "daughter" and "mother" droplet size. For low viscosity fluids, such as water and air, there's an intermediate range of D such that both *Oh* and *Bo* are very small and the size ratio depends only on ρ and μ. For such systems, the size ratio remains constant.[6] For example, for D on the order of hundreds of micrometers, the "daughter"/"mother" droplet size ratio was reported to be approximately 0.5.[2,10,13] Scaling relationships for the drop size ratio were also developed by Chen, Mandre and Feng.[15] Honey and Kavehpour[16] considered

the bouncing height of the daughter droplet, while predictions of cascade features for a variety of different fluids, based on the dimensionless numbers discussed earlier, have been described by Gilet.[2]

A mechanistic model for complete coalescence has been proposed by Bozzano and Dente.[1] Good experimental and theoretical agreement was observed for droplet shape close to the interface. The shape was shown to be similar to an oblate spheroid along the final drainage time and dictated by the effects of hydrostatic and capillary pressure. When the drop gets very close to the interface, viscous resistance created by the displacement of the interposed fluid quickly dissipates the kinetic energy of the drop and velocity immediately reduces.[5] Film drainage time depended mainly on viscosity of the continuous phase.

During droplet-film impact, four regimes can occur: low energy collision-coalescence, bouncing, high energy collision-coalescence and splashing.[17] Bouncing water, ethanol and propanol droplets were investigated on a deep pool of the same liquid. Partial coalescence was observed only for distilled water, likely due to the high viscosities and low surface tensions of alcohols compared to water, weakening the conditions for neck rupture. Distinguishing between the four regimes highlights the importance of system properties.

Bouncing versus coalescence would occur depending on whether the intervening air/fluid drains to a critical thickness, on the order of a few μm, during impact. This critical thickness depends on system properties and cleanness.[18] It should be noted that bouncing dynamics on a liquid pool are difficult to characterize, since both the droplet and pool are undergoing deformation. However, the kinetic

energy available to the droplet when it impacts a thin liquid layer on a solid surface is partially, but not completely, transferred into surface energy.[18]

Granted the focus of this review is the droplet-interface scenario, some studies have utilized bubbles. For example, Li and coauthors investigated bubble transition through an interface of immiscible fluids.[19] When a bubble rises to an interface between two immiscible fluids, it can pass through the interface if this is energetically favorable. Once the intermediate film between the bubble and interface drains sufficiently, the bubble forms a triple-line, producing strong capillary waves, which travel around the bubble and can pinch off a satellite on the opposite side, akin to the dynamics in the coalescence cascade. It's interesting to note that dynamics of the process differs for droplets and bubbles. The drop is pinched off by surface tension, whereas the bubble pinch-off is controlled by inertia of the liquid.[13] The bubble is evacuated by the capillary overpressure and the flow is resisted by inertia of air; coalescence cascade may arise for relatively large bubbles since the effects of gravity are diminished.[20]

2.1.2 Influence of Surface Tension Gradients and Surface-Active Species

While presence of surface tension gradients and surfactants complicates theoretical work, it is more applicable to "real-world" systems.

Blanchette and Bigioni[8] examined the influence of a surface tension difference between a drop and reservoir (fluid 1 ≠ fluid 2 in Fig. 2.1.1) on the coalescence process, as may arise from differences in temperature or composition. Depending on the surface tension ratio of the two fluids, satellite droplets, partial and

complete coalescence were observed. Interactions between two droplets of miscible liquids with different surface tensions sitting on a solid substrate were also investigated through computer simulations.[21] Total, partial coalescence and complete separation were observed after droplet's collision. Partial coalescence occurred for miscible droplets with a surface tension gradient even though droplets of the same composition would coalesce completely.

These studies highlight the effect of surfactant contamination, particularly for aqueous systems where dust particles can decrease surface tension. A "fresh" drop is likely to have a clean surface with a higher surface tension.[9] Therefore even for "clean" systems, a surface tension ratio is likely present to some extent, greatly influencing the outcome of the process. However, surface tension gradients during coalescence of two different liquids arising from the surface tension mismatch between merging liquids are different than those induced by the presence of surfactants.[22]

Early studies focused on the influence of surfactants on the drainage of fluid film separating the drops just before coalescence,[23,24] however only recently studies focused on surfactants affecting droplet coalescence after contact. The dynamics of surfactants affect local surface properties.[4] By locally altering surface tension, surfactants affect flow near fluid interfaces and therefore impact coalescence.[25] More specifically, the presence of surfactants should inhibit partial coalescence.[7]

Contraction of the interfaces affects surfactant concentration, contributing an effective elasticity to the interface.[9] Numerical simulations for surfactant-laden droplets were performed by Lu and Corvalan.[22] Surfactants accumulate on the

meniscus bridge joining the drops due to uneven contraction of the interface. A rapid "neck" contraction leads to strong surface tension gradients, generating tangential Marangoni stresses. These stresses pull the interface from regions of high surface tension and enhance the flow up the side of the drops.

A recent study by Martin and Blanchette further investigated surfactant effects on coalescence dynamics by using the volume of fluid (VOF) method.[25] Simulations showed that surfactant presence led to local surface tension variations, altering the regime of partial coalescence due to uneven distribution of surface forces.

Figures 2.1.6 and 2.1.7 show pressure plots of the coalescing system in the absence (Fig. 2.1.6) and presence (Fig. 2.1.7) of surfactant. The interior and exterior fluids have identical viscosity and density, $Oh = 0.027$; and gravity is not considered. Initially, the qualitative behavior of the droplet in both figures is similar, However, pinch-off fails to occur in Fig. 2.1.7, despite the fact that all parameters are the same except for the presence of surfactant represented by an elasticity coefficient β ($\beta = 0.1$). This elasticity coefficient represents the amount by which the surface tension decreases in response to a unit increase in surfactant concentration. [25]

The thickness of the white curve in Figure 2.1.7 indicates surfactant concentration. Early on, surfactant accumulates at the base of the drop, due to area reduction during initial merging. Surfactant at the crest of the drop initially thins out, as the droplet is stretched by capillary waves, but increases later, as the drop contracts toward the reservoir. The increased surfactant concentration at the base

of the drop and decreased concentration at the crest leads to a lower surface tension at the base and higher at its crest, reducing forces that drive pinch-off. [25]

It should be noted that if Marangoni forces are sufficiently large, they can level out the surfactant distribution, shifting the droplet behavior observed in Fig. 2.1.7 back to that in Fig. 2.1.6. Large Marangoni forces might also counter stretching of the drop, leading to a different balance of forces.[2]

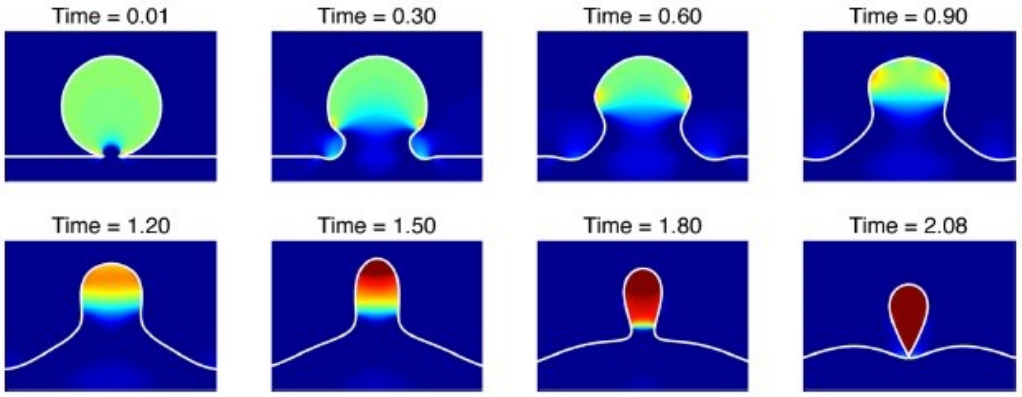

Figure 2.1.6 Pressure plots depicting partial coalescence of a droplet with a reservoir, in the absence of surfactant. The coloring shows the fluid pressure and the interface is shown in white.[25]

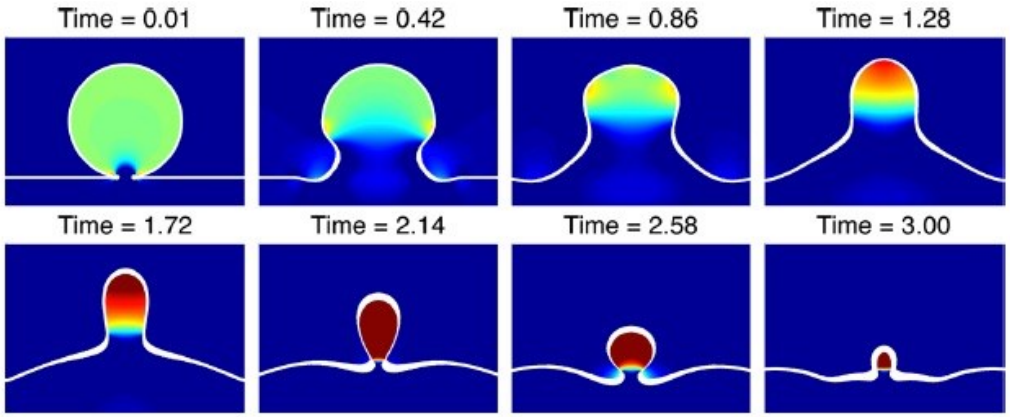

Figure 2.1.7 Pressure plots depicting partial coalescence of a surfactant covered

droplet or bubble on a reservoir. The surfactant concentration is shown as a thickness effect. The elasticity coefficient $\beta = 0.1$, indicating the presence of surfactant.[25]

Experimental studies using polymer solutions demonstrated the importance of viscoelasticity, showing increased droplet coalescence times, smaller "daughter"/"mother" droplet size ratios and an increased minimum droplet size requirement for partial coalescence. However, viscoelasticity in the drop phase appears to have more of an effect than that in the matrix fluid.[5] Partial coalescence may be completely eliminated when the drop fluid is viscoelastic.

Presence of particles coupled with system charge has also been shown to affect the outcome of the coalescence process in electrolyte solutions.[26] The transition from partial to complete coalescence occurs at solid concentration of 20 wt. % and depends on ionic concentration in the dispersed phase, demonstrating the effect of surface rheology/charge on the system. At low and high electrolyte concentrations, the critical particle concentration, at which complete coalescence occurs, corresponds to the onset of non-Newtonian, shear thinning fluid behavior.

It should be noted that if surface-active species are present at the interface at sufficient concentrations, the intervening film drainage would be slowed down significantly, causing an increase in coalescence times, and ultimately resulting in increased emulsion stability.[27] Lower coalescence rates have been experimentally observed for surfactant-laden droplets.[22] For sufficient surfactant concentrations, the critical film thickness required for intervening film rupture may not be reached, thus inhibiting the coalescence process.

2.1.3 Influence of Electric Field/ Charge on the Coalescence Process

In the presence of an electric field, film thinning speed is increased significantly, shortening coalescence time and resulting in smaller droplets. An applied electric field exerts shear stress in the upward direction at the interface between the coalescing drop and the outside dielectric liquid.[4] Effect of electric field stress is intensified in the presence of surfactants due to lower interfacial tension, and jets of very fine droplets may be formed.[3] The deformation and onset of drop breakup can be described by the electrostatic Weber number, *We*,[28] which indicates the significance of electrostatic energy with respect to the interfacial tension energy:

$$We = \frac{D\varepsilon_2\varepsilon_0 E_0^2}{\sigma} \tag{6}$$

where D is the droplet diameter, ε_2 is the dielectric constant of the continuous phase, ε_0 is the permittivity of vaccum, E_0 is the background electric field strength and σ is the surface tension. It's interesting to note that from the fluid mechanics perspective, *We* denotes the importance of inertia to surface tension: [17]

$$We = \frac{\rho v^2 D}{\sigma} \tag{7}$$

where ρ is the density, *v*- velocity, *D*- droplet diameter and σ is the surface tension.

Since *Oh* incorporates the surface tension and viscous drag of the droplet and *We* incorporates electrostatic energy versus surface tension, a combination of *We* and *Oh (We*Oh)* has been successfully used to describe dynamics for droplets in the presence of electric field.[3] This combination represents the ratio of the electrical stress energy over the energy required for pumping of the viscous fluid out of the

droplets, useful for optimizing the design of electro-coalescence systems. It's interesting to note that a similar correlation $We^{*}Oh^{-0.58}$ has been used to characterize the transitions between coalescence and bouncing of droplets.[17]

Overall, these studies highlight the importance of electrical field/ charged interfaces on the partial and complete coalescence. Charged interfaces have been extensively investigated in the last 40 years, and there is still an on-going discussion on the charge at "clean" interfaces. For example, for an air-pure, neutral interface, some studies report negative charge,[29-32] while others-positive charge.[33-36] When a surfactant-free oil in water emulsion is formed, OH^- must be added to keep the pH constant, leading to a conclusion that hydroxide is adsorbed at the oil water interface.[37] However other studies, in particular, molecular dynamics simulations, show surface depletion of hydroxide and accumulation of hydronium ion, leading to further debates on the topic.[35]

Overall, "clean" interfaces are extremely difficult to characterize due to droplet deformation and the significant impact of impurities. Solid system approximations in zeta potential studies can't always be applied due to deformations and coalescing/ sedimentation of the droplets. Obtaining a stable emulsion, particularly for a "clean" system is challenging, especially at low pHs, close to the isoelectric point.[38] Temperature effects may also influence surface charge, for example a difference of 1 °C may induce a shift in the isoelectric point by up to 0.03 pH unit.[39] The pH dependent electrophoretic mobilities should not be used to deduce the net charge of oil droplets in water due to an uneven distribution of partial charges.[40]

In conclusion, based on the studies to date, the occurrence and dynamics of partial coalescence process depend on multiple factors, including the initial droplet diameter, density, viscosity and interfacial tension. The dynamics of the process have been simulated for a variety of fluids and predictions can be made on whether partial or complete coalescence would occur based on system properties. However, the final drop state (stable droplet at the interface or complete coalescence) depends on interactions between the two interfaces in close proximity, charge of the system, etc. and has not received as much investigation. Cascade partial coalescence process may be a useful tool in obtaining the charge of "clean" droplets, a nontrivial task due to deformation.

2.2 STABILIZATION OF WATER–IN-CRUDE OIL EMULSIONS

For the majority of emulsion systems, obtaining a "pure" interface as described in in Section 2.1, is extremely challenging and requires multiple purifications. In industrial systems, trace (or significant) levels of surfactants and impurities are always present and affect emulsion stability and surface forces. The period of emulsion stability strongly depends on characteristics of the interface separating the dispersed and continuous phases.[41] Shear and deformational modes of emulsified droplets contribute greatly to overall emulsion stability.[42]

Oil sand ores are naturally occurring mixtures of bitumen, mineral solids and water. After upgrading of bitumen, the synthetic crude oil can compete with Saudi Arabia's oil.[43] However, the presence of emulsified water droplets in oil poses a major concern in the oil sands industry, leading to a decreased product quality. The chloride ions in the water also affect downstream bitumen upgrading and

cause damage to processing facilities, thus increasing the capital costs.[44] The following sections will briefly review the bitumen extraction and froth treatment process and focus on the mechanism behind the stability of "contaminated" water-in-oil emulsions and ways to "break" these emulsions.

2.2.1 Bitumen Extraction and Recovery from the Oil Sands

Oil sand ores are naturally occurring mixtures of mineral solids (85 wt. %) and bitumen (8-14 wt. %), with a small amount of water.[43] Because of bitumen's high viscosity, it cannot be extracted by conventional methods and open pit mining or in-situ bitumen recovery such as SAGD (steam assisted gravity drainage) are employed. For shallow deposits of oil sands (< 75 m in depth) open-pit mining using trucks and shovels is utilized, while SAGD is used for deeper deposits.

Currently, about 60 % of bitumen is produced by open pit mining, using the Clark hot water extraction method.[43,] The generalized scheme for oil sands processing is shown in Figure 2.2.1.[43] Briefly, oil sands are mined using trucks and shovels. Hot water and chemical additives such as caustic soda are added to the ore to form a slurry. Bitumen is liberated and aerated within the hydrotransport pipeline, with the aerated bitumen skimmed off from the slurry in gravity separation vessels. Some unaerated bitumen is further recovered using either induced air flotation or cyclo-separators and hydrocyclones. The aerated bitumen, separated from water and solids, forms bitumen froth. The typical bitumen recovery in commercial operations, using a 40 - 55 °C slurry, is 88 - 95 %.[43]

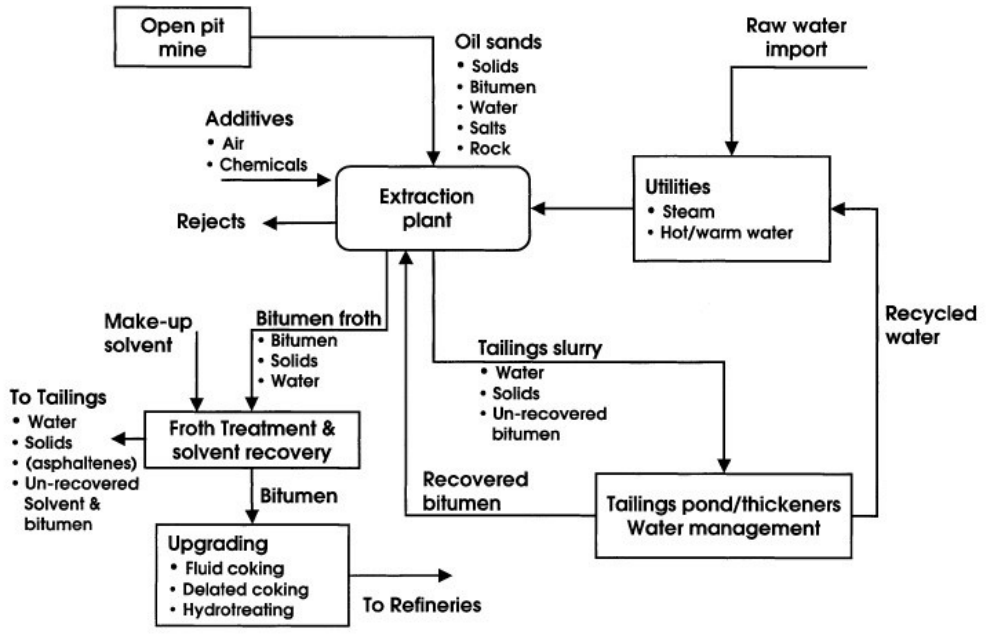

Figure 2.2.1 Generalized scheme for oil sands processing using water-based extraction process.[43]

Bitumen froth typically contains 60 % bitumen, 30 % water and 10 % solids by weight.[43,44] The remaining water and solids are then removed before subsequent upgrading and refining to various types of fuels. This is achieved by diluting bitumen froth with solvent and using a combination of inclined plate settlers, centrifuges and/or gravity settlers.[46] Solvent is added to reduce viscosity of the oil and increase the density difference between oil and aqueous phases.[43,45]

The naphthenic froth treatment (NFT) process, used by Syncrude, Suncor and CNRL, utilizes naphtha, at a naphtha to bitumen mass ratio of 0.6 - 0.7. Shell Canada (Albian Sands) uses the paraffinic froth treatment (PFT) process, where hexane is added to the froth at a solvent to bitumen (S/B) mass ratio of 2.1 - 2.5. Both processes require high operating and capital costs, as multiple froth

recirculations are necessary to remove most of the emulsified water. Even after several stages of separations in NFT process, up to 2 wt. % water and up to 1 wt. % solids remain in diluted bitumen.[47] The tailings stream from the extraction plant goes to tailings ponds for solid-liquid separation; clarified water is then recycled back to the extraction plant.[43]

The water and solids lift behind in the bitumen product are very difficult to remove since they are only a few microns in diameter and covered with a layer of hydrocarbons such as asphaltenes and other bitumen components.[43,45] A micrograph of a typical water-in-oil emulsion is shown in Figure 2.2.2. The "skins" surrounding water droplets prevent droplet coalescence and migration into one of the phases.[48]

Figure 2.2.2 Micrograph of a typical water-in-oil emulsion. One division of the scale on the left is 10 μm.[48]

The emulsified droplets and solids can also form a rag layer, which builds up at the water/oil interface, hindering phase separation. The rag layer is a mixture of flocculated water droplets, fine solids and multiple emulsions. It is extremely

stable because of its intermediate density and the interfacially active materials surrounding the water droplets.[46] The presence of this layer between continuous oil and aqueous phases limits the amount and quality of recoverable oil.[49] However, before investigating the complex multiple emulsion system leading to the development of rag layer, fundamental understanding of a "simple" water-in-crude oil system is necessary.

2.2.2 Role of Asphaltenes, Clays and Other Bitumen Components on Emulsion Stability

Stability of water droplets in crude oil is steric in nature and has been attributed to accumulation of various bitumen components at oil-water interfaces. These surface-active species include asphaltenes, resins, naphthenic acids and suspended fine solids, and form a protective shield or "skin" around water droplets.[50-53]

Asphaltenes are the highest molecular weight fraction of crude oil, soluble in light aromatic hydrocarbons, such as toluene, and insoluble in paraffinic solvents, such as pentane and *n*-heptane.[54] The other components are classified as maltenes and are separated through SARA (saturates, asphaltenes, resins and aromatics) analysis.[43] It should be noted that the amount and composition of asphaltene precipitates strongly depends on solvent type, oil sample and extraction protocols.

Studies of asphaltenes using vacuum feed bitumen showed that when bitumen was diluted with a more paraffinic solvent (higher content of heptane), asphaltenes were more interfacially active as compared to when a more aromatic solvent (toluene) was used.[55] Colloidal forces measured with AFM[56] showed a

repulsive force between asphaltene surfaces in solvents of higher aromaticity, while a week attraction was observed in low aromaticity solvents. Presence of water in the oil also leads to a less favorable environment for asphaltenes, enhancing aggregation even in "good" solvent.[57] However, since soluble asphaltenes are more surface active compared to their precipitates, highest interfacial activity, and hence effectiveness in stabilizing water-in-oil emulsions, occurs just below the onset of precipitation (50 heptol, where heptane:toluene = 50:50 vol. %).[58]

Stability of water-in-oil emulsions has been proven to correlate with compressibility of asphaltene interfacial films.[59,60] Interfacial shear and dilatational rheology show that asphaltenes can form a "gel-like" film,[61] which appears to be viscoelastic and has a high yield stress. Other techniques such as micropipette,[62] Langmuir trough[63] and AFM[56,64] also highlighted the interfacial activity of asphaltenes and their importance in stabilizing water-in-oil emulsions.

Asphaltenes are irreversibly adsorbed at oil-water interfaces and form a rigid film that resists deformation.[65,66] When approaching two water droplets attached to micropipettes in diluted bitumen environment, Yeung and coauthors[62] observed no coalescence between the droplets, even after a forced contact of 5 min, as shown in Figure 2.2.3. Figure 2.2.4 demonstrates the presence of a mechanical barrier or "skin" surrounding the water droplet in 0.1 % bitumen in 50 heptol solution (heptane:toluene = 50:50 vol. %) upon compression of surface area of the droplet.

It has been postulated that only a small fraction of asphaltenes is involved in formation of the interfacial film around the water droplets, rather than all of asphaltenes.[67-69] Only this subfraction may be responsible for emulsion stability.

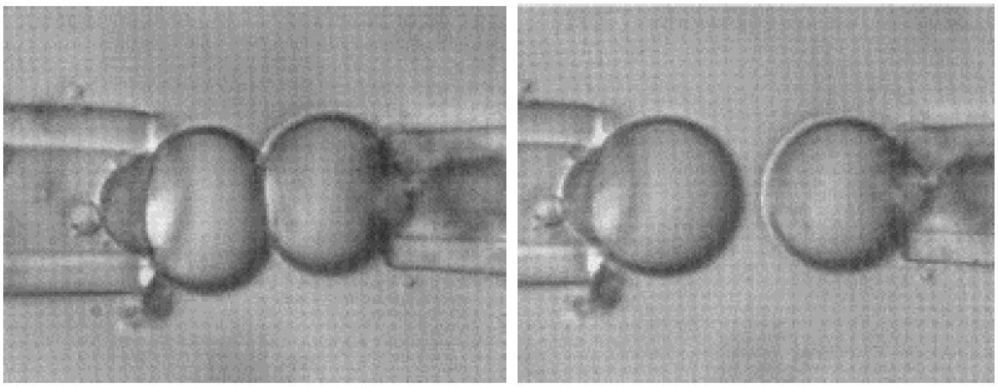

Figure 2.2.3 Demonstration of the stability of water-in-diluted bitumen emulsions by (a) pressing two water droplets together and (b) pulling them apart when oil phase contained 0.01 % bitumen in 50 heptol.[62]

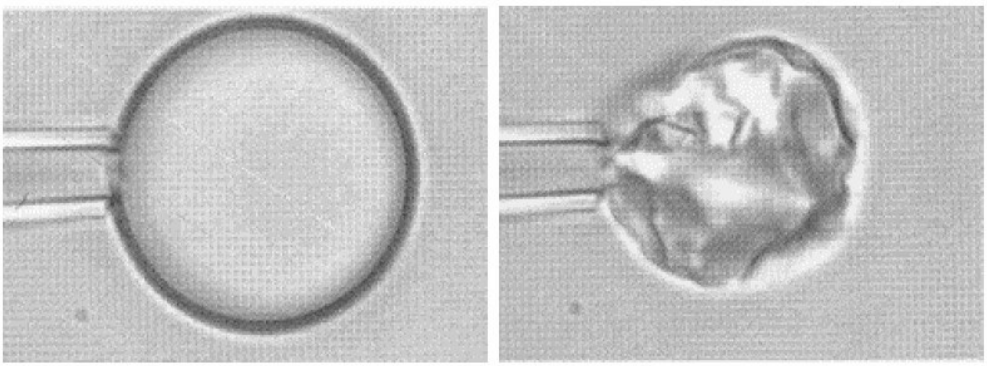

Figure 2.2.4 Deflation of a water droplet by withdrawing fluid back into the water-filled micropipette.[62]

Other bitumen fractions cannot effectively stabilize water in oil emulsions on their own. However, their interactions with asphaltenes play an important role in

stabilizing the water-oil interface. For example, asphaltenes can adsorb on originally hydrophilic solids and change their surface properties, causing them to become bi-wettable and enabling them to migrate and remain at oil-water interfaces.[70] The "contaminated" solids contribute significantly to stabilizing water in oil emulsions and are one of the key components to forming a rag layer.[46,71,72] Due to their small size, they cannot be completely removed by mechanical techniques such as centrifugation, and chemical treatment to make the solids' surface more hydrophilic is required.[73]

Yan and coauthors[53] showed that diluted solids-free bitumen had lower emulsion stabilization potency than bitumen containing solids. However, only solids in the size range of 0.22 - 8 μm could stabilize water-in-oil emulsions. Particles of intermediate hydrophobicity were most effective at stabilizing water-in-oil emulsions due to their ability to remain at the oil-water interface.[74] They can act as a strong mechanical barrier and prevent water droplet coalescence.[75] Both super-hydrophilic and super-hydrophobic particles were ineffective in stabilizing emulsions due to their non-surface active nature and could be dispersed within the respective aqueous and oil phases.[74] Angle and coauthors[48] also showed that surfactant adsorption onto solids changes their wettability and promotes adhesion of the oil droplets to the solids. The accumulation of bi-wettable fine solids at oil-water interfaces reduces the effective density difference between the droplets and continuous phases, hindering oil-water separation.

Resins alone cannot stabilize water-in-oil emulsions, likely due to their nonpolar nature and small-sized molecules.[58] However, when the solvent is changed so that

the resins could precipitate out, they are able to adsorb at the oil-water interface and form a barrier for droplet coalescence. Emulsion stabilization was observed only at small resin to asphaltene (R/A) ratios (R/A<1).[58] Emulsions obtained using such model oils exhibited stabilities similar to those produced from the whole crudes. Mohammed and coauthors[76] investigated the behavior of asphaltene and resin-asphaltene mixture (R/A >1) at oil-water interface under various surface pressures. Solid asphaltene monolayers could withstand surface pressures up to 60 mN/m, while monolayers formed by the mixtures could hold up to only 7 mN/m. It was concluded that resins rearranged asphaltenes by forming a resin-solvated asphaltene aggregate. Because self-association of asphaltenes would be reduced under such conditions, emulsification potency would decrease when R/A >1.

Naphthenic acids are surfactant-like molecules found within crude oil.[55] They adsorb at oil–water interfaces and can significantly reduce interfacial tension of these systems. The area occupied per asphaltene molecule was calculated to be 3 times larger than that of naphthenic acids.[77-79] It has been hypothesized that acid-base interactions between the naphthenic acids and nitrogen from the asphaltenes produced "surface-active naphthenic acid-asphaltene acid-base complexes". These complexes could then aggregate at the oil-water interfaces and reduce oil-water interfacial tension.[78] The reduced interfacial tension promoted water droplet coalescence, reducing stability of water-in-diluted-bitumen emulsions.[54]

Therefore, the main stabilization mechanism of water-in-crude oil droplets arises from asphaltene-asphaltene and asphaltene-clay interactions within crude oil.

2.2.3 Demulsifiers Addition and Role in Emulsion "Breaking"

In order to remove emulsified water, it water droplets have to be brought in contact either by coagulation or flocculation. Droplet coalescence would lead to a larger droplet size, enhancing water removal from emulsion systems.

Emulsion "breaking" can be achieved by a variety of methods including heating, mechanical and chemical methods. Heating can be used to reduce oil viscosity and increase the rate of water settling. Mechanical methods, such as free-water knockout drums and de-salters are also available; another approach utilizes applying an electrical field to facilitate coalescence. However, the aforementioned methods are expensive and may decrease product quality. The most common and least energy consuming approach is to add chemicals to the system.[64,76,80]

When a chemical modifier is added to the water-oil system, it weakens the interfacial film by penetrating the original protective barrier and displacing the interfacial materials.[64] Its presence at the interface provides an opportunity for water droplet flocculation and/or coalescence. Demulsifiers can destabilize emulsions by changing interfacial tension, mechanical strength, elasticity and film thickness, and promoting drop-drop coalescence.[64,81] To break water in oil emulsions, a demulsifier must weaken the strength of interfacial film by interacting with the interfacial materials present, or by displacing them.[48] Therefore, for crude oil systems, demulsifiers have to be oil-soluble for delivery and sufficiently interfacially active to either adsorb on top of hydrocarbons stabilizing the droplet or displace them from the interface.[64] Upon weakening of

the interfacial film, water droplets would coalesce.[72] However, demulsifier overdose may result in deterioration of the separation process performance.[46]

Currently, a mixture of polymers and surface active chemicals is used in the petroleum industry. Ethylene oxide/propylene oxide (EO/PO) copolymer based demulsifiers are used for water removal from naphtha-diluted bitumen and can resolve 90 % emulsified water.[81] At the oil-water interface, EO chains (hydrophilic part) stay in the water droplet and PO structure (hydrophobic part) remains in the oil phase. Such coalescing-type demulsifiers have high interfacial activity to adsorb irreversibly at the interface and break the film, promoting droplets coalescence. Demulsifier addition has been shown to soften asphaltene films, i.e. reduce viscoelastic moduli under both shear and compressional interfacial deformations, ultimately promoting droplet coalescence.[82]

Previous studies have reported a biodegradable and nontoxic polymer, ethyl cellulose (EC) to be an effective demulsifier for water-in-diluted-bitumen emulsions[64,70,83] Addition of 130 ppm of EC removed up to 90 % of emulsified water in naphtha-diluted-bitumen by gravity settling after 1 hour at 80 °C.[64] EC also increased wettability of contaminated solids in the oil phase, enabling them to migrate to the aqueous phase, potentially decreasing emulsion stability.[73]

EC could displace the original interfacial protective materials, breaking up the water in bitumen emulsions by flocculation and coalescence mechanisms.[64] The demulsification schematic of the polymer is shown in Figure 2.2.5. It highlights the ability of EC to adsorb at the interface and disrupt of the original protective films formed by the surface-active components of bitumen.[70] EC addition

decreased interfacial tension of water in diluted bitumen solution and disrupted the original protective films comprised by bitumen's surface-active components.

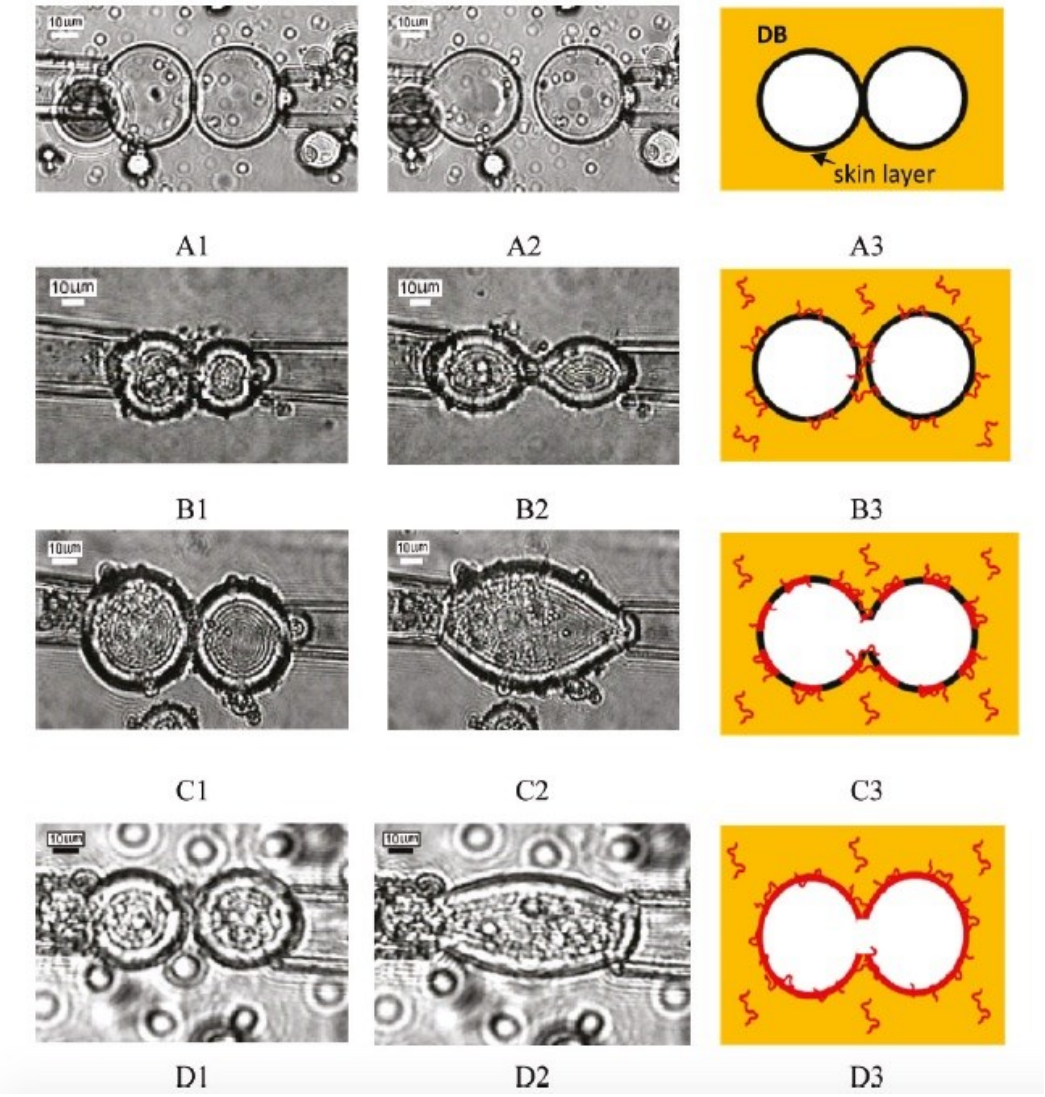

Figure 2.2.5 Interactions between water droplets visualized by the micropipette technique. Water droplets were brought into contact in 0.1 wt% naphtha-diluted bitumen solution (A, B, C) or in naphtha (D). (A1)Water droplets were brought into contact in diluted bitumen (no EC) and detached from each other without a significant change in shape and size (A2); (B1) water droplets were brought into contact in the emulsion with 35 ppm EC and detached after significant

deformation (stretching) of flocculated droplets (B2); (C1) water droplets were brought into contact in the emulsion with 130 ppm EC and coalesced into one large droplet (C2); (D1) water droplets were brought into contact in naphtha with 35 ppm EC and coalesced into one large droplet; A3,B3, C3, and D3 are the schematic representations of the respective conditions.[70]

2.2.4 Presence of Viscoelasticity in Water-Crude Oil Systems

The water-in crude oil system, as described in Sections 2.2.1 and 2.2.2 provides a unique opportunity to study interfaces which exhibit continuously changing surface properties and develop elasticity.[59,60,84,85] A general understanding of the emulsion stabilization mechanism, along with the importance of individual bitumen components, is available from "bulk" studies and coated surfaces.[45,55,58] However, limited knowledge is available on the forces present at the oil-water interface. While interfacial rheology is a useful tool to track the development of interfacial properties and elastic "skin" formation, the surface area to volume ratio for small water droplets is significantly larger than that for planar interfaces, enhancing emulsion stabilization capability of the various crude oil fractions.[85] Droplet curvature and deformation, as well as hydrodynamic forces also enhance repulsion between colliding droplets, further increasing emulsion stability.[86]

To characterize and quantify forces at deformable interfaces, Atomic Force Microscopy (AFM) is often used to study "model" interfaces. Most of the previously reported research focused on interactions between the AFM probe (particle, droplet or bubble) and a bubble or water droplet immobilized on a substrate. [86-91] A detailed description of these can be found in Chapters 4 and 5.

Ultimately, AFM measurements involving a deformable interface are highly nontrivial, and "true" separation between the interacting surfaces is impossible to obtain through AFM measurements alone.[88]

Earlier studies focus on Laplacian interfaces and using the Stokes-Reynolds-Young-Laplace model to predict interfacial shape, deformation and forces present.[88-91] However little information is available about interfaces which exhibit elasticity or, as in the case of interfacially active bitumen components, develop elasticity over time.[59,60] These initially-viscous interfaces become non-Laplacian over time, as demonstrated by the development of a "skin" and in-plane shear at the interface.[62,92] For such systems, where the mechanical barrier causes the interface to behave as a quasi-solid, both the isotropic (for viscous, Laplacian systems) and shear (elastic component) contributions at the interface should be considered to describe droplet deformation.[93,94] However, little information is available on combining interfacial rheology with other measurements for non-Laplacian systems, where the development of viscoelasticity at oil-water interfaces is one of the critical factors responsible for emulsion stability.

In conclusion, the dynamic water-in-crude oil emulsion system is a complex and industrially-relevant topic. Further examination of interactions at the deformable interface is crucial for understanding stabilization and "breaking" of "real-world" emulsions, as well as gauging the effectiveness of interfacially active materials.

2.3 REFERENCES

1. Bozzano, G.; Dente, M. *Comput.Chem.Eng.* **2011**, 35 (5), 901-906.

2. Gilet, T.; Mulleners, K.; Lecomte, J. P.; Vandewalle, N.; Dorbolo, S. *Phys. Rev. E Stat. Nonlin. Soft Matter Phys.* **2007**, 75, 036303.

3. Mousavichoubeh, M.; Shariaty-Niassar, M.; Ghadiri, M. *Chem. Eng. Sci.* **2011**, 66 (21), 5330-5337.

4. Kavehpour, H. P. *Ann. Rev. Fluid Mech.* **2015**, 47, 245-268.

5. Yue, P.; Zhou, C.; Feng, J. J. *Phys. Fluids* **2006***,* 18, 102102.

6. Chen, X.; Mandre, S.; Feng, J. J. *Phys. Fluids* **2006**, 18, 092103.

7. Blanchette, F.; Bigioni, T. P. *Nat. Phys.* **2006***,* 2 (4), 254-257.

8. Blanchette, F.; Bigioni, T. P. *J. Fluid Mech.* **2009**, 620, 333-352.

9. Blanchette, F.; Messio, L.; Bush, J. W. M. *Phys. Fluids* **2009**, 21, 072107.

10. Thoroddsen, S. T.; Takehara, K. *Phys. Fluids* **2000**, 12 (6), 1265-1267.

11. Charles, G. E.; Mason, S. G. *J. Colloid Sci.* **1960**, 15 (3), 236-267.

12. Eggers, J. *Rev. Mod. Phys.* **1997**, 69 (3), 865-929.

13. Thoroddsen, S. T.; Etoh, T. G.; Takehara, K. *Annu. Rev. Fluid Mech.* **2008**, 40, 257-285.

14. Ray, B.; Biswas, G.; Sharma, A. *J. Fluid Mech.* **2010**, 655, 72-104.

15. Chen, X.; Mandre, S.; Feng, J. J. *Phys. Fluids* **2006**, 18, 051705.

16. Honey, E. M.; Kavehpour, H. P. *Phys. Rev. E Stat. Nonlin. Soft Matter Phys.* **2006**, 73 (2), 1-4.

17. Zhao, H.; Brunsvold, A.; Munkejord, S. T. *Int. J. Multiph. Flow* **2011**, 37 (9), 1109-1119.

18. Gilet, T.; Bush, J. W. M. *Phys.Fluids,* **2012**, 24, 122103.

19. Li, E. Q.; Al-Otaibi, S.; Vakarelski, I. U.; Thoroddsen, S. T. *J. Fluid Mech.* **2014***,* 744 (1), R1-R14.

20.Pucci, G.; Harris, D. M.; Bush, J. W. M. *Phys. Fluids* **2015**, 27, 061704.

21. Borcia, R.; Bestehorn, M. *Langmuir* **2013**, 29 (14), 4426-4429.

22. Lu, J.; Corvalan, C. M. *Chem. Eng. Sci* **2012**, 78, 9-13.

23. Hodgson, T. D.; Lee, J. C. *J. Colloid Interface Sci.* **1969**, 30 (1), 94-108.

24. Hodgson, T. D.; Woods, D. R. *J. Colloid Interface Sci.* **1969**, 30 (4), 429-446.

25. Martin, D. W.; Blanchette, F. *Phys. Fluids* **2015**, 27, 012103.

26. Harbottle, D.; Bueno, P.; Isaksson, R.; Kretzschmar, I. *J. Colloid Interface Sci.* **2011**, 362 (1), 235-241.

27. Dreher, T. M.; Glass, J.; O'Connor, A. J.; Stevens, G. W. *AIChE J.* **1999**, 45 (6), 1182-1190.

28. Eow, J. S.; Ghadiri, M.; Sharif, A. *Colloids Surf. A Physicochem. Eng. Asp.* **2003**, 225 (1-3), 193-210.

29. Takahashi, M. *J Phys. Chem. B* **2005**, 109 (46), 21858-21864.

30. Creux, P.; Lachaise, J.; Graciaa, A.; Beattie, J. K.; Djerdjev, A. M. *J. Phys. Chem. B* **2009**, 113 (43), 14146-14150.

31. Creux, P.; Lachaise, J.; Graciaa, A.; Beattie, J. K. *J. Phys. Chem. C* **2007**, 111 (9), 3753-3755.

32. Beattie, J. K.; Djerdjev, A. M.; Warr, G. G. *Faraday Discuss.* **2008**, 141, 31-39.

33. Petersen, P. B.; Saykally, R. J. *Annu. Rev. Phys. Chem,* **2006**, 57, 333-364.

34. Petersen, P. B.; Saykally, R. J. *J. Phys. Chem. B* **2005**, 109 (16), 7976-7980.

35. Dos Santos, A. P.; Levin, Y. *Langmuir* **2012**, 28 (2), 1304-1308.

36. Dos Santos, A. P.; Levin, Y. *J. Chem. Phys.* **2010**, 133 (15), 154107.

37. Gray-Weale, A.; Beattie, J. K. *Phys. Chem. Chem. Phys.* **2009**, 11 (46), 10994-11005.

38. Sonnefeld, J. *Colloids Surf. A Physicochem. Eng. Asp.* **2001**, 190(1-2), 179-183.

39. Kosmulski, M. *J. Colloid Interface Sci.* **2011**, 353 (1), 1-15.

40. Knecht, V.; Levine, Z. A.; Vernier, P. T. *J. Colloid Interface Sci.* **2010**, 352 (2), 223-231.

41. Gunning, A. P.; Kirby, A. R.; Wilde, P. J.; Penfold, R.; Woodward, N. C.; Morris, V. J. *Soft Matter* **2013**, 9 (48), 11473-11479.

42. Erni, P.; Windhab, E. J.; Gunde, R.; Graber, M.; Pfister, B.; Parker, A.; Fischer, P. *Biomacromolecules* **2007**, 8 (11), 3458-3466.

43. Masliyah, J.; Zhou, Z.; Xu, Z.; Czarnecki, J.; Hamza, H. *Can. J. Chem. Eng.* **2004**, 82 (4), 628-654.

44. Gao, S.; Moran, K.; Xu, Z.; Masliyah, J. *Energy & Fuels* **2009**, 23 (5), 2606-2612.

45. Masliyah, J. H.; Xu, Z.; Czarnecki, J. A. *Handbook on Theory and Practice of Bitumen Recovery from Athabasca Oil Sands*, Kingsley Publishing Services, Cochrane (Canada), **2011**, vol. 1.

46. Czarnecki, J.; Moran, K.; Yang, X. *Can. J. Chem. Eng.* **2007**, 85 (5), 748-755.

47. Dabros, T.; Yeung, A.; Masliyah, J.; Czarnecki, J. *J. Colloid Interface Sci.* **1999**, 210 (1), 222-224.

48. Angle, C. W.; Dabros, T.; Hamza, H. A. *Energy & Fuels* **2007**, 21 (2), 912-919.

49. Kiran, S. K.; Acosta, E. J.; Moran, K. *Energy & Fuels* **2009**, 23 (6), 3139-3149.

50. Xu, Y.; Dabros, T.; Hamza, H.; Shefantook, W. *Petrol. Sci. Technol.* **1999**, 17 (9), 1051-1070.

51. Gafonova, O. V.; Yarranton, H. W. *J. Colloid Interface Sci.* **2001**, 241 (2), 469-478.

52. Long, J.; Xu, Z.; Masliyah, J. H. *Energy & Fuels* **2005**, 19 (4), 1440-1446.

53. Yan, Z.; Elliott, J. A. W.; Masliyah, J. H. *J. Colloid Interface Sci.* **1999**, 220 (2), 329-337.

54. Gao, S.; Moran, K.; Xu, Z.; Masliyah, J. *J. Phys. Chem. B* **2010**, 114 (23), 7710-7718.

55. Kiran, S. K.; Acosta, E. J.; Moran, K. *J. Colloid Interface Sci.* **2009**, 336 (1), 304-313.

56. Wang, S.; Liu, J.; Zhang, L.; Masliyah, J.; Xu, Z. *Langmuir* **2010**, 26 (1), 183-190.

57. Andersen, S. I.; Del Rio, J. M.; Khvostitchenko, D.; Shakir, S.; Lira-Galeana, C. *Langmuir* **2001**, 17 (2), 307-313.

58. McLean, J. D.; Kilpatrick, P. K. *J. Colloid Interface Sci.* **1997**, 196 (1), 23-34.

59. Yarranton, H. W.; Sztukowski, D. M.; Urrutia, P. *J. Colloid Interface Sci.* **2007**, 310 (1), 246-252.

60. Yarranton, H. W.; Urrutia, P.; Sztukowski, D. M. *J. Colloid Interface Sci.* **2007**, 310 (1), 253-259.

61. Verruto, V. J.; Le, R. K.; Kilpatrick, P. K. *J. Phys. Chem. B* **2009**, 113 (42), 13788-13799.

62. Yeung, A.; Dabros, T.; Masliyah, J.; Czarnecki, J. *Colloids Surf. Physicochem. Eng. Aspects* **2000**, 174 (1-2), 169-181.

63. Zhang, L. Y.; Lawrence, S.; Xu, Z.; Masliyah, J. H. *J. Colloid Interface Sci.* **2003**, 264 (1), 128-140.

64. Feng, X.; Xu, Z.; Masliyah, J. *Energy & Fuels* **2009**, 23 (1), 451-456.

65. Czarnecki, J.; Tchoukov, P.; Dabros, T. *Energy & Fuels* **2012**, 26 (9), 5782-5786.

66. Kilpatrick, P. K. *J. Am. Chem. Soc.* **2012**, 4017-4026.

67. Yang, F.; Tchoukov, P.; Pensini, E.; Dabros, T.; Czarnecki, J.; Masliyah, J.; Xu, Z. *Energy & Fuels* **2014**, 28 (11), 6897-6904.

68. Yang, F.; Tchoukov, P.; Dettman, H.; Teklebrhan, R. B.; Liu, L.; Dabros, T.; Czarnecki, J.; Masliyah, J.; Xu, Z. *Energy & Fuels* **2015**, 29 (8), 4783-4794.

69. Tchoukov, P.; Yang, F.; Xu, Z.; Dabros, T.; Czarnecki, J.; Sjoblom, J. *Langmuir* **2014**, 30 (11), 3024-3033.

70. Feng, X.; Mussone, P.; Gao, S.; Wang, S.; Wu, S.; Masliyah, J. H.; Xu, Z. *Langmuir* **2010**, 26 (5), 3050-3057.

71. Saadatmand, M.; Yarranton, H. W.; Moran, K. *Ind. Eng. Chem. Res.* **2008**, 47 (22), 8828-8839.

72. Gu, G.; Zhang, L.; Xu, Z.; Masliyah, J. *Energy & Fuels* **2007**, 21 (6), 3462-3468.

73. Wang, S.; Segin, N.; Wang, K.; Masliyah, J. H.; Xu, Z. *J. Phys. Chem. C* **2011**, 115 (21), 10576-10587.

74. Hannisdal, A.; Ese, M.; Hemmingsen, P. V.; Sjoblom, J. *Colloids Surf. Physicochem. Eng. Aspects* **2006**, 276 (1-3), 45-58.

75. Yan, Y.; Masliyah, J. H. *Colloids Surf. A Physicochem. Eng. Aspects* **1993**, 75 (C), 123-132.

76. Mohammed, R. A.; Bailey, A. I.; Luckham, P. F.; Taylor, S. E. *Colloids Surf. Physicochem. Eng. Aspects* **1993**, 80 (2-3), 223-235.

77. Varadaraj, R.; Brons, C. *Energy & Fuels* **2007**, 21 (1), 195-198.

78. Varadaraj, R.; Brons, C. *Energy & Fuels* **2007**, 21 (1), 199-204.

79. Varadaraj, R.; Brons, C. *Energy & Fuels* **2007**, 21 (3), 1617-1621.

80. Mohammed, R. A.; Bailey, A. I.; Luckham, P. F.; Taylor, S. E. *Colloids Surf. Physicochem. Eng. Aspects* **1993**, 80 (2-3), 237-242.

81.Zhang, L. Y.; Xu, Z.; Masliyah, J. H. *Langmuir* **2003**, 19 (23), 9730-9741.

82. Pensini, E.; Harbottle, D.; Yang, F.; Tchoukov, P.; Li, Z.; Kailey, I.; Behles, J.; Masliyah, J.; Xu, Z. *Energy & Fuels* **2014**, 28 (11), 6760-6771.

83. Hou, J.; Feng, X.; Masliyah, J.; Xu, Z. *Energy & Fuels* **2012**, 26 (3), 1740-1745.

84. Rane, J.P.; Pauchard, V.; Couzis, A.; Banerjee, S. *Langmuir* **2013**, 29 (15), 4750-4759.

85. Harbottle, D.; Chen, Q.; Moorthy, K.; Wang, L.; Xu, S.; Liu, Q.; Sjoblom, J.; Xu, Z. *Langm*uir **2014**, 30 (23), 6730-6738.

86. Krasowska, M.; Prestidge, C. A.; Beattie, D. A. Atomic force microscopy for determining surface interactions of relevance for food foams and emulsions. In: Dar, Y. L.; Light, J. M. (Eds.). *Food Texture Design and Optimization* **2014**, 402-422, doi: 10.1002/9781118765616.ch16.

87. Filip, D.; Uricanu, V. I.; Duits, M. H. G.; Agterof, W. G. M., Mellema, J. *Langmuir* **2005**, 21 (1), 115-126.

88.Chan, D. Y. C.; Klaseboer, E.; Manica, R. *Soft Matter* **2011**, 7, 2235-2264.

89. Manor, O.; Chau, T. T.; Stevens, G. W.; Chan, D. Y. C.; Grieser, F.; Dagastine, R. R. *Langmuir* **2012**, 28 (10), 4599-4604.

90.Shi, C.; Zhang, L.; Xie, L.; Lu, X.; Liu, Q.; Mantilla, C. A.; van den Berg, F. G. A.; Zeng, H. *Langmuir* **2016**, 32 (10), 2302-2310.

91. Tabor, R. F.; Grieser, F.; Dagastine, R. R.; Chan, D. Y. C. *J. Colloid Interface Sci.* **2012**, 371 (1), 1-14.

92. Langevin, D.; Argillier, J-F. *Adv Colloid Interface Sci* **2015**, http://dx.doi.org/10.1016/j.cis.2015.10.005.

93. Yeung, A.; Dabros, T.; Masliyah, J. *Langmuir* **1997**, 13 (24), 6597-6606.

94. Erni, P. *Soft Matter* **2011**, 7 (17), 7586-7600.

CHAPTER 3 CASCADE PARTIAL COALESCENCE PHENOMENA AT ELECTROLYTE–OIL INTERFACES AND DETERMINATION OF BOUNDS FOR THE SURFACE POTENTIAL*

3.1 INTRODUCTION

The value of the surface electric potential (or that of the closely related ζ potential[1]) of fluid–fluid interfaces is a crucial parameter for, *e.g.*, the stability of oil in water emulsions, which are extensively used in the food, cosmetics, pharmaceutical, and oil industries. For example, in the oil sands industry the value of ζ potential is used to characterize and quantify interactions between various bitumen components.[2] Determining ζ potential of liquid–liquid interfaces using classic colloid methods initially designed for solid particles, such as measuring the electrophoretic mobility of drops/bubbles, remains a very challenging task since these interfaces are deformable (see, *e.g.*, refs. 3 and 4). In many cases, the results are prone to controversy; for example, there is an on-going debate on whether an air-pure, neutral pH water interface is negatively[3,5–9] or positively[10–14] charged. This has stimulated extensive discussion in the literature (see the concise summary in ref. 14) on the value of the electric potential difference across such interfaces. An intrinsic surface potential of a water–air (or oil) interface is

* A version of this chapter has been published in: Kuznicki, N.; Krasowska, M.; Sellaperumage, P. M. F.; Xu, Z.; Masliyah, J.; Ralston, J.; Popescu, M. N. *Soft Matter* **2013**, 9, 4516-4523.

expected due to the dipolar nature of the water molecules; however, the recent analysis in refs. 13 and 14 indicates that this intrinsic surface potential is negligibly small. For electrolytes, the presence of the interface disturbs the distribution of ions from their uniform state in the bulk and gives rise to an electric potential difference across the interface (the Gibbs dividing surface for the solvent, water). Accounting for the size and polarizability of the ions, and their hydration and cavitation energies, this surface electrostatic potential has been calculated theoretically in refs. 13 and 14. The theory provides reasonable estimates for the experimentally measured electric potential difference across the interface *once* an ordered dipolar structure (which cannot be directly accounted for within the continuum dielectric assumptions of the theory, see ref. 13) of the adsorbed layer of ions is assumed.

For a variety of fluids it has been observed that a small drop of liquid 1 slowly approaching through an immiscible liquid 2 a quasi-planar liquid 2- liquid 1 interface may experience a phenomenon of partial coalescence upon colliding with the interface.[15–19] During this process, only part of the "mother" drop passes through the interface and a smaller "daughter" drop is left behind.[1] This process may continue in a "cascade", finishing either with complete coalescence of the mother drop or when a threshold size for the daughter drop, below which the drop stays adjacent to the interface but remains stable, is reached.[15–19,25]

[1] Partial coalescence was also observed in more complicated systems, such as electrically driven collisions between drops or drops and fluid–fluid interfaces (see, *e.g.*, the studies in refs. 20–23) or particle-laden drops colliding with planar fluid–fluid interfaces.[24]

The occurrence (upon a drop touching the interface) and dynamics of partial coalescence are governed by the viscosities and densities of the two liquids as well as their interfacial tension.[15–19,25,26] On the other hand, the final state in the cascade: complete coalescence or stable drop near the interface (as well as the time between successive partial coalescence events) is expected to depend on the interactions between the two interfaces in close proximity.

In this paper we present results for cascade partial coalescence of oil (toluene, *n*-heptane, and various toluene–*n*-heptane mixtures) drops at a water or salt solution–oil interface. For neutral pH water and for salt solutions of concentrations up to 10^{-2} M, a stable drop near the interface emerges as the final state of the cascade. (In our study, a drop near the interface was considered to be stable if no coalescence occurred during observation times of 45 to 75 min. This is much longer than the few seconds required for the whole cascade coalescence process; see the movies provided in the ESI (available online with the article)[2] and, *cf.*, Fig. 3.1. Therefore, a delayed coalescence due solely to hydrodynamic slowing down of film drainage as droplet size decreases[16,17] can be ruled out. In contrast, for solutions of high salt concentrations (1 M), the cascade sequence

[2] Electronic supplementary information (ESI) available online: (1) Movies of the cascade partial coalescence for toluene and *n*-heptane droplets in water (toluene_in_water.mp4 and heptane_in_water.mp4) and in 1 M salt solutions (toluene_in_1MKCl.mp4 and heptane_in_1MKCl.mp4). See DOI: 10.1039/c3sm27772k. (2) The sequence of drops undergoing partial-coalescence, up to the final stable drop, at the heptane-, toluene- and various heptol-water (Appendix A, Figure A-1), toluene–salt solutions (Appendix A, Figure A-2), and heptane–salt solution (Appendix A, Figure A-3) interfaces, respectively.

ends with complete coalescence within a few seconds. We therefore attribute the occurrence of stable-drop states to an electrically charged oil-water (salt solution) interface.[3,4,9] We then show that within the framework of the Derjaguin-Landau-Verwey-Overbeek (DLVO) theory, the spontaneously-occurring cascade partial coalescence can be exploited to estimate, from the last partial coalescence event in the sequence, the lower- and upper- bounds for the absolute value of the surface potential of oil-water (or salt solution) interfaces. (In the context of our system, "surface potential" refers to the value of the electrostatic potential of mean-force, *i.e.*, the solution of the Poisson-Boltzmann equation of the electrical double layers, at the Stern layer- the oil drop plus adsorbed ions of the interface.) The approach presented here can be developed into a simple method to determine the absolute value of the surface potential for a variety of liquid-liquid interfaces.

---

[3] The charging mechanism of oil–water, as well as that of air-water, interfaces is a subject of ongoing debate (see refs. 3–14). Computer simulations, theoretical models, and measurements of surface tension of air–electrolyte and oil-electrolyte interfaces[10–14] suggest that hydronium ion would strongly adsorb at the air-water interface and thus the interface would be positively charged. (However, as noticed in refs. 13 and 14, yet the electrostatic potential difference across the air–water or oil–water interface may turn out to be negative if the dipolar structure of the adsorbed hydronium ion is accounted for.) On the other hand, electrophoretic, streaming potential, and thin-film stability measurements[3–9] show behavior compatible with a negatively charged interface, which is interpreted to indicate preferential adsorption of OH^- ions. Moreover, the pH-dependence of the ζ potential obtained in these experiments seems to be consistent with charging due to adsorption of OH^- ions.[3,4,8]

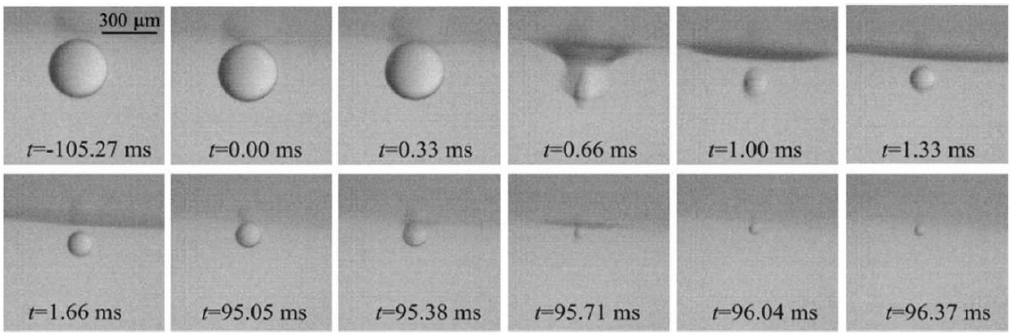

Figure 3.1 A typical cascade partial coalescence of an *n*-heptane droplet at a water- *n*-heptane interface. Two such partial coalescence events are captured in the frames at t = 0.66 ms and t = 95.38 ms. The origin of time is set arbitrarily, t = 0 being close to the occurrence of the first partial coalescence event.

3.2 MATERIALS AND METHODS

3.2.1 Materials

Commercially available toluene (AR, Chem-Supply) and *n*-heptane (99%, spectrophotometric grade, Sigma-Aldrich) were thoroughly purified through a combination of chemical treatments and fractional distillation. For both toluene and *n*-heptane, 200 ml of oil was stirred with 50 ml of concentrated H_2SO_4 for 1 hr. In order to avoid sulphonation, the temperature of the acid-oil (here oil refers to either *n*-heptane or toluene) mixture was maintained below 30 ^oC. In each case, the oil was then carefully separated from the acid-oil mixture and rinsed successively with Milli-Q water, 0.1 M NaOH aqueous solution, and Milli-Q water until neutral pH of the water running through the aqueous phase was reached. The oils were separated from the water phase and dried over anhydrous

$MgSO_4$. The last purification step was fractional distillation, where the first 10 % and last 20 % of distilled oils were discarded.

Toluene, *n*-heptane and their mixtures (heptol) were used for all of the experiments. Heptol solutions were prepared by either mixing 80 mL of *n*-heptane with 20 mL of toluene (heptol 80:20, "H_{80}") or 50 ml of *n*-heptane with 50 ml of toluene (heptol 50:50, "H_{50}").

KOH (AR) and KCl (99.9 %) were obtained from Merck. KCl was further purified via recrystallization and calcination for 8 hrs at 550 ^{o}C in order to remove organic impurities. Ethanol (AR, 99.5 %), purchased from Chem-Supply, was used for surface cleaning.

High purity Milli-Q water with a resistivity of 18.2 Ω·cm, surface tension of 72.4 $mN \cdot m^{-1}$ at 22 ^{o}C, and a total organic carbon component of less than 5 ppm was supplied by an Advantage A10 system (Millipore, USA) and used in all of the experiments.

3.2.2 Cleaning

A microfluidic chip with two channels in a T-geometry was used to generate oil droplets of well-defined sizes. Prior to experiments, the channels were flushed with ethanol and 1 M KOH for 30 min each. Milli-Q water was then pumped until neutral pH was reached. For all of the above steps the flow rate was kept constant and equal to 1 $mL \cdot hr^{-1}$. The channels were then dried by pumping air through the system.

All glassware was soaked in 1 M KOH solution for 2 hrs and subsequently rinsed with Milli-Q water until neutral pH was reached. Prior to each experiment, the borosilicate glass column and the Pyrex glass microfluidic chips were cleaned in a plasma cleaner (Harrick, PDC-OD2) for 60-90 s.

3.2.3 Droplet Collision Experiments

Oil droplet collisions with the water (or KCl aqueous solution)-oil interface were recorded using high-speed video photography. The time required for (partial) droplet coalescence with the water-oil interface, the number of such events (cascade), and the sizes of droplets prone to, or resisting, coalescence were then determined.

The experimental set-up consisted of a square (30 *x* 30 mm) borosilicate glass column mounted on a Teflon microfluidic chip holder. The column was filled with either Milli-Q water or KCl solutions of various concentrations. Single (more precisely, widely spaced) oil droplets were generated at the T-junction of a Pyrex glass microfluidic chip following well-established protocols (see, *e.g.*, ref. 27) and allowed to rise freely. The column is sufficiently tall so that terminal velocity of the rising droplet is reached well before approaching the liquid-liquid interface, located at 80 mm above the point of droplet release. This interface is formed by topping the water column with a thick (~3 mm) layer of oil, and its shape is quasi-planar due to the significant width of the column. Oil evaporation during experiments was prevented by sealing the column. During droplet collision with the water (or KCl solution)-oil interface, the thin liquid film

between the two surfaces slowly drained. Partial coalescence occurred upon droplet contact with the interface and a smaller "daughter" droplet pinched-off in a rapid fashion (shown in Figure A-1 in Appendix A and in videos available in the ESI online).

These phenomena were observed with a stereo-microscope (Olympus SZ4511TR) and recorded with a high speed camera (Photron 1024 PCI) at a frame rate of 10^3 to 10^4 Hz (on a case by case basis, as imposed by the characteristic time scales of the partial coalescence events). The recorded images were later analyzed using the image analysis software Image Pro Plus (v. 4.5.0.29).

3.2.4 Model and Theoretical Analysis

The net force F acting on a drop of liquid 1 (oil) rising through a liquid 2 (water or KCl solution) towards a liquid 2- liquid 1 interface is given by (as shown in Figure 3.2):

$$F = -(F_b + F_{vW} - F_{el} - F_v)\hat{e}_x := (\tilde{F} + F_v)\,\hat{e}_x \qquad (1)$$

Here F_b, F_{vW}, F_{el}, and F_v denote the magnitudes of the apparent weight of the drop, van der Waals force, electrostatic double layer force, and viscous resistance, respectively, and $\hat{e}_x$ is the unit vector corresponding to the x-direction. $\tilde{F}$ denotes the combination of the first three terms in the RHS of eqn (1) and is independent of the velocity of the rising drop. Note that the orientation of the various forces is accounted for by the corresponding signs in Eqn. (1). Since the interacting interfaces are identical (symmetric

case), the van der Waals contribution is attractive (along the $-\hat{e}_x$ direction) while the electrostatic contribution is repulsive (along the $+\hat{e}_x$ direction).[1,28] Before proceeding, we note that the similar approach of mapping onto the colloid framework and applying DLVO theory,[1] *i.e.*, using an analogy between the drop plus the adsorbed ions layer and a charged colloid, has been successfully employed to quantitatively model atomic force microscopy and surface force apparatus measurements of interactions through liquids between drops or bubbles and surfaces or other drops/bubbles (see, *e.g.*, refs. 29–31).

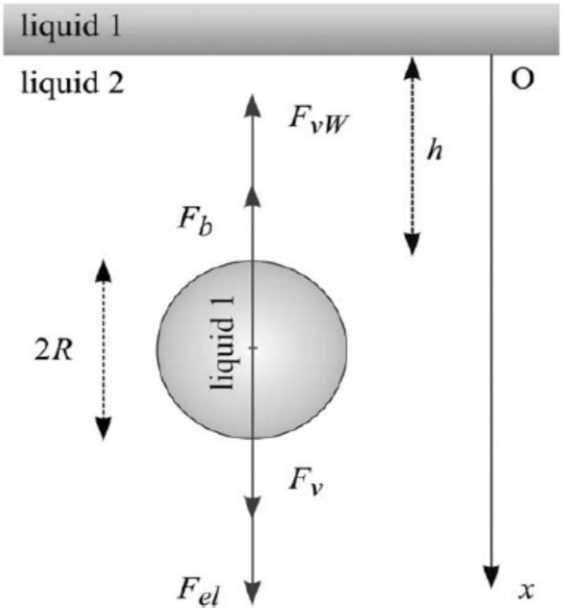

Figure 3.2 Forces acting on a buoyancy-driven droplet of radius R slowly rising through an immiscible liquid towards a quasi-planar liquid-liquid interface.

In the regime of very small Reynolds numbers, which in our experiments is the case for small drops near the interface, the net force on a drop is vanishingly small, *i.e.*,

$$\tilde{F} \approx -F_v. \tag{2}$$

In order for a slowly rising drop to collide with (touch) the interface, its velocity should be non-zero and pointing towards the interface at all distances $h > 0$, *i.e.*, the viscous resistance F_v must be positive at all distances h. Combined with Eqn. (2), this implies

$$\tilde{F}(h) < 0, \text{ for any } h > 0 \leftrightarrow \max_{h>0}\tilde{F}(h) < 0, \tag{3}$$

On the other hand, if the drop reaches a state of stable rest near the interface, its velocity must become zero at some distance h_{eq} from the interface and thus the viscous resistance will vanish there, *i.e.*,

$$\tilde{F}(h_{eq}) = 0, \text{ for some } h_{eq} > 0 \rightarrow \max_{h>0}\tilde{F}(h) \geq 0. \tag{4}$$

For given liquids and known van der Waals forces, the inequalities in (3) and (4), applied to the last pair of coalescing "mother" (of radius R_1)-stable "daughter" (of radius R_2) drops, depend only on the absolute value of the surface potential ψ of the electrolyte-oil interface. Therefore, bounds on $|\psi|$ can be obtained once the explicit dependence of $\tilde{F}$ on ψ is known. (Note that only the magnitude of the potential enters in the description because the system is symmetric, *i.e.*, the two interacting interfaces are identical.)

In order to connect the general conclusions above with the observables of interest, *i.e.* the surface electric potential, an expression of the electrostatic interaction must be provided. In the following we carry out such an example calculation with a number of simplifying assumptions: (i) the drop shape remains quasi-spherical and the top liquid-liquid interface

remains quasi-planar (except during the coalescence event), at all times and down to very small separations h.[4] This assumption is well supported by the experimental findings (see Fig. 3.2 and the videos in the ESI); (ii) the van der Waals and electrostatic interactions between the drop and the liquid–liquid planar interface are well described by the Derjaguin approximation;[1] (iii) the electrostatic double-layer interaction can be described by the Debye-Hückel theory (*i.e.* linearized Poisson-Boltzmann equation) for a symmetric 1:1 electrolyte.[51] While there is no conceptual problem in using the non-linear Poisson-Boltzmann description, it would restrict the study to numerical analysis only. We therefore prefer to work within the assumptions of the linearized equation, which provides analytical results and physical insight. For the state of the interface we

[4] It is reasonable to expect that the bending elasticity and the surface tension of the interface will play a role whenever significant deformations, like formation of "dimples", [29] are to be expected. This is likely the case of drops hitting, and bouncing from the liquid–air interface, as, e.g., in the experiments of Zou *et al.*[32] In contrast, in the case of our experiments, where the density difference between the drop and the surrounding electrolyte is relatively small, the drops (and in particular the smaller "daughter" ones) do approach the interface very slowly. This leads to small hydrodynamic pressure in the draining film, thus small deformations of the interfaces (see also ref. 29) and reduced influence of the bending elasticity (except if it happens that the interface is extremely soft, which does not seem to be the case of our oil–electrolyte interfaces).

[5] In the following we treat water as a weak electrolyte of $5 \cdot 10^{-6}$ M concentration.

assume either "constant potential" or "constant charge" conditions,[6] which are typically viewed as providing limiting cases for the magnitude of the electrostatic interactions;[33,34] (iv) the van der Waals interaction is approximated by the non-retarded form at all separations h, with a Hamaker constant A determined by the "static" dielectric constants of water and the corresponding oil;[28] (v) all of the coalescence events observed experimentally occur as a result of a drop moving towards and coming into direct contact with the interface, *i.e.*, collisions induced by thermal fluctuations of otherwise mechanically stable configurations are disregarded. This is a reasonable assumption as long as the drop diameter is larger than approximately 10 μm (such that its Brownian motion does not play a significant role) and the equilibrium separation distance between a stable drop and the interface is larger than few nm (such that the sharp-interface approximation is justified, the amplitude of the thermal fluctuations in the outline of the interfaces is negligible, and the continuum media approximation required by the DLVO theory holds).

We will focus below on the case of constant potential conditions. The case of constant charge conditions is treated in a similar manner, with the only change being that in the second of Eqns. (5) the term $\cosh(\kappa h/2)$ is

[6] This assumption can be replaced by any other physically meaningful boundary conditions, such as the one of "charge regulation".[33,34] The argument is essentially unchanged, but the calculations are more involved; moreover, in this case bounds would be derived either for the corresponding surface potential or for the regulation parameter, respectively.

replaced by sinh(κ*h*/2).[33] Therefore, for the latter case, present only the final results.

Following the assumptions (i)-(v) above and for constant electric potential conditions the components of $\tilde{F}$ are written as:[7]

$$F_{vW} = 2\pi R\left(\frac{A}{12\pi h^2}\right),$$

$$F_{el} = 2\pi R\left(\frac{2n_0}{\beta\kappa}\phi^2\frac{exp(-\frac{\kappa h}{2})}{cosh(\frac{\kappa h}{2})}\right),$$

$$F_b = \frac{4}{3}\pi R^3(\rho_W - \rho_H)g. \qquad (5)$$

Here n_0 denotes the number density of the electrolyte, $\boldsymbol{\beta} = 1/(k_B T)$, where k_B is the Boltzmann constant and T- absolute temperature, $\kappa = 1/\lambda_D$, where λ_D is the Debye length at the corresponding electrolyte concentration, $\phi = \boldsymbol{\beta} e\psi$, where e is the electron charge and ψ is the electric potential of the (isolated) interface, $\rho_{W,H}$ are the densities of water and corresponding oil, respectively, and g is the gravitational acceleration. Since dielectric constants of toluene (refractive index $n \sim 1.499$) and *n*-heptane (refractive index $n \sim 1.388$) are much smaller than that of water, for all of the oils employed, the Hamaker constant is approximated by $A \sim 3/4\boldsymbol{\beta}$, which corresponds to $A \sim 3\cdot10^{-21}$ J at room temperature.

---

[7] We note that this relies on the assumption of a homogeneous charge density. For the oil-electrolyte interface, for which the charging is presumed to occur *via* adsorption of ions (note, again, the on-going debate on whether OH^- (refs. 3–9) or H^+ (refs. 10–14) ions adsorb preferentially at the interface), charge fluctuations, and even charge polarisation, in the electrolyte layer adjacent to the oil-electrolyte interface may play a role at very small separations.[35]

Introducing the force scale $F_0 = R\kappa^2/(8\boldsymbol{\beta})$, defining the dimensionless separation and force by $u = \kappa h$ and $\tilde{f} = \tilde{F}/F_0$, respectively, and introducing the parameters:

$$p := \frac{32\pi n_0}{\kappa^3}\boldsymbol{\phi}^2 > 0 \tag{6}$$

$$q := \frac{32\pi}{3}\frac{\beta(\rho_W - \rho_H)g}{\kappa^2} > 0 \tag{7}$$

(p is dimensionless, q has units of m^{-2}), one obtains:

$$\tilde{f} = -\frac{1}{u^2} + p\frac{exp(-\frac{u}{2})}{cosh(\frac{u}{2})} - qR^2 := g(u) - qR^2 \,. \tag{8}$$

The effect of the apparent-weight (*i.e.*, of the term $-qR^2$) on $\tilde{f}$ is simply a vertical down-shift of $g(u)$, as shown in Fig. 3.3. In order for a stable drop to exist, as observed in the experiments, the condition (4) requires $\tilde{f}$ to be positive in a range of separation values u. In conjunction with the asymptotic behavior $g(u \to 0_+) \to -\infty$, $g(u \to \infty) \to 0_-$, this means that $g(u)$ must have a positive maximum: $g_M(p) > 0$. This constraint establishes a lower bound (although a very weak one) for the surface potential. For example, in the case of drops in neutral pH water the requirement $g_M(p) > 0$ leads to $p \geq 1.04$, *i.e.*, the surface potential $|\psi| \geq 0.95$ mV. (For the case of constant charge conditions, the corresponding result is $p \geq 0.77$ and $|\psi| \geq 0.82$ mV.)

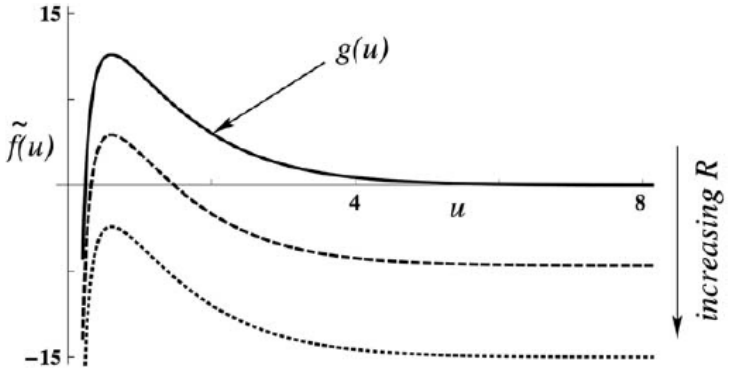

Figure 3.3 The effect of droplet radius R (equivalently, of buoyancy) on the scaled force $\tilde{f}$. The lines correspond to $p = 20$ and $qR^2 = 0$ (solid), 7 (dashed), and 15 (dotted).

The conditions (3) and (4) applied for R_1 (last "mother" drop) and R_2 (stable "daughter" drop), respectively, together with the observations described above, allow us to establish an upper bound on the magnitude of the surface potential and to tighten the lower bound. The inequality in (3) requires the shift qR_1^2 to be larger than, or at least equal to, the value $g_M(p)$ (see Fig. 3.3). Since the value $g_M(p)$ is an increasing function of p and $p:=p(\psi)$ increases with ψ, the magnitude of the surface potential is bounded from above by ψ_M, which is the positive solution of the equation:

$$g_M\big(p(\psi_M)\big) = qR_1^2. \tag{9}$$

Similarly, the inequality in (4) requires that $\tilde{f} \geq 0$ for some values of u; therefore the shift qR_2^2 must be smaller than the maximum $g_M(p)$ (see Fig. 3.3). The magnitude of the surface potential is thus bounded from below by ψ_m, which is again the positive solution of the equation:

$$g_M\big(p(\psi_m)\big) = qR_2^2. \tag{10}$$

3.3 RESULTS AND DISCUSSION

We have carried out experiments with drops of various oils: toluene, *n*-heptane, and heptol of various compositions approaching neutral pH water-oil planar interfaces. Toluene and *n*-heptane drops approaching salt solution–oil interfaces were also investigated. In all cases studied, cascade partial coalescence occurred (see Figure 3.1 and Figures A-1 to A-3 in Appendix A). For each pair of liquids, the reproducibility of cascade partial coalescence process is very good, *i.e.*, the number of steps in the cascade is identical and the radii of each "daughter" drop do not vary by more than 5 %; small variations in the radius of the drop starting the cascade led solely to similarly small variations in the radii of the "daughter" drops. These observations agree with the behavior reported in previous studies of this phenomenon.[15-19,25,26] When liquid 2 was chosen to be neutral pH water or KCl solution of concentration up to 10^{-2} M, a stable drop near the interface emerged as the final state of the cascade (see Fig. 3.1 and Figures A-1 to A-3 in Appendix A). In contrast, when liquid 2 was chosen to be a higher concentration (1 M) KCl solution, experiments with either toluene or *n*-heptane employed as liquid 1 showed (within the resolution of our microscope) complete coalescence at the end of the cascade (see the videos provided in the ESI online).[8] This strongly

[8] We note here that oil and salt purity is crucial in obtaining reliable and reproducible results at large salt concentrations. If these are used as purchased and the rest of the cleaning and preparation steps are left unchanged, the experiments at 1 M KCl concentration would have poor reproducibility and

supports our argument that electrostatic interactions, and thus a charged oil-electrolyte interface, are determinant in the emergence of a stable drop as the final state of the cascade partial coalescence process. While for salt concentrations below 10^{-2} M the electrostatic interactions are relevant (Debye lengths of a few to hundreds of nm), for 1 M concentration their range is decreased to atomic distances. Therefore, in the latter case, they cannot prevent even very small drops (very small apparent weight) from touching the interface.

Our results show that high salt concentrations promote coalescence of the oil drops with the bulk oil phase, in contrast to earlier studies (see the discussion and references in ref. 36) on coalescence of gas bubbles in electrolytes where high electrolyte concentration was reported to prevent bubble coalescence. This conclusion was reexamined and challenged in a number of recent studies. Browne *et al.*[36] noted that whether or not a stabilizing effect with increasing salt-concentration is observed, it is seemingly dependent on the exact type of the experimental setup. While

---

often would show the cascade partial coalescence ending with a stable drop. On the other hand, for all other experiments no significant differences were observed between outcomes when using either purified or as purchased oils and salt. This can be rationalized by the fact that organic impurities in the "as purchased" oils and salt can act as surfactants. Even in minute amounts, they can provide an additional stabilizing short-ranged steric repulsion by adsorbing at the oil-salt solution interface. This becomes effective if the range of the electrostatic repulsion is drastically reduced, as in the case for large salt concentrations (Debye length < 1 nm for a salt concentration of 1 M).

swarms of bubbles in the bulk electrolyte indeed seem to behave in that manner, AFM measurements of driven collisions between isolated pairs of argon bubbles in pure water show the contrary: the argon bubbles are stable against coalescence. But coalescence of those argon bubbles is promoted by the addition of even small amounts of salt (see Fig. 6 in ref. 36). The same conclusion, that bubbles in pure water do not coalesce, was drawn by Tabor *et al.*[30] from similar AFM studies; this study concludes with a "stability map", *i.e.*, a minimum "push to approach" force is needed to induce coalescence between two identical bubbles in water as a function of the bubbles radii and the pH of water (Fig. 5 in ref. 30). Based on dynamic AFM measurements of driven collision between isolated bubble pairs in high concentration salt solutions, Vakarelski *et al.*[29] observed excellent agreement between experimental results and theory predictions which invoke only van der Waals and hydrodynamic interactions, providing indirect support that a salt-stabilizing effect does not occur in their experiments. From the perspective of these recent experiments, there is no difference, in respect to the effect of added salt, between our observations on oil-electrolyte systems and the coalescence behavior of two bubbles in electrolyte solution, at least when studied as a collision process between an isolated pair (which is closer to our setup of a collision between a single oil drop and a planar electrolyte-oil interface).

By applying the method outlined in Section 3.2.4, we estimated bounds for the electric potential corresponding to the interfaces between various oils

and neutral pH water or KCl solutions of various (up to 10^{-2} M) salt concentrations. The values of temperature, T = 297 K, densities, ρ_T = 870 kg·m^{-3} (toluene), ρ_H = 680 kg·m^{-3} (*n*-heptane), ρ_{H50} = 775 kg·m^{-3} (heptol H_{50}), ρ_{H80}= 718 kg·m^{-3} (heptol H_{80}), and ρ_W = 997 kg·m^{-3} (water), and concentrations of salt solutions are known experimental parameters. The radii R_1 and R_2 in each experiment are determined by using image analysis of the corresponding video recordings. Eqns. (9) and (10) are then solved numerically for each pair R_1 and R_2 to extract the corresponding bounds ψ_m and ψ_M for the electric potential of the interface. The results of this analysis are summarized in Tables 3.1–3.3.

Table 3.1 Bounds on the electric potential of oil-neutral pH water interfaces for the constant potential (CP) and constant charge (CC) models, respectively. "T" denotes toluene and "H" *n*-heptane. The last column shows the ζ-potential measured using the Zetasizer ($\zeta < 0$ in all cases), representing the solution conditions of the cascade partial coalescence measurements, with ± 6.0 mV confidence interval for T, H_{50}, and H_{80}, and ± 3.0 mV for H, respectively.

			CP		CC		
Oil type	R_1 (μm)	R_2 (μm)	ψ_m (mV)	ψ_M (mV)	ψ_m (mV)	ψ_M (mV)	$\lvert\zeta\rvert$ (mV)
T	152.0	72.0	31	64	5.2	7.6	64
H_{50}	62.0	27.0	16	35	3.7	5.6	38
H_{80}	84.0	40.0	26	52	4.8	6.9	42
H	31.5	18.0	13	22	3.3	4.4	22

Table 3.2 Bounds on the electric potential of toluene-KCl solution interfaces at various KCl concentrations for the constant potential (CP) and constant charge (CC) models, respectively.

			CP		CC	
KCl (M)	R_1 (μm)	R_2 (μm)	ψ_m (mV)	ψ_M (mV)	ψ_m (mV)	ψ_M (mV)
10^{-4}	166.5	55.5	13	35	4.8	8.0
10^{-3}	205.0	77.0	12	26	5.9	9.1
10^{-2}	136.5	51.5	9	14	6.4	8.5

Table 3.3 Bounds on the electric potential of heptane-KCl solution interfaces at various KCl concentrations for the constant potential (CP) and constant charge (CC) models, respectively.

			CP		CC	
KCl (M)	R_1 (μm)	R_2 (μm)	ψ_m (mV)	ψ_M (mV)	ψ_m (mV)	ψ_M (mV)
10^{-4}	55.5	21.5	9	19	3.8	5.9
10^{-3}	64.0	25.5	8	15	4.6	6.6
10^{-2}	38.5	13.0	7	9	5.7	6.7

The first observation is that the range $\Delta\psi = \psi_M - \psi_m$ set by the bounds depends on the specific liquid-liquid interface as well as on the choice of charge model (constant potential or constant charge). For all cases studied the constant charge model predicts very low surface potential and tight bounds (basically determining the absolute value of the potential). These predictions are significantly different from those of the constant potential model. If the physical picture is not *a priori* clear but complementary information on the magnitude of the surface potential is available, these

results provide a means to discriminate between various models. For example, in our system, the results of independent ζ-potential measurements (when possible) seem to support the constant potential assumption. We thus focus the rest of the discussion on the results corresponding to this case.

In the case of heptol-water interfaces, the bounds for heptane in water are much tighter than those for toluene; however, no clear trend with increasing % of toluene in the heptol mixtures can be inferred. The range $\Delta\psi$ varies between approximately 33 mV for the toluene-water interface and approximately 9 mV for the heptane-water interface.

For the case of oil-salt solution interfaces, the bounds estimated are much tighter. If there was no specific adsorption of K^+ or Cl^-, the surface electric potential would be independent of the salt concentration. Therefore the bound estimates in Tables 3.2 and 3.3, respectively, would basically determine the toluene–water surface potential as 13 mV $\leq |\psi| \leq$ 14 mV and the heptane–water surface potential as $|\psi|$ = 9 mV. (The results at 10^{-2} M KCl concentration should be considered with caution: the Debye length is approximately 3 nm, and therefore this is a borderline case since, as noted in Section 3.2.4, thermal fluctuations of the interfaces may play a destabilizing role if the equilibrium separation for a drop near the interface is within this range.)

However, a comparison with the results in Table 3.1 shows that these bounds are outside the range allowed by the direct oil-neutral water

measurements. Therefore, we conclude that specific adsorption of K^+ or Cl^- at the oil-water interfaces occurs.

One of the causes of $\Delta\psi$ variability from system to system is that the constraints of our experimental setup allow basically a single size of the initial mother drop (in practice, a very narrow size distribution), for any given pair of liquids among the ones we investigated. It is known that for given surface tension and viscosities the cascade partial-coalescence leads to an almost deterministic ratio of sizes of daughter and mother drops.[17,19] Therefore, for any pair of liquids in our experiments, we explored only one such possible cascade sequence, and consequently only one (R_1, R_2) pair, among the many possible. While it can happen that the sequence explored is an optimal one (in the sense that the mother and stable daughter drop radii are sufficiently close to one another to allow tight bounds on the potential), this cannot be the generic situation. For any of the pairs of liquids we used, the range $\Delta\psi$ can be in principle improved (decreased) by being able to significantly vary the size of the drops released towards the interface, *i.e.*, by exploring a few sequences of cascade coalescence. Since these would provide various pairs (R_1, R_2), and since the bounds ψ_m and ψ_M depend on R_1 and R_2, not only on their ratio, overlapping the bounds from various sequences should lead to the mentioned decrease of $\Delta\psi$. Unfortunately, such modifications were not possible for our present experimental setup.

It remains unclear whether the lack of optimization discussed above could

fully explain the non-monotonic variation of the bounds in the case of heptols with increasing concentration of *n*-heptane. A systematic investigation of these aspects, the effects of salt type and pH of the water, as well as of the assumptions on which the model is based (in particular the effect of drop shape and of possible deformations of the top interface) will be conducted in the future.

3.4 CONCLUSIONS

We have presented proof-of-concept results that a spontaneously occurring cascade partial coalescence of an oil drop at water (electrolyte)-oil interface, where a stable drop emerges as the final state, allows one to set lower- and upper-bounds on the absolute value of the surface potential. In some cases, these are very close and the result is an accurate estimate of the surface potential. When combined with complementary studies, the analysis outlined can provide a means to discriminate between various physical models for the charging state of the interface. For a given pair of liquids, straightforward improvements of this approach are in principle possible by varying the size of the released droplets. In this case, various sequences of cascade partial coalescence events would be explored, providing tight bounds for the surface potential by overlapping the resulting ψ ranges. Finally, we note that the method discussed can be employed for a wide variety of interfaces, where a cascade partial coalescence occurs[15,17,19] and a stable drop near the interface emerges as the final state.

3.5 REFERENCES

1. Derjaguin, B. V.; Churaev N. V.; Muller, V. M. *Surface Forces,* Consultants Bureau, New York, **1987**.

2. Masliyah, J. H. J.; Czarnecki, J.; Xu, Z. *Handbook on Theory and Practice of Bitumen Recovery from Athabasca Oil Sands*, Theoretical aspects, Kingsley Publishing Services, Cochrane (Canada), **2011**, vol.1.

3. Takahashi, M. *J. Phys. Chem. B* **2005**, 109, 21858–21864.

4. Marinova, K. G.; Alargova, R. G.; Denkov, N. D.; Velev, O. D.; Petsev, D. N.; Ivanov, I. B.; Borwankar, R. P. *Langmuir* **1996**, 12, 2045–2051.

5. Ciunel, K.; Arm´elin, M.; Findenegg, G. H.; von Klitzing, R. *Langmuir* **2005**, 21, 4790–4793.

6. Hänni-Ciunel, K.; Schelero, N.; von Klitzing, R. *Faraday Discuss.* **2009**, 141, 41–53.

7. Creux, P.; Lachaise, J.; Graciaa A.; Beattie, J. K. *J. Phys. Chem. C* **2007**, 111, 3753–3755.

8. Beattie, J. K.; Djerdjev, A. M.; Warr, G. G. *Faraday Discuss.* **2009**, 141, 31–39.

9. Creux, P.; Lachaise, J.; Graciaa, A.; Beattie, J. K.; Djerdjev, A. M. *J. Phys. Chem. B* **2009**, 113, 14146–14150.

10. Petersen, P. B.; Saykally, R. J.; Mucha, M.; Jungwirth, P. *J. Phys. Chem. B* **2005**, 109, 10915–10921.

11. Jungwirth P.; Winter, B. *Annu. Rev. Phys. Chem.* **2008**, 59, 343–346.

12. Petersen, P. B.; Saykally, R. J. *Chem. Phys. Lett.* **2008**, 458, 255–261.

13. dos Santos, A. P.; Levin, Y. *J. Chem. Phys.* **2010**, 133, 154107.

14. dos Santos, A. P.; Levin, Y. *Faraday Discuss.* **2013**, 160, 75-87.

15. Charles, G. E.; Mason, S. G. *J. Colloid Sci.* **1960**, 15, 236– 267.

16. Thoroddsen, S. T.; Takehara, K. *Phys. Fluids* **2000**, 12, 1265-1267.

17. Blanchette, F.; Bigioni, T. P. *Nat. Phys.* **2006**, 2, 254–257.

18. Vandewalle, N.; Terwagne, D.; Mulleners, K.; Gilet, T.; Dorbolo, S. *Phys. Fluids* **2006**, 18, 091106.

19. Gilet, T.; Mulleners, K.; Lecomte, J. P.; Vandewalle. N.; Dorbolo, S. *Phys. Rev. E: Stat., Nonlinear, Soft Matter Phys.* **2007**, 75, 036303.

20. Ristenpart, W. D.; Bird, J. C.; Belmonte, A.; Dollar, F.; Stone, H. A. *Nature* **2009**, 461, 377–380.

21. Bird, J. C.; Ristenpart, W. D.; Belmonte, A.; Stone, H. A. *Phys. Rev. Lett.* **2009**, 103, 164502.

22. Mousavichouhbeh, M.; Ghadiri, M.; Shariaty-Niassar, M. *Chem. Eng. Process.* **2011**, 50, 338–344.

23. Hamlin, B. S.; Creasey, J. C.; Ristenpart, W. D. *Phys. Rev. Lett.* **2012**, 109, 094501.

24. Harbottle, D.; Bueno, P.; Isaksson, R.; Kretzschmar, I. *J. Colloid Interface Sci.* **2011**, 362, 235–241.

25. Charles, G. E.; Mason, S. G. *J. Colloid Sci.* **1960**, 15, 105–122.

26. Manga, M.; Stone, H. A. *J. Fluid Mech.* **1995**, 287, 279–298.

27. Xu, J. H.; Li, S. W.; Tan. J.; Luo, G. S. *Microfluid. Nanofluid.* **2008**, 5, 711–717.

28. Parsegian, V. A. *Van der Waals Forces: a Handbook for Biologists, Chemists, Engineers, and Physicists*, Cambridge University Press, New York, **2006**.

29. Vakarelski, I. U.; Manica, R.; Tang, X.; O'Shea, S. J.; Stevens, G. W.; Grieser, F.; Dagastine, R. R.; Chan, D. Y. C. *Proc. Natl. Acad. Sci. U. S. A.* **2010**, 107, 11177–11182.

30. Tabor, R. F.; Grieser, F.; Dagastine, R. R.; Chan, D. Y. C. *J. Colloid Interface Sci.* **2012**, 371, 1–14.

31. Manor, O.; Vakarelski, I. U.; Stevens, G. W.; Grieser, F.; Dagastine, R. R.; Chan, D. Y. C. *Langmuir* **2008**, 24, 11533–11543.

32. Zou, J.; Wang, P. F.; Zhang, T. R.; Ruan, X. *Phys. Fluids* **2011**, 23, 044101.

33. Carnie, S. L.; Chan, D. Y. C. *J. Colloid Interface Sci.* **1993**, 161, 260–264.

34. Borkovec, M.; Behrens, S. H. *J. Phys. Chem. B* **2008**, 112, 10795–10799.

35. Pincus. P. A.; Safran, S. A. *Europhys. Lett.* **1998**, 42, 103–108.

36. Browne, C.; Tabor, R. F.; Chan, D. Y. C.; Dagastine, R. R.; Ashokkumar, M.; Grieser, F. *Langmuir* **2011**, 27, 12025– 12032.

CHAPTER 4 DYNAMIC INTERACTIONS BETWEEN A SILICA SPHERE AND DEFORMABLE INTERFACES IN ORGANIC SOLVENTS STUDIED BY ATOMIC FORCE MICROSCOPY [*♦]

4.1 INTRODUCTION

Emulsions are widely encountered in a variety of industries, including food processing, formulation of cosmetics, manufacture of pharmaceuticals, materials processing and oil production. For some applications, stable emulsions are desirable. For instance, well-dispersed oil-in-water (milk) and water-in-oil (facial creams) emulsions are necessary to extend the shelf life of consumer products. However, emulsions encountered in the oil industry require rapid phase separation to remove water and associated ions from oil, thus improving product quality and minimizing the potential for equipment corrosion and fouling in downstream processing. Emulsion stability strongly depends on characteristics of the interface separating the dispersed and continuous phases. Partitioning of surface-active agents such as surfactants, polymers and nanoparticles can influence the interactions between two approaching droplets as well as droplet deformation.[1-3]

---

[*] A version of this chapter has been published in: Kuznicki, N. P.; Harbottle, D.; Masliyah, J. H.; Xu, Z *Langmuir* **2016**, DOI: 10.1021/acs.langmuir.6b02306.

♦This chapter uses the term "Natural Polyaromatic Molecules" (NPAMs) as a general description for asphaltenes. The findings from this study can be applied to other non-Laplacian systems of significant viscoelastic contributions, such as biological cell membranes or polymer blends.

In emulsion systems, hydrodynamic forces, corresponding to the momentum of two interacting droplets, contribute to the overall interaction force. In addition, as the distance between droplets decreases, surface forces including van der Waals and electrical double layer force become more significant and determine whether the droplets coalesce or remain dispersed. These forces contribute to the overall disjoining pressure of the intervening liquid film. Other surface forces such as hydration, hydrophobic, steric, depletion and/or bridging forces can be dominant in determining the stability of the intervening liquid film, depending on the nature of the system, which includes the presence of surface active species and/or polymers residing at or near the liquid-liquid interface.[2]

AFM has been extensively used to study nano-scale forces between rigid surfaces. Knowing the spring constant of the AFM cantilever, the magnitude of the force as a function of separation distance between rigid surfaces can be readily obtained. This measurement is achieved by calibrating the optical pass of laser detecting systems, using the slope of the constant compliance region where cantilever deflection has a linear dependency on piezo displacement.[4] Such an approach becomes invalid for determining interaction forces involving deformable surfaces. To understand interactions between two deformable interfaces in emulsion systems or between biological cells, researchers have previously measured interaction forces between two solid substrates coated (deposited or adsorbed) with surface-active species or biomolecules. Combined with theoretical modelling, these measurements have shed light on interactions between emulsion droplets stabilized by surface active species.[5] The scaling theory developed by de-

Gennes, for example, has been used to describe steric hindrance between polymer brushes responsible for steric stabilization.[6,7] However, establishing a direct link between the measured interaction forces using "model" emulsion surfaces and bulk emulsion stability is difficult, if not impossible, due to the deformable nature of the system. Deformable surfaces are also known to be more sensitive to interaction forces compared to rigid solid surfaces.[2]

To address this critical issue, pioneering AFM work by Butt[8] and Ducker[9] demonstrated the feasibility of direct force measurements for bubble-particle systems using scanning probe microscope. Since these influential studies, a variety of complex interfaces have been investigated. Force measurement for particle-bubble/droplet systems using AFM is nontrivial, since both the cantilever and bubble/droplet can deform under surface forces and/or compression by the AFM cantilever. In such systems, the contact area between the particle and bubble/droplet changes as the colloidal probe is pressed down on the interface.[10] Interpretation of the corresponding force curves is further complicated by the presence of surface active species, which add yet another deformable layer to the system.[7] Since interfacial deformation occurs prior to contact, due to an extended range of surface forces, there is no sharp transition between non-contact and contact regions. In such systems, zero separation between solid and droplet or bubble surfaces cannot be determined in the same way as for rigid bodies.[5,11] Other methods such as confocal microscopy or theoretical modeling are required to obtain "true" separation between the probe and droplet/bubble. When an AFM probe approaches a droplet, the droplet will deform when the disjoining pressure

exceeds the Laplace pressure. Therefore, instead of reducing the distance between the solid-fluid interface (as is the case for solid-solid interaction), the droplet will deform (flatten) while separation distance remains constant during further movement of the probe towards the droplet.[10]

In some cases of measuring interactions between solid probe and liquid droplets or bubbles, particle "snap-in" upon approach is observed, establishing a three-phase contact line where interactions are dominated by capillary forces.[11-13] However, when surfactants are present, fluid "wrapping" around the particle or dimple formation is more commonly observed, with a thin liquid film of the continuous phase remaining between the two surfaces without three phase contact.[14-16] Force measurements between titania particles and air bubbles in electrolyte solutions at different pHs highlighted the effect of surface charge in flotation.[17] A large adhesion force was observed for pHs between isoelectric points of titania and bubble, a system where an attractive electrostatic interaction exists due to opposite surface charges. In contrast, weak adhesion was measured at pHs above the isoelectric point of titania. Experiments between air bubbles and mica in aqueous solutions demonstrated no bubble attachment to hydrophilic mica, while jump-in was recorded for partially hydrophobized mica.[18]

Droplet deformation has been experimentally shown by a reduction in slope of the constant compliance region of the force curves, which provides a qualitative comparison between systems, where higher slopes indicate a more rigid or "solid-like" interface. In early studies, bubbles and deformable bodies were described as linear Hookean springs.[9] The complex spring constant of the system, which

correlates with interfacial tension, was calculated from the constant compliance region of force-displacement curve.[16,19] However, detailed theoretical investigation using the augmented Stokes-Reynolds-Young-Laplace (SRYL) equation• showed the nonlinear behavior of force (F) versus interfacial tension (γ), and accurate quantitative predictions were achieved by the Chan-Dagastine-White model.[20] The augmented SRYL equation is a type of equation of state (EOS) which relates droplet or bubble deformation to the applied force, analogous to Hooke's law for springs. The assumptions required for this model include Stokes flow of the liquid between interacting surfaces and a boundary condition for the interface, with the drop shape described by the Young-Laplace equation. Although tangentially immobile or mobile boundary conditions can be applied for the various interfaces, tangentially immobile condition produces a better fit in the majority of the studies due to the presence of impurities even in "clean" systems.

The SRYL model has been successfully applied to predict deformation for a number of systems with low Reynolds (*Re)* and Capillary (*Ca*) numbers, and to calculate the force exerted on the probe by the disjoining pressure from the interface as a function of separation distance.[18] In addition to film thickness, the augmented SRYL equations were used to predict the shape of droplets or bubbles, such as the formation of "pimple", "dimple" or "wimple" from the spatial variation of the hydrodynamic and disjoining pressures due to surface and capillary forces.[21] By including the electrical double layer and van der Waals interactions in the disjoining pressure term, good agreement between

• A description of the full SRYL model is included at the end of Appendix B.

experimental data and calculated forces has been shown for two decane droplets in aqueous systems of different electrolyte concentrations.[21] To predict interactions between two oil droplets with adsorbed polymer layers in electrolyte solutions, a steric term accounting for compression of the adsorbed polymer brushes was found essential to be incorporated into the disjoining pressure.[22] Interaction forces for two surfactant-free oil droplets (toluene) in electrolyte solutions could also be well fitted by the classical DLVO theory. However, additional steric interactions had to be included in the presence of natural polyaromatic molecules (NPAMs) of surface active nature, such as asphaltenes, present in petroleum oil.[23] In addition to the type and concentration of NPAMs in crude oil, stability of oil droplets in aqueous solution is also significantly influenced by the pH, as well as the type and concentration of ions in the aqueous phase. Good agreement between the calculated and measured drop deformations and magnitude of measured forces has been demonstrated for a variety of clean interfaces and polymer-covered droplets.[10,20-25] Ultimately, one can successfully predict droplet deformation based on the force applied, provided that the size and boundary conditions of the particle and droplet are known. It should be noted that most oil-water deformable interface studies consider oil droplets in water, with few studies investigating interactions between water droplets in oil, an important system for many industrial applications.[26]

The augmented SRYL model assumes that the mechanical response of the bubble or droplet is dominated by interfacial tension and Laplace pressure.[20] However, Laplacian shape of the droplet upon deformation may not always be maintained

when surface active species, such as proteins and particles, are irreversibly partitioned at the interface. For such systems, the surface may exhibit a significant restoring force under shear, i.e., an elastic interface that resists the change in area.[27,28] This solid-like behavior is manifested in many systems as "crumpling" or wrinkle formation upon droplet volume reduction.[29] In this case, elasticity has to be included to differentiate surface energy as observed in "solid-like" systems from surface tension for "fluid-like" systems.

The current study demonstrates the need to include interfacial elasticity in the augmented SRYL model in order to accurately predict the deformation of water droplets under the compression force of AFM probe in an oil containing NPAMs (asphaltenes), that are soluble in toluene and less soluble in 50 heptol.[30] It should be noted that the NPAMs encompass a wide range of molecular structures. Some of the NPAMs are permanently trapped at the interface while others may be mobile to escape the interfaces during interface deformation. The overall properties of the interface come from the net effect of NPAMs, with the major contributions from the irreversibly adsorbed interfacially active species. By taking advantage of self-assembly of NPAMs at the oil-water interface, we are able to form interfacial films of variable elasticities due to the continual adsorption/association (structuring) of NPAMs at the interface.[31] In previous studies, the interfacial film formed by NPAMs has shown a progressive and time-dependent rheological property, transitioning from a viscous dominant interface at short aging times to elastically dominant responses with longer aging.[30-35] Upon reduction of droplet volume the interface is seen to crumple.[29] This elastic

interfacial film often leads to poor water separation in petroleum emulsions by inhibiting droplet coalescence.[7,29,32-37] However, such time-dependence and irreversibility of NPAM adsorption/self-assembly at the oil-water interface provide an opportunity to study the applicability of the augmented SRYL model predicting interfacial compressibility and interaction forces of a solid probe interacting with a water droplet in petroleum oil that progressively migrates from a Laplacian to a non-Laplacian response. Extending the existing SRYL equations to non-Laplacian interfaces is the focus of this study.

4.2 MATERIALS AND METHODS

4.2.1 Materials Preparation

Vacuum distillation feed bitumen was kindly provided by Syncrude Canada Ltd. High-performance liquid chromatography (HPLC)-grade toluene and *n*-heptane (Fisher Scientific) were used as solvent (toluene) or to prepare 50 heptol (a mixture of 50:50 vol. % *n*-heptane and toluene).

Deionized water with a resistivity of 18.2 MΩ cm was prepared with an Elix 5 system, followed by purification with a Millipore-UV plus system. Silicon wafers were purchased from NanoFab (University of Alberta) and used as substrates. Tipless silicon nitride cantilevers were purchased from Bruker Scientific (Camarillo, CA) and used for the force measurement. Silica microspheres (D ≈ 8 μm) were purchased from Duke Scientific Co. (Palo Alto, CA) and glued to the tipless cantilevers to form colloidal probes.

4.2.2 Precipitation of Natural Polyaromatic Molecules (Asphaltenes) and Solution Preparation

Details on precipitation of asphaltenes, a class of natural polyaromatic molecules (NPAMs), have been described elsewhere.[38] Briefly, vacuum distillation feed bitumen was diluted with HPLC-grade toluene at a toluene/bitumen volume ratio of 5:1. The mixture was centrifuged at 35,000 g for 30 min to remove fines, usually mineral solids. Toluene was then allowed to evaporate from the diluted bitumen in a clean fume hood for one week to obtain solids-free bitumen. The NPAMs (asphaltenes) were extracted from the solids-free bitumen by adding *n*-heptane at an *n*-heptane-to-bitumen volume ratio of 40:1. The mixture was agitated for 2 hr to achieve full precipitation, followed by gravity settling to separate the precipitates from the remaining solution. After settling, the supernatant was removed. To wash away the trapped solvent, the precipitates were repeatedly washed by adding additional *n*-heptane-shaking-settling until the supernatant appeared clear. The remaining *n*-heptane trapped in the precipitates of the final washing was then allowed to evaporate. The resulting precipitates of NPAMs accounted for 13 wt. % of the original bitumen sample.

Fresh solutions of NPAMs in toluene or 50 heptol were prepared prior to each experiment by dissolving NPAMs in the desired solvent under sonication in an ultrasonic bath for 15 min.

4.2.3 Preparation of Cantilever and Substrate

A silica sphere (D ≈ 8 μm) was glued onto either a long wide-beam or a short narrow-beam AFM cantilever (model NP-O10) at its apex location using a two-component epoxy (EP2LV, Master Bound, Hackensack, NJ). The modified cantilevers were placed in a vacuum desiccator for 24 hr, after which the probes were exposed to an ultraviolet light for 1 hr to remove organic contaminants from the silica sphere (probe). The spring constant of the modified cantilever was measured prior to and after AFM force measurements and did not show any significant change over the course of the measurements (< 5 %). The spring constants for the long wide-beam and short narrow-beam modified cantilevers were in the range of 0.12-0.22 N/m. For a given system, equivalent and reproducible force profiles were obtained using both the long wide-beam and short narrow-beam cantilevers.

Silicon wafers, used as substrates, were first treated with piranha solution for 1 hr to remove impurities. The cleaned wafers were then soaked in 1 mM octadecyltrichlorosilane (OTS) (ACROS Organics, Geel, Belgium) in toluene solutions for 30 s to partially hydrophobize the surfaces. The substrates were then rinsed with copious amounts of toluene and gently dried with nitrogen gas. This procedure resulted in an intermediate contact angle of 45-50° measured through the water droplet in air. Wafers of intermediate hydrophobicity were required to keep water droplets immobilized on the substrate in NPAM solutions during AFM measurements.

4.2.4 AFM Force Measurements

Interactions between a silica sphere and a water droplet in NPAM solutions were measured using an Agilent 5500 Molecular Imaging Microscope (Agilent Technologies Inc., Chandler, USA). Force profiles were collected in NPAM-in-toluene or 50 heptol solutions using the vendor-provided liquid cell. The experimental setup for the measurement of probe-droplet interaction forces is shown in Figure 4.1 (a). Also shown in this figure is a top view optical microscope image of the cantilever positioned over a water droplet (shown in the inset) in NPAM solution. After adding 0.5 vol. % water to the freshly prepared NPAM solution, the mixture was sonicated for 5 s. The resulting emulsion was slowly injected into the AFM liquid cell using a glass pipette. In our AFM system, the static electricity interference was not observed.

The water drop size on the treated substrate obtained using this method was of a diameter range of 60 - 100 μm. The cantilever was then positioned over a selected droplet (D ≈ 70 μm) and allowed to approach the interface. The setpoint of the AFM was kept at 0 V, and the piezo travel distance was constant at 4 μm during force measurements. Since the "true" separation between the probe and droplet cannot be determined due to droplet deformations under cantilever load and the nontransparent nature of the system, the measured force in this study is plotted as a function of unprocessed piezo displacement. In AFM measurements, only the distance between "hard" substrates is known, i.e., between the probe and underlying substrate. Other complementary techniques, such as confocal microscopy[25] or theoretical calculations using SRYL model,[21] are required to

obtain "true" separation between a probe and a soft interface. Cantilever velocity was kept at 1 μm/s in order to avoid the effect of hydrodynamics.[10]

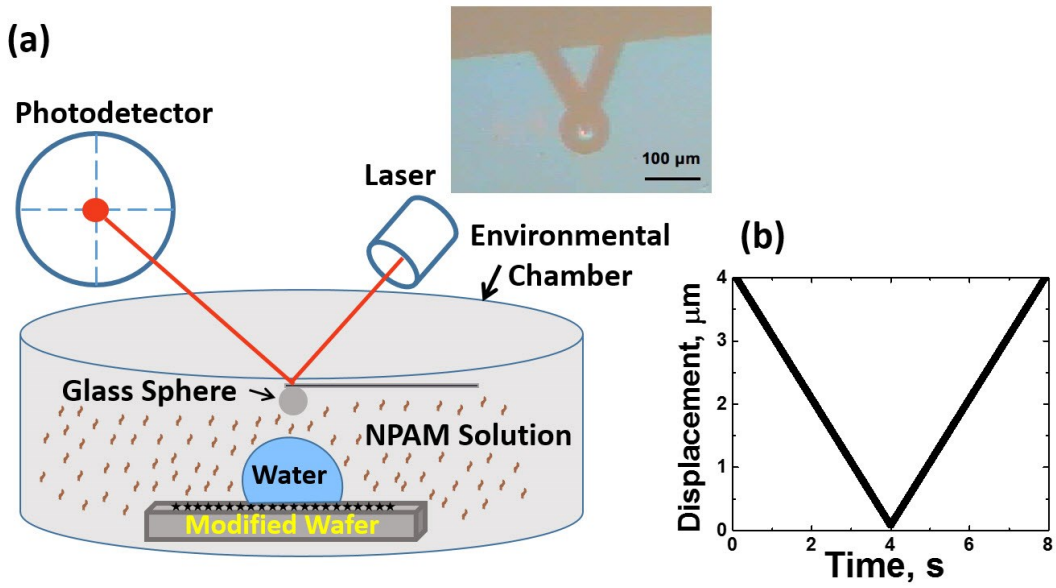

Figure 4.1 (a) Experimental setup for measurement of interaction forces between a silica sphere (D ≈ 8 μm) and water droplet (D ≈ 70 μm) in 0.1 g/L NPAM solution, (b) AFM piezo movement as a function of time. The inset shows the top view of AFM cantilever positioned over a selected water droplet on the treated substrate NPAM solution. Note that the glued glass sphere is on the underside and hence not visible using the top view camera.

Figure 4.1 (b) shows the piezo displacement as a function of time. A single AFM force profile was acquired in 8 s. Deflection sensitivity and spring constant values of the colloidal probe against the underlying OTS-treated substrate were calculated prior to and after force measurements using the Thermal K function available in Agilent 5500 AFM software. All measurements were carried out at room temperature (24 °C). One limitation of this experimental setup is that the

NPAM concentration in the continuous phase has to remain fairly low ($\leq$ 0.1 g/L), as the solution should be sufficiently translucent to obtain a high laser sum and reduce scattering. The Agilent 5500 AFM is equipped with an environmental chamber, suitable for measurements using volatile organic solutions as in our case. However, even with the seals in place, measurements were kept to a maximum of 1 hr for toluene and 30 min for 50 heptol solutions in order to minimize any effect that might result from solvent evaporation.

4.2.5 Measurement of the Contact Angle, Interfacial Tension and Crumpling Ratio

Interfacial characterization studies were conducted using a Theta Optical Tensiometer T200 (Biolin Scientific, Stockholm, Sweden) at room temperature (24 °C). The contact angle of water droplets on untreated hydrophilic substrates soaked in NPAM solution was measured in air. Similar measurements were made on the OTS-treated substrates in air, toluene, 50 heptol as well as in 0.1 g/L NPAM-in-toluene or 50 heptol solutions. For measurements in air, a water droplet (V $\approx$ 9 μL) was carefully placed on the substrate and contact angle measured for 3 min at 3 fps. For measurements in NPAM solutions, a fresh solution was prepared prior to each measurement. The treated substrate was placed in a rectangular quartz cell and a water droplet (V $\approx$ 9 μL) was deposited on the substrate and brought into focus. The NPAM solution was then added to the cell mimicking the setup used for the force measurement using AFM probe technique. The time-dependent contact angle was recorded over 60 min (3 fps), a time span

comparable to the AFM force measurement. All experiments were repeated 3 times and the error was within 5 %.

Prior to each interfacial tension and crumpling ratio measurement, fresh NPAM solution was transferred into a rectangular quartz cell and a water droplet (D ≈ 2 mm) was generated from a 1 mL gastight Hamilton syringe with an 18 gauge needle (Reno, NV). The droplet profile was recorded and analyzed using the Theta software. Tensiometer camera was calibrated prior to each experiment and droplet images were recorded at 12 fps for 60 min. The tests were repeated a minimum of 3 times for each condition with the measurement error less than 10 %. Edge detection was used for pendant drop shape analysis and the interfacial tension was determined using the Young-Laplace equation. The interfacial tension relates to the drop shape by:

$$\gamma = \Delta\rho g \frac{R_0^2}{\beta} \quad (1)$$

where γ is the interfacial tension, $\Delta\rho$ is the density difference between fluids, g is the gravitational acceleration constant, R_0 is the radius of drop curvature at apex, and β is the shape factor.

Crumpling of the water droplet was measured in 0.1 g/L NPAM solutions to demonstrate the development of viscoelastic interfacial film[39] by deviation of water droplet from its pendant shape in response to volume reduction.[40] To measure the crumpling ratio, a water droplet (V ≈ 6 μL) was generated at the tip of an 18-gauge needle in NPAM solution and allowed to age for up to 1 hr (0, 5, 15, 30, 60 min), after which droplet volume was slowly reduced at a rate of 50

μL/min until "folds" or "crumpling" was observed at the interface. The crumpling ratio is defined as the apparent projected area of the droplet prior to crumpling (A_f) divided by the initial droplet area (A_i):[40]

$$\mathrm{CR} = \frac{\mathrm{A_f}}{\mathrm{A_i}} = \left(\frac{R_f}{R_i}\right)^2 \quad (2)$$

With the CR defined as such, a large CR would indicate a more rigid interface.

4.2.6 Dilatational Rheology

There are different methods to follow the development of interfacial elasticity. Forth et al. for example studied the development of interfacial elasticity by tracking the drop shape of the constant volume and calculating the discrepancy between the predicted shape by using the Young-Laplace equation and the measured droplet shape.[41] In the current study, the more conventional oscillatory pendant drop method was used to quantify the interfacial dilatational elasticity. The pulsating droplet module (PD 200) of the Theta Optical Tensiometer T200 was used to measure dilatational viscoelastic complex modulus (*E*) and hence the dilatational elastic modulus (*E'*) of the NPAM-stabilized oil-water interface. A water droplet of V ≈ 5-6 μL was formed at the tip of an 18-gauge needle in 0.1 g/L NPAM solution (toluene or 50 heptol), and sinusoidally oscillated to vary the drop volume and hence interfacial area. The tracking of interfacial tension and area during a given measurement is shown in Appendix B (Figure B-1).

Dependence of *E* on oscillation frequency is linked to characteristics of the relaxation process of NPAMs at the interface. Since the freshly created expanding interface is exposed to bulk phase for a longer period of time, diffusion controlled

adsorption occurs at low frequencies, in contrast to intrinsic elasticity at higher frequencies.[32] However, due to hydrodynamic effects associated with the oscillation, this method loses accuracy at high frequencies.[42] For NPAM-stabilized interfaces a good frequency range was determined to be 0.1-0.5 Hz. In the current study the droplet volume change was set to be 10 % during sinusoidal oscillation, and the frequency of oscillation was set at 0.1 Hz. Each measurement of the interfacial viscoelasticity comprised of ten oscillations with a 10 s delay.

The complex viscoelastic modulus *E* can be separated into *E'* (elastic modulus) and *E''* (viscous modulus) through the well-established relationship:[42-47]

$$E = \frac{\Delta\gamma}{\Delta A/A_0} = E' + iE'' = E' + 2\pi i\nu\mu \qquad (3)$$

where $\Delta\gamma$ is the change in interfacial tension, ΔA is the amplitude, A_0 is the reference area, *E'* is the dilatational elasticity, *E''* is the loss (viscous) modulus, *i* is the imaginary unit, *v* is the oscillation frequency, and μ is the viscosity of the droplet liquid. For the systems considered, the viscous modulus was found to be very low (1-2 mN/m) and did not change over time. Therefore, only the elastic modulus is reported in this study.

4.3 RESULTS AND DISCUSSION

4.3.1 Interaction Forces between a Rigid Sphere and Deformable Interfaces in Organic Solvents

Interaction forces between a silica sphere and a micron-sized water droplet in NPAM solutions were measured using AFM to investigate the effect of oil-water interfacial aging. Figure 4.2 (a) shows the time-dependent interaction forces

between a silica sphere (D ≈ 8 μm) and water droplet (D ≈ 70 μm) immersed in 0.1 g/L NPAM-in-toluene solution for up to 1 hr. A higher slope in the "high force" constant compliance region implies a more rigid or "solid-like" interface, which is readily observed as the interface ages. The slope of the constant compliance region increases from 27 mN/m at aging time t = 5 min to 41 mN/m at t = 1 hr. The time-dependent change in the slope of the constant compliance region is mainly due to adsorption/association of NPAMs at the oil-water interface. This time-dependent change was shown in our previous study as an increase in the extended range of repulsion over time when the interaction forces were measured between two mica surfaces in similar NPAM solutions using SFA.[48] On approach, the nature of the interaction forces between the two surfaces in NPAM-in-toluene solutions is purely repulsive, attributed to steric repulsion of swollen NPAM layers on silica and/or the oil-water interface. It is interesting to note a significant increase in the adhesion force (and force range) during cantilever retraction as the cantilever "hold time" at the interface is increased (Figure 4.2 (b)) and the intervening film is given more time to drain. When the interfacial materials (aggregates) become compressed as the colloidal probe gets closer to the interface, an increase in interpenetration and bridging of NPAMs/aggregates is anticipated, which accounts for the observed increase in adhesion upon probe retraction. Since the electrical double layer is negligible in the non-aqueous environment, the forces of interaction for the system of interest are attributable to steric and van der Waals forces.

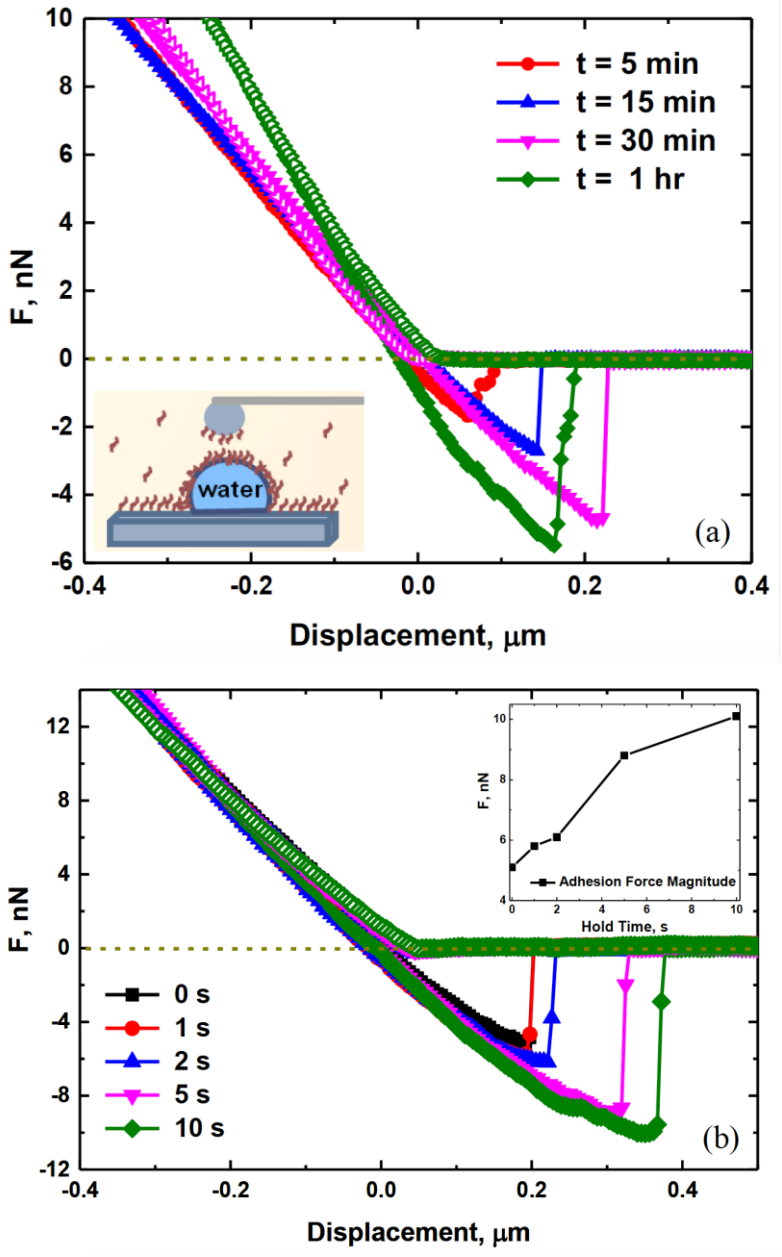

Figure 4.2 (a) Interactions between silica probe (D ≈ 8 μm) and water droplet (D ≈ 70 μm) in 0.1 g/L NPAM-in-toluene solution upon cantilever approach (open symbols) and retract (filled symbols), as a function of droplet aging time; (b) Effect of cantilever 'hold time' on the adhesion force between the colloidal probe and an NPAM-stabilized interfacial layer at the oil-water interface (D ≈ 75 μm) after 30 min aging time. Inset: the adhesion force magnitude versus hold time.

For 50 heptol (see Appendix B, Figure B-2), the aging effect was found to be less pronounced and the interfacial deformation and force magnitude did not change significantly during 30-min aging. This reduced time dependency in 50 heptol is likely due to a much faster adsorption and/or association of NPAMs in 50 heptol than in toluene on solids and at the oil-water interface, which will be discussed further in the following sections. Since the interfacial stiffening occurred mostly during the first colloidal probe approach to the interface (approach time ~ 5 min), only one representative force curve at 15 min aging time will be discussed further. The AFM force measurements were stopped after 30 min aging in order to minimize the change in solution composition due to a higher evaporation rate of heptane over toluene. Measuring further interfacial stiffening at longer aging times in NPAM in 50 heptol solution would be extremely interesting once the limitation of possible composition change in the AFM liquid cell is resolved.

4.3.2 SRYL Prediction for Droplet Deformation

To better understand and predict the measured changes in drop deformation, the high force formula of the augmented SRYL equations was applied to our system. With proper boundary conditions the Chan-Dagastine-White model has been successfully used to predict the equilibrium force (F) as a function of relative piezo displacement (ΔD) for interactions between a particle and a bubble/droplet or between two bubbles or droplets.[10,20,21] This model utilizes the augmented SRYL equations to predict film drainage and deformations based on the force applied. It should be emphasized that this model applies the Young-Laplace equation for droplet shape, which is accurate only for "fluid-like" systems of

minimal viscoelasticity. By using the high force equation with a specified boundary condition of the augmented SRYL model (Eqns. 4-6), droplet deformation under given loads can be accurately predicted.[21]

$$\Delta D(y) \equiv \frac{F(t)}{4\pi\sigma}\left[\ln\left(\frac{F(t)R_{ds}}{8\pi\sigma R_o^2}\right) + 2B(\theta) - \frac{4\pi\sigma}{K} - 1\right] \quad (4)$$

$$B(\theta) = 1 + \frac{1}{2}\ln\left[\frac{1+\cos(\theta)}{1-\cos(\theta)}\right] \quad (5)$$

$$R_{ds} \equiv \frac{1}{\left[\frac{1}{R_O}+\frac{1}{R_S}\right]} \quad (6)$$

Where ΔD is the predicted displacement, $F(t)$ is the measured force, R_{ds} is linked to R_o and R_s, the radii of the unperturbed droplet and sphere, respectively; θ is the contact angle of the droplet on the substrate in solution, σ is the interfacial tension and K is the spring constant of the cantilever.

The extent of droplet deformation depends on the boundary conditions selected- a pinned three-phase contact line or constant contact angle as the probe is pressed on the droplet. Considering the much smaller size of the probe than the droplet and small displacement of the probe in our experiment, deformation of the interface in the context of the entire droplet can be considered negligible, to ensure a pinned three phase contact line given by Eqn. 5.

Water droplet contact angles in toluene on substrates of different hydrophobicity can be found in Appendix B (Figure B-3). The selected intermediate contact angle of 50$^{\mathbf{o}}$ in air resulted in contact angles of 86° and 74° in NPAM-in-toluene and 50 heptol solutions respectively, with the droplet firmly anchored on the substrates.

AFM imaging of the substrate surface features revealed that NPAMs adsorbed on the substrate within 15 min, and no significant change was observed at longer exposure times (Figure B-4). Surface properties and roughness of the underlying OTS-treated substrates were also checked prior to and after force measurements for each system (Table B-1). The SEM images presented in Appendix B (Figure B-5) confirmed that the contact area of the silica sphere did not change upon exposure to NPAMs. Therefore, by considering the results in Figures B-3 to B-5, one can conclude that the changes in slopes of the constant compliance region of force curves reported in Figure 4.2 (a) are indeed due to the changes in the physical properties of the oil/water interface.

To apply the augmented SRYL model to the force profiles as a function of droplet aging time, shown in Figure 4.2, the dynamic interfacial tension ($\sigma(t)$) of the system needs to be determined. The measured dynamic interfacial tension of a water droplet in 0.1 g/L NPAM-in-toluene and 50 heptol solutions is shown in Figure 4.3. For a clean oil-water interface, baseline interfacial tensions of 36 mN/m and 43 mN/m were measured for water-toluene and water-50 heptol, respectively. A rapid decrease in the interfacial tension of water in contact with NPAM solutions was observed within the first 10 min for both solutions, indicating a rapid adsorption of the interfacially active material. This initial rapid decrease in interfacial tension was followed by a slower secondary decay which is often associated with reorganization and relaxation of NPAMs at the oil-water interface.[49] After 15 min aging time the interfacial tensions for both systems equaled 26.8 mN/m, and slowly approached a steady-state value of ~ 24.5 mN/m

after 1 hr. However, the initial slope of interfacial tension versus time is quite different for the two solutions, indicating a significant effect of solvent aromaticity on interfacial activity of NPAMs.

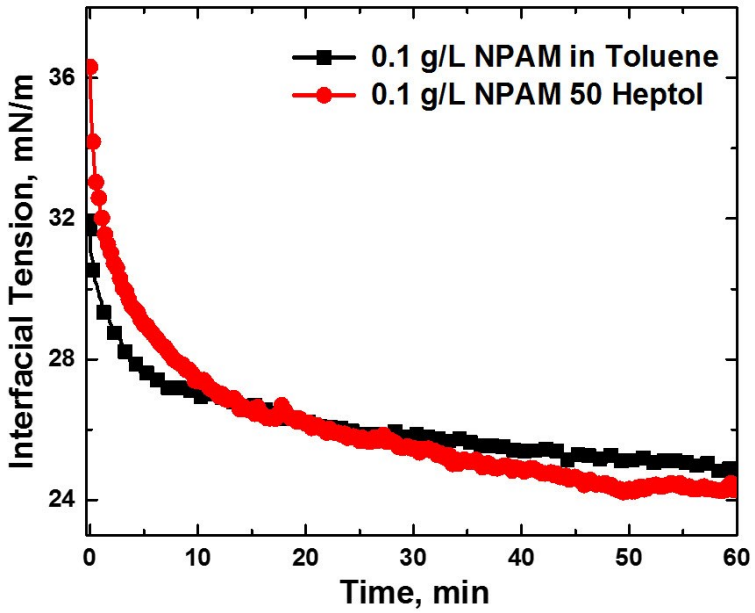

Figure 4.3 Interfacial tension of a water droplet in 0.1 g/L NPAM-in-toluene or 50 heptol solution.

Using the dynamic interfacial data, the measured forces acting upon the colloidal probe during approach (system: NPAM-in-toluene solution at 15 min and 1 hr water droplet aging) are compared with the predictions from the theoretical model in Figure 4.4. The model provides a good fit for the force profile at a short aging time, t = 15 min, but deviates from the experimental result at a longer aging time of 1 hr. Since $B(\theta)$, R_{ds} and K are constant during the droplet aging, as shown in Appendix B (Figures B-3, B-4, and Table B-1), and σ decreases only by ~2 mN/m from 15 min to 1 hr aging as shown in Figure 4.3, the observed deviation of the measured force profiles by the model at longer aging times cannot be explained

by considering only the change in interfacial tension. For interfaces of substantial viscoelasticity due to highly cross-linked nature of interfacially active NPAMs, as in the current study, the extent of deformation could be greatly influenced by interfacial rheology. For such systems, it is not surprising that the current SRYL model could not predict droplet deformation and interaction force, as the NPAMs irreversibly partitioned at the interface exhibit a significant restoring force under shear. To understand the observed deviation, a closer look at the interfacial properties is therefore warranted.

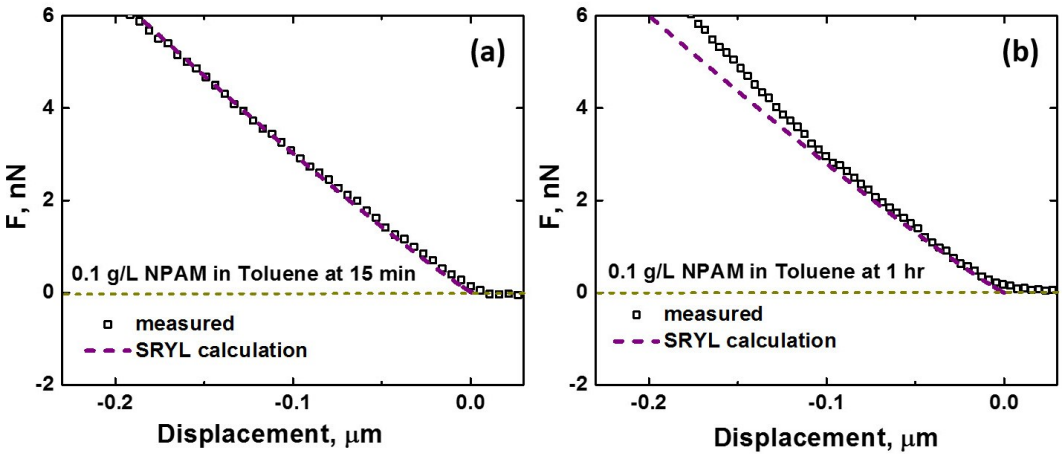

Figure 4.4 Comparison of measured forces over the constant compliance (high force) region (symbols) in 0.1 g/L NPAM-in-toluene solution upon approach at (a) 15 min and (b) 1 hr with the predictions from the SRYL model (dashed lines).

4.3.3 Development of Viscoelasticity at the Oil-Water Interface

To illustrate the crosslinking of NPAMs and "stiffening" of the interface, the time-dependent crumpling ratio of a water droplet aged in NPAM solutions (toluene and 50 heptol) was determined. The results in Figure 4.5 show that for both solvents the crumpling ratio increases with increasing interfacial aging,

indicating an increased resistance of the interface to in-plane shear. Interfacial crumpling upon droplet volume reduction demonstrates the development of a mechanical barrier at the interface and deviation from a classical Laplacian response. Crumpling occurs due to the irreversible adsorption of NPAMs at the oil-water interface,[49] as a critical interfacial concentration is eventually reached during droplet contraction to cause "jamming" of the interfacial network. For crumpling to occur, the compressional elasticity should be non-zero while the interfacial shear elasticity should be significant.[50]

Development of a rigid "skin" and hence deviation from Laplacian shape can qualitatively explain the lack of agreement between the measured and predicted forces by existing SRYL equation after 1 hr aging, as shown in Figure 4.4 (b).

For 0.1 g/L NPAM-in-toluene solution, the crumpling ratio (CR) after 1 hr droplet aging was 0.12, indicating interfacial crumpling at an 88 % reduction in drop volume. For 50 heptol, the crumpling ratios are higher compared to toluene at equivalent aging times, with CR = 0.37 after 1 hr droplet aging. However, due to the AFM setup limitations, force measurements at an equivalent time could not be conducted. The force curve after 15 min aging time in 50 heptol NPAM solution is equivalent (if not slightly more rigid) compared to the corresponding toluene case after 1 hr aging time, as indicated in Figure 4.5. A higher crumpling ratio in 50 heptol indicates that the interfacial film is more resistant to compression and hence more rigid than the film formed in toluene. Higher crumpling ratios in poorer solvents correlate well with the findings from earlier studies showing that NPAM molecules are most effective at stabilizing emulsions in "poorer" solvents

(~50 heptol) when NPAM concentration is below the critical precipitation concentration.[34] It is interesting to note that while the interfacial tensions for both toluene and 50 heptol systems are similar at 15 min and 1 hr aging time, the crumpling ratios are considerably different with $CR_{50\ heptol} > CR_{toluene}$. This finding confirms that interfacial tension alone cannot fully describe changes occurring at the oil-water interface when irreversibly adsorbed and self-associating molecules such as NPAMs are present. The significant increase in crumpling ratio and a marginal decrease in the interfacial tension, ~2 mN/m between 15 min and 1 hr aging time, confirms the likelihood that molecular association of NPAMs at the oil-water interface dominates the interfacial response.

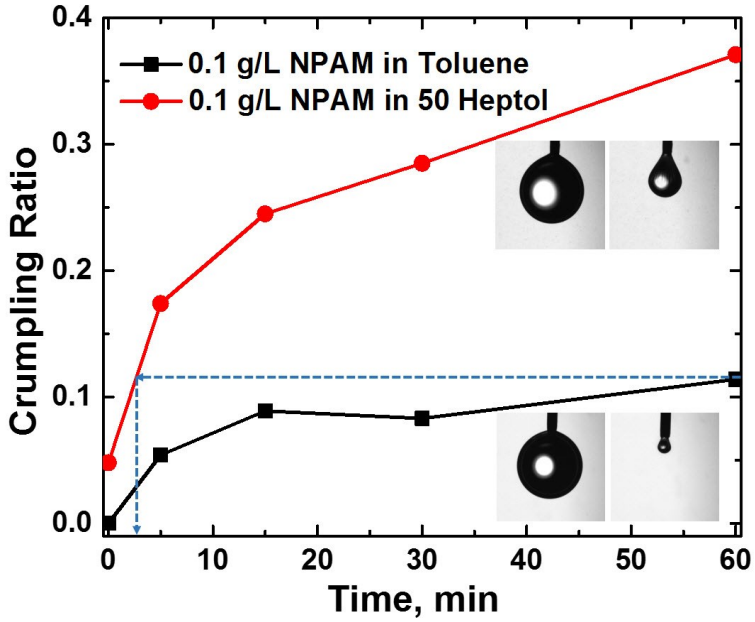

Figure 4.5 Crumpling ratio of water droplets aged in NPAM-in-toluene and 50 heptol solutions. The images shown in the inset compare the initial water droplet shape and that at the onset of crumpling after 1 hr of interfacial aging.

Time-dependent dilatational elasticity of water droplets aged in NPAM solutions was therefore measured. The results in Figure 4.6 show that for both systems interfacial elasticity increases with increasing droplet aging, indicating the formation of more "solid-like" and mechanically stronger interfacial films. A higher dilatational elasticity is measured for an interfacial film formed in 50 heptol. This finding is consistent with higher crumpling ratios (Figure 4.5) and relates to faster interfacial adsorption dynamics (Figure 4.3) and stronger intermolecular interactions between NPAMs in poorer solvents. It is evident that the ability to form a cohesive interlinking network is enhanced in less aromatic solvent. Previous research investigating surface forces between NPAMs deposited/ adsorbed on mica showed an increased attraction and stronger adhesion forces of NPAMs in heptol than in toluene.[7]

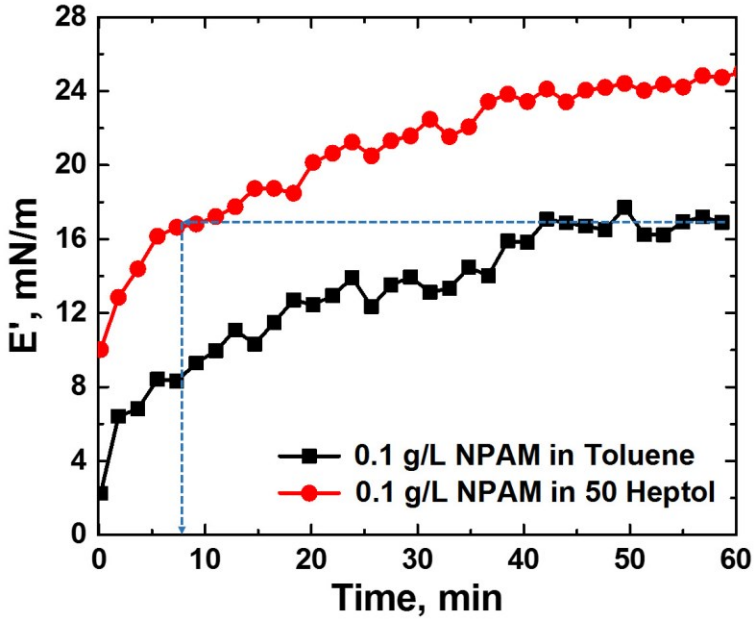

Figure 4.6 Time-dependent dilatational elastic modulus for a water droplet aged in NPAM solutions.

Such rapid adsorption of NPAMs from 50 heptol as shown in Figures 4.3 and 4.6 explains the lack of time-dependent changes in the 50 heptol force curves (see Figure B-2), as a rapid increase in the interfacial elasticity to ~16 mN/m occurs in the first 5 min. As indicated in Figure 4.6, it takes an equivalent of 1 hr aging for NPAM-in-toluene solution to reach the same level of interfacial elasticity.

Our interfacial characterization studies confirm that NPAMs adsorb at the oil-water interface to form strongly elastic films which exhibit resistance to in-plane shear (non-Laplacian behavior).

The dynamics of this process are accelerated in "poorer" solvents (50 heptol) due to the increase in interfacial activity and stronger interaction between NPAM aggregates. While these characteristics are often probed on planar surfaces or millimeter size droplets, the research described in this study demonstrates the potential of AFM to measure such dynamic interfacial changes and the requirement to account for the interfacial elasticity in the widely used high force droplet deformation equation of the augmented SRYL model.

4.3.4 Viscoelasticity Correction Factor to Modify the High Force SRYL Equation

For complex interfaces where deviation from Laplacian behavior occurs and interfacial crumpling is observed, the Young-Laplace equation does not provide a good approximation for droplet shape. When crumpling is observed, interfacial tension/surface energy (σ) should not be substituted for surface stress (τ), similar

to that observed for solid surfaces.[27,28,51] Gibbsian formulation of thermodynamics of interfaces given below is more representative of the case, i.e.:

$$\Delta p = \tau\left(\frac{1}{R_1} + \frac{1}{R_2}\right) \tag{7}$$

where Δp is the increment in pressure, and R_1 and R_2 are local radii of curvature. With the replacement $\tau = \sigma$, Eqn. 7 simplifies to the Young-Laplace equation. However, this replacement is allowable only for interfaces of non-viscoelastic nature.[27] For solid-like surfaces and similarly for interfaces with elasticity and surface strain ε, the surface stress tensor given by Eqn. 8 instead of surface tension (equivalent to surface energy) should be used.[28]

$$\tau = \sigma + \frac{\partial\sigma}{\partial\varepsilon} \tag{8}$$

As shown in Figure 4.4 (b), the slope of the constant compliance region at 1 hr aging time is higher than that predicted by the existing SRYL model, indicating a more "rigid" interface. This mechanical stiffness as the colloidal probe is pushed against the interface can be addressed by inclusion of a viscoelastic correction factor ($\frac{\sigma}{E\prime}$ similar to $\frac{\partial\sigma}{\partial\varepsilon}$ in Eqn. 8 for solid surfaces) inside the brackets in Eqn. 4. As a result, the high force formula (Eqn. 4) becomes:

$$\Delta D(y) \equiv \frac{F(t)}{4\pi\sigma}\left[\ln\left(\frac{F(t)R_{ds}}{8\pi\sigma R_o^2}\right) + 2B(\theta) - \frac{4\pi\sigma}{K} - 1 + \frac{\sigma}{E'}\right] \tag{9}$$

Applying the corrected formula (Eqn. 9) to both systems that exhibit significant interfacial crumpling upon drop volume reduction (water droplet aging in 0.1 g/L NPAM-in-toluene solution at 1 hr and in 50 heptol solution at 15 min), the results in Figure 4.7 show a negligible discrepancy between experimental data and the

theoretical prediction in the high force region during approach. It is interesting to note that for the toluene system after 1 hr aging, the elasticity is 15.8 mN/m and the slope of constant compliance = 41 mN/m, while for the 50 heptol system after 15 min aging time, the elasticity is 17 mN/m and the slope of constant compliance = 44mN/m. Hence, independent of the solvent type, there is a very good agreement between the dilatational elasticity and the interfacial stiffness as measured under normal load deformation.

The interplay between interfacial tension and interfacial elasticity is crucial for non-Laplacian systems where deformation is not well-predicted by the high force equation of SRYL. As the deviation from Laplacian behavior increases, for example due to higher cross-linking of molecules, interfacial rheology will play a more significant role in the interfacial dynamics. Tracking the changes in interfacial tension and interfacial elasticity explains the deviations from the traditional high force calculation and provides better predictions for droplet deformation, an important factor in emulsion stability.

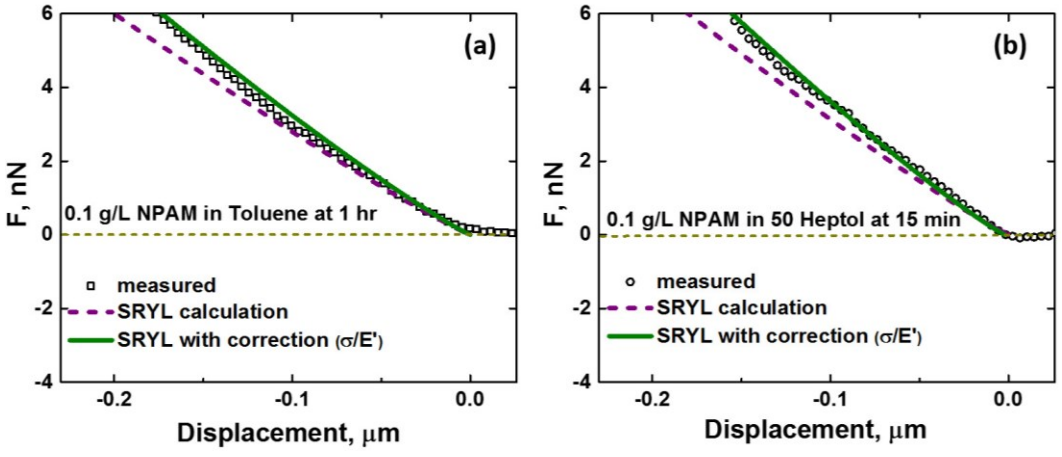

Figure 4.7 Measured forces upon approach in 0.1 g/L NPAM solution (a) in

toluene after 1 hr aging and (b) 50 heptol after 15 min aging, plotted in comparison with predictions using SRYL model (Eqn. 4) and the modified SRYL model to account for interfacial elasticity (Eqn. 9).

4.4 CONCLUSIONS

In this study, interactions between a silica probe and a viscoelastic interface, formed by the continual accumulation of natural polyaromatic species at an oil-water interface, have been examined. Our system of interest showed progressive rheological aging of the interface, resulting in the formation of a rigid 'skin' and quasi-solid-like behavior of a water droplet. The development of an interfacial mechanical barrier is a contributing factor to enhanced emulsion stability as a result of interfacial aging and decreased solvent quality. This non-Laplacian behavior leads to a discrepancy between the measured droplet deformation and that predicted by the SRYL equation in the "constant compliance" (high force) region. A viscoelastic correction term is introduced into the equation to account for the increased interfacial dilatational rheology. This critical modification is shown to provide excellent theoretical prediction of the deformation of an interface of non-Laplacian nature.

4.5 REFERENCES

1. Wilde, P. J. *Curr. Opin. Colloid Interface Sci.* **2000**, 5 (3-4), 176-181.

2. Krasowska, M.; Prestidge, C. A.; Beattie, D. A. Atomic force microscopy for determining surface interactions of relevance for food foams and emulsions.

In: Dar, Y. L.; Light, J. M. (Eds.). *Food Texture Design and Optimization* **2014**, 402-422, doi: 10.1002/9781118765616.ch16.

3. Langevin, D. *Adv. Colloid Interface Sci.* **2000**, 88 (1-2), 209-222.

4. Butt, H. J.; Cappella, B.; Kappl, M. *Surf. Sci. Rep*. **2005**, 59 (1-6), 1–152.

5. Gromer, A.; Penfold, R.; Gunning, A. P.; Kirby, A. R.; Morris, V. J. *Soft Matter* **2010**, 6, 3957-3969.

6. de Gennes, P. G. *Adv. Colloid Interface Sci.* **1987**, 27, 189-209.

7. Wang, S.; Liu, J.; Zhang, L.; Masliyah, J.; Xu, Z. *Langmuir* **2010**, 26 (1), 183-190.

8. Butt, H.J. *J. Colloid Interface Sci.* **1994**, 166 (1), 109-117.

9. Ducker, W. A.; Xu, Z.; Israelachvili, J. N. *Langmuir* **1994**, 10 (9), 3279-3289.

10. Tabor, R. F.; Grieser, F.; Dagastine, R. R.; Chan, D. Y. C. *J. Colloid Interface Sci.* **2012**, 371 (1), 1-14.

11. Gillies, G.; Prestidge, C. A.; Attard, P. *Langmuir* **2002**, 18 (5), 1674-1679.

12. Gillies, G.; Prestidge, C. A. *Langmuir* **2005**, 21 (26), 12342-12347.

13. Nguyen, A. V.; Evans, G. M.; Nalaskowski, J.; Miller, J. D. *Exp. Therm. Fluid Sci.* **2004**, 28 (5), 387-394.

14. Connor, J. N.; Horn, R. G. *Faraday Discuss.* **2003**, 123, 193-206.

15. Chen, L.; Heim, L.-O.; Golovko, D. S.; Bonaccurso, E. *Appl. Phys. Lett.* **2012**, 101, 031601.

16. Filip, D.; Uricanu, V. I.; Duits, M. H. G.; Agterof, W. G. M., Mellema, J. *Langmuir* **2005**, 21 (1), 115-126.

17. Krasowska, M.; Carnie, S. L.; Fornasiero, D.; Ralston, J. *J. Phys. Chem. C* **2011**, 115 (22), 11065-11076.

18. Shi, C.; Chan, D. Y. C.; Liu, Q.; Zeng, H. *J. Phys. Chem. C* **2014**, 118 (43), 25000-25008.

19. Munz, M.; Mills, T. *Langmuir* **2014**, 30 (15), 4243-4252.

20. Chan, D. Y. C.; Dagastine, R. R.; White, L. R. *J. Colloid Interface Sci.* **2001**, 236 (1), 141-154.

21. Chan, D. Y. C.; Klaseboer, E.; Manica, R. *Soft Matter* **2011**, 7, 2235-2264.

22. Manor, O.; Chau, T. T.; Stevens, G. W.; Chan, D. Y. C.; Grieser, F.; Dagastine, R. R. *Langmuir* **2012**, 28 (10), 4599-4604.

23. Shi, C.; Zhang, L.; Xie, L.; Lu, X.; Liu, Q.; Mantilla, C. A.; van den Berg, F. G. A.; Zeng, H. *Langmuir* **2016**, 32 (10), 2302-2310.

24. Webber, G. B.; Manica, R.; Edwards, S. A.; Carnie, S. L.; Stevens, G. W.; Grieser, F.; Dagastine, R. R.; Chan, D. Y. C. *J. Phys. Chem. C* **2008**, 112 (2), 567-574.

25. Tabor, R. F.; Lockie, H.; Mair, D.; Manica, R.; Chan, D. Y. C.; Grieser, F.; Dagastine, R. R. *J. Phys. Chem. Lett*. **2011**, 2 (9), 961-965.

26. Vakarelski, I. U.; Li, E. Q.; Thoroddsen, S. T. *Colloids Surf. A* **2014**, 462, 259-263.

27. Shuttleworth, R. *Proc. Phys. Soc.* **1950**, A63, 444-457.

28. Cammarata, R. C. *Prog. Surf. Sci.* **1994**, 46 (1), 1-38.

29. Yeung, A.; Dabros, T.; Masliyah, J. *Langmuir* **1997**, 13 (24), 6597-6606.

30. Harbottle, D.; Chen, Q.; Moorthy, K.; Wang, L.; Xu, S.; Liu, Q.; Sjoblom, J.; Xu, Z. *Langm*uir **2014**, 30 (23), 6730-6738.

31. Masliyah, J.; Zhou, Z. Z.; Xu, Z.; Czarnecki, J.; Hamza, H. *Can. J. Chem. Eng.* **2004**, 82, 628-654.

32. Yarranton, H. W.; Sztukowski, D. M.; Urrutia, R. *J. Colloid Interface Sci.* **2007**, 310 (1), 246-252.

33. Yarranton, H. W.; Sztukowski, D. M.; Urrutia, R. *J. Colloid Interface Sci.* **2007**, 310 (1), 253-259.

34. McLean, J. D.; Kilpatrick, P. K. *J. Colloid Interface Sci.* **1997**, 196 (1), 23-34.

35. Langevin, D.; Argillier, J-F. *Adv. Colloid Interface Sci.* **2015**, DOI: http://dx.doi.org/10.1016/j.cis.2015.10.005.

36. Taylor, S.D.; Czarnecki, J.; Masliyah, J. *J. Colloid Interface Sci.* **2002**, 252 (1), 149-160.

37. Jestin, J.; Simon, S.; Zupancic, L.; Barré,L. *Langmuir* **2007**, 23 (21), 10471-10478.

38. Zhang, L. Y.; Lawrence, S.; Xu, Z.; Masliyah, J. H. *J. Colloid Interface Sci.* **2003**, 264 (1), 128-140.

39. Woodward, N. C.; Gunning, A. P.; Maldonado-Valderrama, J.; Wilde, P. J.; Morris, V. J. *Langmuir* **2010**, 26 (15), 12560-12566.

40. Gao, S.; Moran, K.; Xu, Z.; Masliyah, J. *Energy & Fuels* **2009**, 23 (5), 2606-2612.

41. Forth, J.; French, D. J.; Gromov, A. V.; King, S.; Titmuss, S.; Lord, K. M.; Ridout, M. J.; Wilde, P. J.; Clegg, P. S. *Langmuir* **2015**, 31 (34), 9312-9324.

42. Rane, J.P.; Pauchard, V.; Couzis, A.; Banerjee, S. *Langmuir* **2013**, 29 (15), 4750-4759.

43. Miller, R.; Ferri, J. K.; Javardi, A.; Krägel, J.; Mucic, N.; Wüstneck, R. *Colloid Polym. Sci.* **2010**, 288 (9), 937-950.

44. Pauchard, V.; Rane, J. P.; Banerjee, S. *Langmuir* **2014**, 30 (43), 12795-12803.

45. Liggieri, L.; Santini, E.; Guzmán, E.; Maestro, A.; Ravera, F. *Soft Matter* **2011**, 7, 7699-7709.

46. Ravera, F.; Loglio, G.; Kovalchuk, V. I. *Curr. Opin. Colloid Interface Sci.* **2012**, 15 (4), 217-228.

47. Maldonado-Valderrama, J.; Rodríguez Patino, J. M. *Curr. Opin. Colloid Interface Sci.* **2010**, 15 (4), 271-282.

48. Natarajan, A.; Kuznicki, N.; Harbottle, D.; Masliyah, J.; Zeng, H.; Xu, Z. *Langmuir* **2014**, 30 (31), 9370-9377.

49. Freer, E. M.; Radke, C. J. *J. Adhesion* **2004**, 80 (6), 481-496.

50. Erni, P.; Jerri, H. A.; Wong, K.; Parker, A. *Soft Matter* **2012**, 8, 6958-6967.

51. Erni, P. *Soft Matter* **2011**, 7 (17), 7586-7600.

CHAPTER 5 PROBING MECHANICAL PROPERTIES OF WATER-CRUDE OIL EMULSION INTERFACES USING ATOMIC FORCE MICROSCOPY*

5.1 INTRODUCTION

Water-in-crude oil emulsions pose a significant challenge in the petroleum industry. Small water droplets and solids, a few microns in diameter, cannot be completely removed during surface processing and thus migrate downstream, accelerating corrosion and equipment malfunctions which can lead to production losses.[1-3] These fine water droplets are stabilized by a layer of hydrocarbons and do not coalesce, even upon contact under applied load. The main hydrocarbon fraction responsible for the high emulsion stability is believed to be asphaltenes, the most problematic surface-active component in crude oils.[4] Asphaltenes are soluble in toluene and insoluble in *n*-heptane.[1] Steric stabilization from the interfacial asphaltene layers and non-uniform drainage of the intervening liquid films as water droplets are pressed together lead to enhanced emulsion stability.[5-7] The strongly elastic interfacial layers act as a mechanical barrier between water droplets and must be deformed beyond the shear yield strength to initiate droplet coalescence.[4,5,7,8] Although other bitumen components such as resins and naphthenic acids cannot stabilize water-in-oil emulsions alone, they interact with asphaltenes to enhance emulsion stability.[9,10] Asphaltenes are also known to

* A version of this chapter has been submitted to the special edition of *Energy & Fuels*, dedicated to the Petrophase 2016 conference.

change the surface properties of hydrophilic solids (clays), making them bi-wettable and enhancing their potential to partition at the oil-water interface.[11-13] Solids of intermediate hydrophobicity (water contact angles close to 90^{o}) and in the size range of 0.22 - 8 μm were shown to be most effective in stabilizing water-in-oil emulsions.[14]

Demulsifiers are commonly added to crude oil to enhance phase separation of water-in-oil emulsions.[15] Gradual accumulation of demulsifier molecules at the oil-water interface weakens the interfacial protective layer. Once a sufficient concentration of demulsifier molecules at the interface is reached, water droplet flocculation and/or coalescence occurs upon contact.[16] Previous studies reported a biodegradable polymer, ethyl cellulose (EC), to be an effective demulsifier for water-in-diluted bitumen emulsions. Addition of EC increased the flocculation-enhanced coalescence of water droplets through displacement of the protective interfacial layer.[11,16,17]

Methods such as bottle tests and/or measurements of water content in oil (titration) are frequently used to determine the stability of emulsions. However, a much deeper understanding of emulsion stabilization mechanisms can be derived from studying the mechanical properties of the oil-water interfacial layer under compression and shear.[18-20] Shear rheology, a relatively new experimental technique,[20-22] is sensitive to layer growth and structural changes at the interface, whereas dilatational rheology highlights the interfacial coverage of surface active species and provides insights into dynamic changes of interfacial properties.[18] However, a direct link between experimental results and emulsion stability of

"real" process systems, where emulsified droplets collide randomly due to Brownian motion or under imposed shear, is often difficult to establish.

Droplet coalescence, which promotes the phase separation of immiscible liquids, is often inhibited by the presence of surface-active species, such as asphaltenes at the oil-water interface. These adsorbed species influence the surface forces acting between neighboring droplets and affect emulsion stability by controlling the drainage rate and rupture of the thin liquid film separating two droplets.[23] Measuring the interaction forces as the oil-water interfaces deform due to the close proximity of neighboring droplets is fundamental to understanding emulsion stabilization mechanisms.

Atomic force microscopy (AFM) has been widely used to investigate forces between solid surfaces (clean or coated). It has been extended to study deformations of oil-water and air-water interfaces and to measure surface forces between droplets or gas bubbles in aqueous systems.[24] Measurement of surface forces between a probe and rigid substrate using AFM has been well described, and true separation between the colloidal probe and rigid substrate can be determined from the slope of constant compliance, where the force (F) depends linearly on piezo displacement. For systems involving a deformable interface, zero separation distance becomes more difficult to determine due to the coupling effect of interfacial deformation and cantilever bending upon applied force.[25-30]

Adsorbed interfacial species can greatly influence interaction forces and also govern the degree of droplet deformation under applied load, with the latter greatly influenced by interfacial rigidity.[31] In the absence of hydrodynamic

effects, droplet deformations result from the interaction forces exceeding the Laplace pressure.[29,32] When droplets are pushed together, instead of reducing the distance of closest approach between the droplet interfaces, as in the case of rigid substrates, the droplets flatten to increase their effective interaction area, with the separation distance unchanged under the condition of disjoining pressure of the intervening liquid film being equal to the Laplace pressure.[33]

A theoretical approach has been developed to calculate the forces and deformations for particle-droplet, particle-bubble, droplet-droplet and bubble-bubble systems by utilizing the augmented Stokes-Reynolds-Young-Laplace (SRYL) equations.[29,35] Droplet deformation can be well predicted for viscous interfaces where droplet shape is described by the Young-Laplace equation.[29,32,35-40] However, there is limited research which considers industrially relevant systems, such as water droplets in oil,[42] or interfaces with significant elasticity, for which the criterion of a Laplacian response no longer holds.[43] Our previous study[44] explored viscoelastic effects encountered in water-in-crude oil emulsion systems. Oil-water interfacial stiffening and "skin" formation was observed upon water droplet aging in asphaltene solution, leading to the gradual formation of a viscoelastic oil-water interface. Incorporating dilatational elasticity into the SRYL equations was shown to accurately describe the deformation of aged water droplets under applied load.

The current research measures interaction forces between a silica sphere ($D \approx 8$ μm) and water droplets ($D \approx 70$ μm) in asphaltene- or bitumen-in-toluene solutions. The importance of interfacial deformation and hydrodynamics is

investigated. Interaction forces and droplet deformations were measured with AFM for aged interfaces, and following demulsifier (EC) addition. This approach allows tracking of droplet deformation and forces *in-situ*, moving away from bulk and planar studies to industrially-relevant coalescing systems, with interfaces exhibiting elasticity. The water-crude oil system provides a unique opportunity to study interfaces which are originally viscous-dominant (Laplacian) and develop elasticity over time (non-Laplacian), while demulsifier addition reverts the interfacial aging. Tracking of these properties with AFM allows one to estimate the effectiveness of various surface active species, and the forces required to create and break emulsion systems.

5.2 MATERIALS AND METHODS

5.2.1 Materials

Vacuum distillation feed bitumen was kindly provided by Syncrude Canada Ltd. High-performance liquid chromatography (HPLC)-grade toluene and *n*-heptane were purchased from Fisher Scientific (Canada). Deionized water with a resistivity of 18.2 MΩ·cm was prepared with an Elix 5 system and purified with a Millipore-UV plus system. Silicon wafers, purchased from NanoFab (University of Alberta), were used as substrates. Tipless cantilevers for force measurements and silicon nitride cantilevers for imaging were purchased from Bruker Scientific (USA). Silica microspheres (D ≈ 8 μm) were purchased from Duke Scientific (USA) and mounted on the tipless cantilevers to form colloidal probes. Ethyl cellulose with an ethoxyl content of 48 % and viscosity of 4 cP (EC-4; CAS 9004-57-3) was purchased from Sigma Aldrich (Canada).

5.2.2 Asphaltene Precipitation and Solution Preparation

Details on the asphaltene precipitation method have been reported elsewhere.[45] Briefly, vacuum distillation feed bitumen was diluted with HPLC-grade toluene and centrifuged to remove fine solids. Toluene was then evaporated from the supernatant and *n*-heptane was added to the solids-free bitumen at a ratio of 40:1 by weight; the mixture was subsequently shaken on a mechanical shaker for 2 hr. After the supernatant was removed from the *n*-heptane-bitumen mixture, fresh *n*-heptane was added to wash away entrained maltenes in the precipitated asphaltenes. The centrifugation- maltenes removal process was repeated until the supernatant appeared clear.

Fresh asphaltene- and bitumen-in-toluene solutions were prepared for each experiment by dissolving the required amount of asphaltenes or bitumen in toluene, and sonicating the solution for 15 min in an ultrasonic bath. To compare the two systems, bitumen concentration was adjusted to produce an equivalent asphaltene concentration, i.e. 0.588 g/L bitumen-in-toluene equaled 0.1 g/L asphaltene-in-toluene. The bitumen: asphaltene ratio was determined from the asphaltene precipitation method previously described. Two additional asphaltene concentrations (0.05 and 0.2 g/L) were also considered in this study.

EC-4 stock solution of 1 g/L was prepared by adding the required amount of EC to toluene and sonicating the mixture for 15 min in an ultrasonic bath. The role of EC-4 as an effective demulsifier was assessed by dosing EC-4 at 0.13 g/L into asphaltene or bitumen solutions with an immersed water droplet. The dosing

concentration was based on previous findings which showed effective demulsification of water-in-oil emulsions at 130 ppm (0.13 g/L).[16]

5.2.3 Cantilever and Substrate Preparation

Silica spheres (D ≈ 8 μm) were glued onto the tip of the long wide-beam or short narrow-beam AFM cantilever (model NP-O10 (Bruker, USA)) using a two-component epoxy (EP2LV, Master Bound, USA). The modified probes were placed in a vacuum desiccator for 24 hr and subsequently exposed to UV for 1 hr. Cantilever spring constant values were ~ 0.12 N/m for the short narrow-beam and ~ 0.22 N/m for the long wide-beam probes. These values did not change significantly during force measurements (< 10 %).

Silicon wafers used as underlying substrates for anchoring water droplets in oil, were treated with piranha solution for 1 hr, then soaked in 1 mM Octadecyltrichlorosilane-in-toluene solution (OTS; ACROS Organics, Belgium) for 30 s. The substrates were subsequently rinsed with toluene and dried with nitrogen, resulting in an intermediate contact angle of 45-50° in air. The contact angle of these substrates was measured to be 84° in toluene and 86° in asphaltene- and bitumen-in-toluene solutions, as shown in Appendix C, Figure C-1.

For force measurements between two water droplets, the underlying substrate was treated with 1 mM OTS-in-toluene solution for 2 min, resulting in a contact angle of 86° in air and 150° in toluene. This resulted in weakly attached water droplets to the substrate in solution and enabled easy pick-up of the water droplets by the AFM cantilever for droplet-droplet measurements.

5.2.4 The Measurement of Contact Angle and Interfacial Tension

The water droplet contact angles on the solid substrate in air and in solvent as well as the interfacial tension for water/asphaltene solution and water/bitumen solution were measured using a Theta Optical Tensiometer T200 (Biolin Scientific, Stockholm, Sweden). The tensiometer camera was calibrated prior to each experiment and fresh asphaltene/bitumen solutions prepared for each test.

Contact angle measurements for treated silicon wafers were conducted either in air or in asphaltene- and bitumen-in-toluene solutions. For measurements in air, a water droplet ($V \approx 9$ μL) was deposited on the treated substrate and brought into focus. The droplet profile was recorded for 3 min at 3 fps and the contact angle determined using the Theta software. For measurements in solvent, the substrate was placed in a quartz cell and a water droplet ($V \approx 9$ μL) deposited on the substrate before gently adding asphaltene or bitumen solution to the quartz cell. The water droplet contact angle was recorded over 60 min at 3 fps to provide comparison with the AFM study.

For interfacial tension measurements a water droplet ($V \approx 6$ μL) was generated from a 1 mL gastight Hamilton syringe with an 18 gauge needle (Reno, NV). The water droplet profile in either asphaltene or bitumen solution was captured at 12 fps for 60 min and analyzed using the Theta software. Three measurements were conducted per test condition and the variation in the measured values was less than 10 %. To measure the effect of demulsifier the EC-4 stock solution was added to the quartz cell following the aging of a water droplet in asphaltene or

bitumen solutions for 1 hr. The interfacial aging time and demulsifier concentration (0.13 g/L) were consistent with the AFM study.

5.2.5 AFM Force Measurements

Interaction forces between a silica sphere and water droplets were measured using the Agilent 5500 AFM, equipped with a sealed environmental chamber. Deflection sensitivity and spring constant values of the cantilevers against the substrate were calculated by the Thermal K function in the AFM software before and after force measurements.

Water (0.5 wt. %) was added to the various asphaltene and bitumen solutions and sonicated for 5 s to form an emulsion which was then injected into the AFM liquid cell. The setpoint for the force measurements was set to 0 V, while the piezo displacement- to 4 μm. All measurements were conducted at room temperature (24 °C). To eliminate the effect of solvent evaporation and subsequent changes in solvent concentration, interfacial aging was limited to 1 hr.

In this study, the following AFM force measurements were conducted:

1. **Probe-droplet interactions with a cantilever velocity of 1 μm/s.** For probe-droplet force measurements water droplets (D ≈ 60 - 80 μm) remained strongly anchored on a partially hydrophobized (86°) substrate in asphaltene or bitumen solutions. The water droplets were aged for a predetermined time before the cantilever with the 8 μm silica particle was centered over the selected droplet and approached the oil-water interface at 1 μm/s. Following 1 hr aging, EC-4 stock solution was added to the AFM liquid cell (1 mL total

volume) at a net EC concentration of 0.13 g/L. The first force profile following the addition of EC-4 was collected at 7 min due to the intricate experimental setup and cantilever approach time.

2. **Effect of hydrodynamics for the probe-droplet system.** To measure the effect of hydrodynamics the cantilever velocity was varied between 0.5 and 20 μm/s. Force curves between the silica particle and water droplet were collected following 15 min aging in 0.1 g/L asphaltene-in-toluene solution. A 5 s delay between each force measurement was selected to allow the interface to equilibrate and dissipate any interference between consecutive force measurements, especially at high velocities. Interfacial aging was not observed during these measurements, as verified by the slope of the high force constant compliance region (k = 28.5 mN/m) remaining unchanged within the experimental time frame. It should be noted that the Force-Displacement curves reported in this study show unprocessed piezo displacement instead of "true" separation between the probe and droplet. Additional techniques such as confocal microscopy, or theoretical analysis are required to obtain "true" separation when the measurements involving a deformable interface are conducted.[29,39]

3. **Droplet-droplet interactions.** For droplet-droplet measurements in asphaltene solution, the cantilever was first positioned above a fresh water droplet on the hydrophobized substrate (150°) and lowered into contact using the same setpoint voltage as for the case of particle-droplet interaction. For freshly prepared water droplets in asphaltene solution (aging time less than 5

min), the droplet readily spreads on the surface of the cantilever. This was achieved by holding the cantilever in contact with the droplet for 5 s before retracting the cantilever and removing the droplet from the underlying substrate. The selected droplet (D ≈ 70 μm) was subsequently used to measure droplet-droplet interactions in 0.1 g/L asphaltene-in-toluene solution after 15 min aging. The cantilever approach and retract velocity was fixed at 1 μm/s.

5.3 RESULTS AND DISCUSSION

5.3.1 Force Interactions between Rigid and Deformable Interfaces

The geometrical configuration of adsorbed layers on solid surfaces is frequently extrapolated to explain interactions in the presence of surface active agents, as encountered in emulsion systems. However, direct comparisons between "model" planar surfaces and "real" emulsion interfaces are difficult to make, since droplet curvature and deformation greatly affect the adsorption and displacement of surface-active species.[31]

For the crude oil system, AFM was used to compare the interaction forces between asphaltenes adsorbed on solids and those at liquid interfaces (Figure 5.1). To ensure the development of a uniform asphaltene layer the surfaces/interfaces were allowed to age for 15 min.[12]

Case I: Force curves were collected at 15 min following the injection of 0.1 g/L asphaltene-in-toluene solution between the silica particle and planar substrate (i.e. two rigid surfaces). During approach and retraction, short-range steric repulsion and weak adhesion (0.5 nN), with a relatively abrupt pull-off was observed

(Figure 5.1). The occurrence of repulsion is in agreement with previously published data, where the swollen asphaltene structure of polyaromatic core and aliphatic branches led to steric hindrance in good solvent (toluene).[46,47] Interpenetration of the aliphatic branches of asphaltenes leads to the observed adhesion between the two asphaltene layers. The slope of the constant compliance region is very high at 1457 mN/m (Table 5.1), as expected for interactions between rigid surfaces.

Case II: 0.1 g/L asphaltene-in-toluene solution was injected into the AFM liquid cell, and the interaction forces between a silica particle and a deformable oil-water interface (water droplet pinned on the silica substrate) was measured at 15 min interfacial aging. Upon cantilever approach (Figure 5.1) the slope of the high force constant compliance region is much lower (28.9 mN/m) than that for coated substrates (Case I), indicating a more deformable interface. Upon cantilever retraction, the net adhesion force between the two interacting surfaces is significantly greater than that between the two rigid surfaces (2.4 nN versus 0.5 nN). The substantial increase in adhesion likely results from an increase in the contact area, as the solid particle is surrounded by the deformable oil-water interface (see schematic in Figure 5.1). It should be noted that the colloidal silica probe did not break the oil-water interface, since the laser signal would be lost in that case.

Case III: 0.1 g/L asphaltene-in-toluene solution was injected into the AFM liquid cell prior to measuring the interaction forces between two water droplets. The AFM cantilever with the attached water droplet ($D \approx 70$ μm) was positioned over

a second water droplet of similar size (D ≈ 80 μm) and interaction forces measured at 15 min aging. In this case, the slope of the high force constant compliance region was 10.6 mN/m; this reduced slope is once again attributed to increased deformation in the system (Figure 5.1). The presence of a second deformable droplet led to a further increase in the adhesion force on retraction (5.4 nN), likely from the increased contact area and "flattening" of the interface as droplets are brought together. For the various systems considered in this study, it should be noted that the reported adhesion forces in Figure 5.1 (b) and Table 5.1 represent the total adhesion force, which is influenced by the geometry of the interacting surfaces, i.e. contact area for droplet-droplet >> particle-substrate.

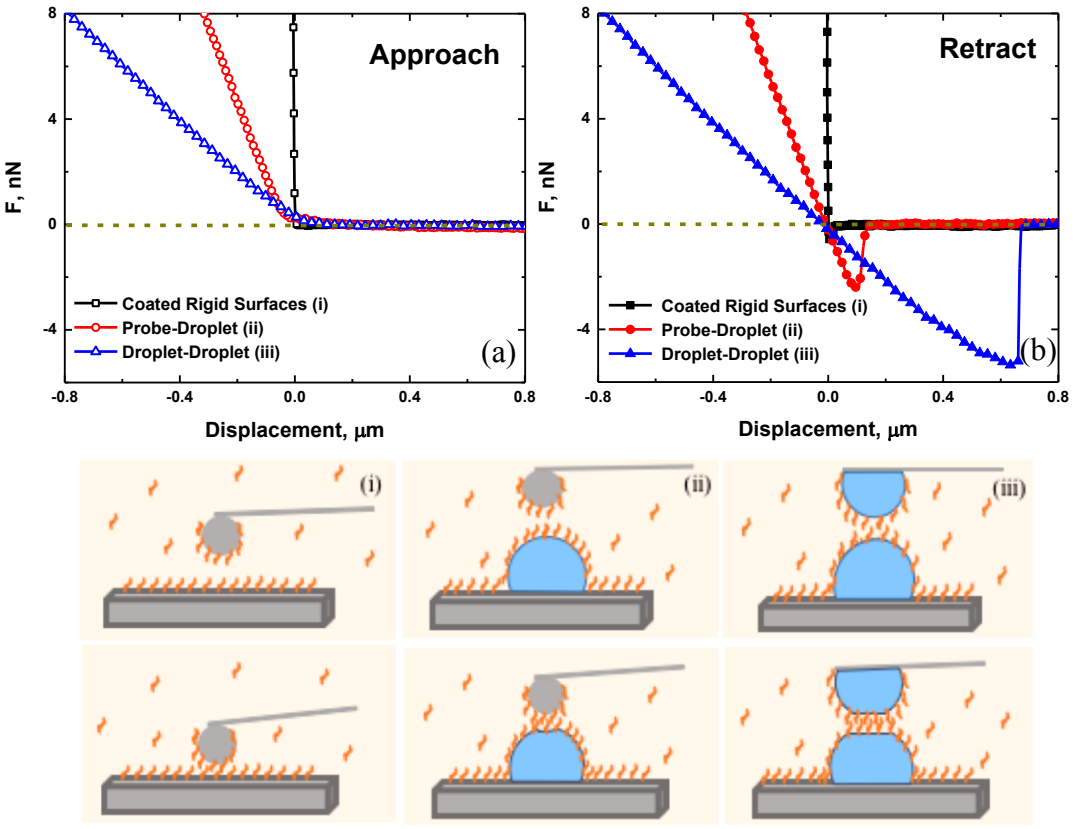

Figure 5.1 Interactions between various surfaces upon (a) approach (open

symbols) and (b) retract (filled symbols) after 15 min aging in 0.1 g/L asphaltene-in-toluene solution. Symbols: interactions between (i) coated rigid surfaces; (ii) a silica probe (D ≈ 8 μm) and water droplet (D ≈ 80 μm); (iii) two water droplets of similar size (D ≈ 70 and 80 μm). The schematic below the experimental data features the different systems far apart (top row) and in close proximity (bottom row), demonstrating the likely interfacial deformations.

Table 5.1 The net adhesion force (F_{ad}) and slope of the constant compliance region (k) from Figure 5.1.

	k (mN/m)	**F_{ad} (nN)**
Coated Rigid Surfaces in Asphaltene Solution (i)	1457	0.5
Probe-Droplet in Asphaltene Solution (ii)	28.9	2.4
Droplet-Droplet in Asphaltene Solution (iii)	10.6	5.4

5.3.2 Effect of Hydrodynamics on the Interaction Forces

In most surface forces studies, cantilever approach and retract velocities are often set in the range of 0.5 - 2 μm/s to minimize the effect of hydrodynamics.[29,40] However, hydrodynamic forces can affect interactions between droplets in "real" emulsion systems, where flows are present.[25,48]

Figure 5.2 shows the effect of cantilever velocity on interaction forces between the colloidal probe and water droplet following 15 min aging in 0.1 g/L

asphaltene-in-toluene solution. The cantilever approached the interface followed by an immediate retraction. Two distinct features are clearly observed as the cantilever velocity is varied between 0.5 μm/s and 20 μm/s. Firstly, an increase in the cantilever velocity results in a longer-ranged repulsion force on approach. At low velocities, the repulsion arises from a combination of surface forces (steric force) and droplet deformation,[38,41] while hydrodynamic drainage dominates the interactions at higher approach velocities. The droplet will flatten as the combination of disjoining and hydrodynamic pressures exceed the Laplace pressure. The extended range over which repulsion is measured upon approach at higher velocities relates to the relative inability of the thin liquid film between the probe and water droplet to drain.[29,32,40] The "trapping" of the intervening liquid results in a buildup of pressure and an increase in repulsion force.[29]

Secondly, on retraction, an increase in the magnitude and range of the attractive force minimum (adhesion) is observed due to the limitation of the liquid drainage rate compared to the separation rate of the two interacting surfaces, which would result in hydrodynamic suction.[40,49] Hysteresis between the approach and retract force curves becomes more significant at higher cantilever velocities due to the increase in hydrodynamic pressure, with similar findings reported for particle-oil droplet and two oil droplets interacting in aqueous solutions.[29] The hysteresis shown in Figure 5.2 is higher than that reported for droplet-planar substrate systems,[50] likely due to the high local interfacial curvature.[40] Due to the rapid nature of these force measurements (within a few minutes), interfacial aging

effects were assumed to be negligible, as confirmed by an unchanged slope of the constant compliance region (k = 28.5 mN/m).

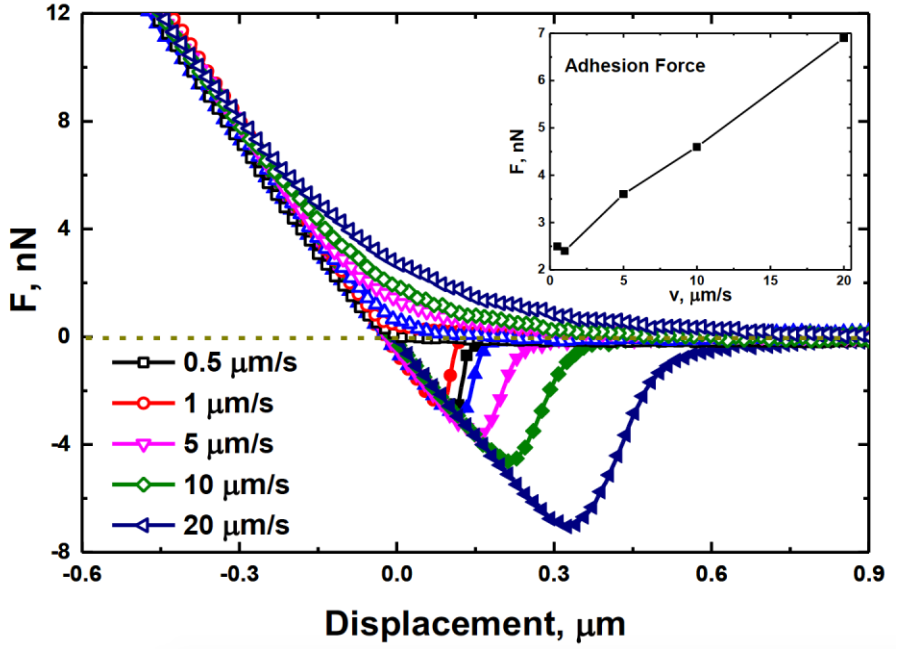

Figure 5.2 Interaction forces between silica probe (D ≈ 8 µm) and water droplet (D ≈ 70 µm) in 0.1 g/L asphaltene-in-toluene solution after 15 min aging. Cantilever approach and retraction force curves represented by the open and filled symbols, respectively. The inset shows adhesion forces as a function of cantilever velocity.

5.3.3 Adhesion forces in Asphaltene- and Bitumen-Stabilized Systems

A comparison between adhesion forces measured in asphaltene and bitumen solutions is shown in Table 5.2. Interaction forces were measured between a silica colloidal probe and water droplet at 15 min following the injection of the test solution. Asphaltene concentration was varied between 0.05 and 0.2 g/L, with the corresponding bitumen concentration equal to 0.284 and 1.117 g/L, respectively.

Studying equivalent asphaltene concentrations in toluene and bitumen with AFM allows us to directly compare *in-situ* the forces acting between interfaces stabilized by asphaltenes and other interfacially active components in bitumen, such as resins and naphthenic acids.[9,10]

The adhesion force between the silica particle and water droplet was shown to be in the range of 3.2 - 4.1 nN and 3.8 - 4.7 nN for asphaltene and bitumen solutions, respectively. While the range of measured adhesion is attributed to the changes in asphaltene concentration, it is worth noting that the adhesion forces measured in bitumen solutions are consistently slightly higher than those measured in asphaltene solutions. While asphaltenes are expected to be the dominant interfacial component,[6,7] the presence of other indigenous species in bitumen clearly contribute to the overall adhesion between two interacting interfaces.[51] The 'jump' in adhesion force at the highest asphaltene concentration may be justified by the increased interpenetration of voluminous asphaltene layers. At high asphaltene concentrations, previous research using surface forces apparatus (SFA), showed that the asphaltene layer thickness increases more rapidly, forming thick (multi-layer) interfacial layers which exhibit significant compressibility under normal force (i.e. soft, voluminous layers). Increased layer compressibility contributes to higher adhesion forces due to increased interpenetration and contact area between asphaltene layers.[46,52]

Table 5.2 The adhesion force (F_{ad}) between a silica probe (D ≈ 8 μm) and water droplet in asphaltene and bitumen solutions of equivalent asphaltene concentrations after 15 min aging.

Asph. Conc. (g/L)	**Adhesion Force F_{ad} (nN)**	**Bit. Conc. (g/L)**	**Adhesion Force F_{ad} (nN)**
0.05	3.2 ± 0.6	**0. 284**	3.8 ± 0.6
0.1	3.3 ± 0.6	**0.588**	3.6 ± 0.6
0.2	4.1 ± 0.8	**1.117**	4.7 ± 0.9

5.3.4 The Effect of Interfacial Aging and Demulsifier Addition

Water-oil interfaces have been shown to age as surface active species such as asphaltenes, fine particles, and surfactants partition at the liquid-liquid interface to form an interfacial layer in crude oil systems.[4,8,20] The dominant interfacially active species in bitumen is asphaltenes, as inferred from Table 2 and from other studies.[1-7,9,10] Asphaltene layers have been shown to exhibit time-dependent elasticity, with increased aging time resulting in a stable (solid-like) interfacial layer that can resist yielding.[7,53] The rheological properties of the interfacial layer, more specifically the elastic modulus, has been shown to correlate to emulsion stability.[54]

Our previous study demonstrated interfacial "stiffening" upon aging of a water droplet in asphaltene solution, and non-Laplacian behavior of the interface was highlighted by interfacial crumpling upon droplet volume reduction.[44] The same

phenomena of interfacial stiffening for a water droplet in bitumen solution is shown in the inset of Figure 5.3. For 0.588 g/L bitumen-in-toluene the slope of the constant compliance region after 15 min aging is 32 mN/m and increases to 45 mN/m after 1 hr aging, comparable to the results for the asphaltene systems previously reported.[44] The increasing slope of constant compliance in bitumen solution is also attributed to an increase in dilatational elasticity, since the change in water-bitumen interfacial tension (15- 60 min), as shown in Figure 5.4, cannot suitably describe the measured changes in the slope of the constant compliance region.

To reduce the stiffness of the interfacial layer, amphiphilic demulsifier molecules are typically dosed at the ppm level in the organic phase to disrupt the interfacial network. The interaction forces between the silica probe ($D \approx 8$ μm) and water droplet ($D \approx 70$ μm) aged in 0.1 g/L asphaltene- and 0.588 g/L bitumen-in-toluene solutions for 1 hr and subsequently dosed with 0.13 g/L EC-4 are shown in Figure 5.3.

Firstly, considering the asphaltene system, the slope of the constant compliance region following 1 hr aging and in the absence of EC-4 is 41 mN/m, and the associated adhesion force between the particle and water droplet is 5.6 nN. Upon addition of EC-4, the slope of the constant compliance region and the particle-water droplet adhesion force continually decreases with demulsification time. Unfortunately, due to the complexity of the measurement technique, we were unable to collect data within the first several minutes following demulsifier addition. The resulting time delay led to a significant reduction in the slope of

constant compliance with k = 18.5 mN/m and 18.2 mN/m at 7 and 8 min demulsification time, respectively. While gradual softening of the interfacial layer is clearly measured at longer demulsification times, the significant reduction in the slope of constant compliance within the first 7 min indicates that the demulsification process is rather rapid. To study the competitive adsorption of EC-4 at the oil-water interface, the interfacial tension of a water droplet in asphaltene solution was measured, as shown in Figure 5.4. During the first hour of aging the interfacial tension reduced from 32 mN/m to 25 mN/m, confirming asphaltene adsorption, which has been shown to be a diffusion-limited process at short aging times.[46] At 1 hr interfacial aging, EC-4 was dosed to the asphaltene solution at a concentration of 0.13 g/L, with the interfacial tension was continuously measured. The oil-water interfacial tension reduced to 12 mN/m in less than one minute, and further reduced by 2 mN/m in the next 15 min. The reduction in interfacial tension following EC-4 addition confirms that the competition of EC-4 molecules for available surface sites at the oil-water interface is rapid, followed by a secondary dynamic which is much slower and possibly related to the relaxation and reorganization of EC-4 molecules. The slower secondary dynamic supports the softening of the oil-water interface at longer demulsification times, as measured using the AFM technique (Figure 5.3). It is worth noting that after 15 min demulsification time, the oil-water interfacial tension is almost equivalent to the equilibrium EC-4 only solution in toluene (IT = 9.5 mN/m), confirming significant displacement of the pre-formed asphaltene layer. While interfacial tension measurements are useful to study the competitive

adsorption of surface active molecules, the reduction in oil-water interfacial tension alone is not always a suitable indicator for demulsification, and rather an approach to track the mechanical properties of the interfacial layer, for example with AFM, is favored. Overall, the AFM results show a reduction in the mechanical stiffness of the interfacial layer following the addition of EC-4 demulsifier. These findings are consistent with interfacial shear rheology measurements conducted at an asphaltene-stabilized planar oil-water interface, reporting diminished elasticity of the interface upon demulsifier addition.[15,56]

A similar effect of interfacial layer softening was observed for the bitumen system in our study. It is interesting to note that the interfacial tensions for the asphaltene and bitumen systems almost overlap (likely indicating asphaltenes to be the dominant interfacial component), and show a similar reduction in the interfacial tension following addition of EC-4 (Figure 5.4). At 1 hr aging, EC-4 was dosed into the bitumen solution and the slope of constant compliance decreased from 45 mN/m to 17.9 mN/m (demulsification time = 10 min). The adhesion force between silica particle-water droplet was shown to reduce with increasing demulsification time. AFM is able to track in situ in real time the changes in the mechanical properties of interfacial network. The reduction in adhesion force upon addition of EC confirms the rearrangement of the molecules at the interface and likely the formation of fractures in the network. Previous work highlighted ability of EC to flocculate water droplets at low concentrations. At high concentrations, however, EC addition promotes droplet coalescence, which would only occur upon rearrangement and/or “breaking” of the original stabilizing

interfacial network.[16] EC-4 has also been shown to reduce the thickness of the asphaltene/ bitumen interfacial film and irreversibly displace the asphaltenes/ bitumen from the interface.[17]

With the addition of EC-4, the interfacial properties of the stabilized water droplet became sufficiently modified as such that the silica probe was engulfed by the water droplet upon cantilever approach. The critical demulsification time at which the silica particle would break the oil-water interface was 10 min and 12 min in asphaltene and bitumen solutions, respectively. Engulfment of the colloidal probe in the water droplet was easily identified by a loss of the laser signal. It is interesting to note that force measurements could not be conducted in EC-only solution and in "pure" toluene, as the probe was engulfed into the droplet immediately. Therefore, at the critical demulsification time for asphaltene and bitumen solutions, the film has softened significantly, and fractures in the asphaltene/bitumen network led to particle immersion in the droplet. It should be noted that for water droplets in oil, the double layer forces are negligible, and the interaction forces are attributed to steric and van der Waals forces.

To ensure that the measured changes in the slope of constant compliance result from changes to the interfacial layer mechanical properties, the colloidal probe and water droplet were individually assessed in the different solvent environments. Hydrophilic silica was exposed to asphaltene and bitumen solutions, and subsequently to EC-4, to represent changes to the surface properties of the colloidal probes. AFM topographical images of the substrates, given in Appendix C (Figure C-2 and Table C-1), show no significant change in aggregate

height and roughness with increasing asphaltene/ bitumen concentration after demulsifier addition. Therefore, the changes in force and droplet deformation observed in Figure 5.3 are due to the changes in the structure of the layer at the oil-water interface.

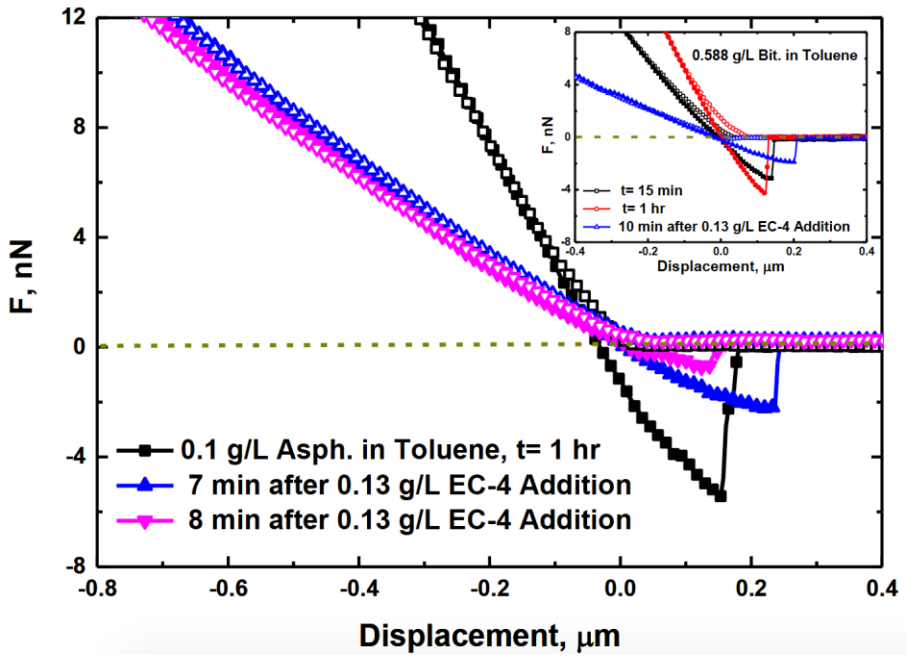

Figure 5.3 Interaction forces between silica probe (D ≈ 8 μm) and water droplet (D ≈ 70 μm) in 0.1 g/L asphaltene-in-toluene at 1 hr aging and following the addition of 0.13 g/L EC-4. Cantilever approach and retraction force curves represented by the open and filled symbols, respectively. The cantilever velocity remained fixed at 1 μm/s. Inset: force profiles for a water droplet in 0.588 g/L bitumen-in-toluene solution (D ≈ 60 μm) prior to and after EC-4 addition.

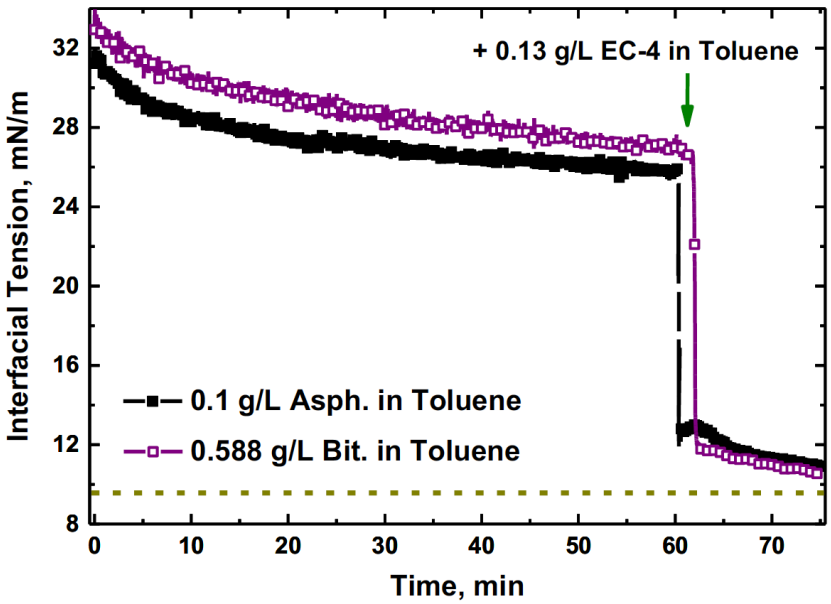

Figure 5.4 Time-dependent interfacial tension (IT) of a water droplet in 0.1 g/L asphaltene- and 0.588 g/L bitumen-in-toluene solution. EC-4 was added (indicated by the arrow) to the solutions at a net concentration of 0.13 g/L. The dashed line represents the equilibrium IT value of a water droplet in 0.13 g/L EC-4-in-toluene solution.

To further understand the mechanisms of droplet deformation, the high force SRYL model was applied to predict water droplet deformation in asphaltene solution upon aging and after demulsifier addition (Figure 5.5). The widely used high force SRYL equations with a pinned contact line boundary condition, developed for viscous Laplacian interfaces are given by:[29, 32, 33]

$$\Delta D(y) \equiv \frac{F(t)}{4\pi\sigma}\left[\ln\left(\frac{F(t)R_{ds}}{8\pi\sigma R_o^2}\right) + 2B(\theta) - \frac{4\pi\sigma}{K} - 1\right] \quad (1)$$

$$B(\theta) = 1 + \frac{1}{2}\ln\left[\frac{1+\cos(\theta)}{1-\cos(\theta)}\right] \quad (2)$$

$$R_{ds} \equiv \frac{1}{\left[\frac{1}{R_O}+\frac{1}{R_S}\right]} \quad (3)$$

where ΔD is the predicted displacement, $F(t)$ is the measured force, R_o is the radius of the unperturbed droplet and R_s is that of the spherical probe; θ is the contact angle of the droplet on the substrate, σ is the interfacial tension, and K is the spring constant of the cantilever.

To predict the deformation of a water droplet, both the contact angle and oil-water interfacial tension should be known. The water droplet contact angle in asphaltene solution was measured to be 86° and remained independent of droplet aging, and even following the addition of EC-4 (Appendix C, Figure C-1). However, the oil-water interfacial tension slowly decreased during asphaltene adsorption, and rapidly decreased following the addition of EC-4 (Figure 5.4).

Using the appropriate measured values, Figure 5.5 shows the discrepancy between the experimental data and droplet deformation predicted by the SRYL equations for a water droplet aged for 1 hr in 0.1 g/L asphaltene-in-toluene solution. As shown in our previous study, the change in interfacial tension upon droplet aging (Figure 5.4) is not sufficient to explain the time-dependent "stiffening" of the oil-water interface. The elasticity of the interface after 1 hr aging, measured by dilatational rheology, increased to 16 mN/m (data not shown), confirming the formation of a rigid asphaltene network.[44] To account for this high elasticity contribution an experimentally measured viscoelasticity parameter (σ/E') is included as an extra term inside the brackets of Eqn. 1. Inclusion of the viscoelasticity parameter provides good agreement between experiment and theory when the interfacial elasticity is a significant contribution to the overall

interfacial stress. Interestingly, following the addition of EC-4, the modified SRYL model provides poor agreement to the experimental data. Due to the significant softening of the interfacial layer and a return to a Laplacian-like response, the dilatational elasticity is no longer a substantial component of the total interfacial stress; hence, the experimental data is best fitted using the SRYL equations, as shown in Figure 5.5. This behavior is consistent with a diminishing interfacial elasticity following demulsifier addition,[15] which correlates with reduced emulsion stability.[56]

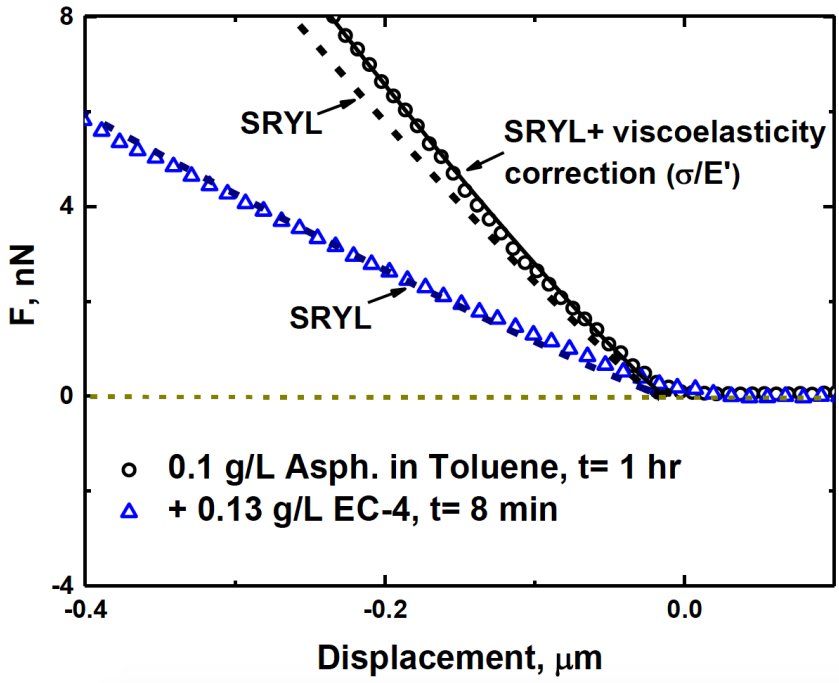

Figure 5.5 Measured forces (symbols) in 0.1 g/L asphaltene-in-toluene solution and after EC-4 addition upon approach, plotted against SRYL model predictions.

5.4 CONCLUSIONS

This study considered the interactions between a silica probe and water droplet in asphaltene- and bitumen-in-toluene solutions. The net force observed in

deformable systems was an order of magnitude higher than that for coated solid substrates, and hydrodynamics played a significant role in controlling the force magnitude and range. During the aging of water droplets in asphaltene and bitumen solutions, interfacial elasticity significantly contributed to the overall deformation of the water droplet under applied load and had to be incorporated into the high force Stokes-Reynolds-Young-Laplace equation. However, after the addition of EC-4, the slope of the constant compliance region confirmed a significant softening of the interfacial layer, and the mechanical response was similar to "fresh" water droplets in the asphaltene solution. Under this condition, the slope of the constant compliance region was suitably fitted using the SRYL equations. The results from this study highlight the application of AFM to study interactions in industrially relevant systems, where droplet deformation has a significant effect on emulsion stability and multiple interfacially active species are present. Utilizing techniques that mimic the real systems (emulsions) provides an opportunity to better understand the micro-scale properties which govern the macro-scale behaviors.

5.5 REFERENCES

1. Masliyah, J.; Zhou, Z.; Xu, Z.; Czarnecki, J.; Hamza, H. *Can. J. Chem. Eng.* **2004,** 82 (4), 628-654.

2. Masliyah, J. H.; Xu, Z.; Czarnecki, J. A., - *Handbook on Theory and Practice of Bitumen Recovery from Athabasca Oil Sands.* - Kingsley Publishing Services, Cochrane (Canada), **2011**, vol.1.

3. Czarnecki, J. In *Stabilization of water in crude oil emulsions. part 2*, 2009; American Chemical Society: 1253-1257.

4. McLean, J. D.; Kilpatrick, P. K. *J. Colloid Interface Sci.* **1997,** 196 (1), 23-34.

5. Tchoukov, P.; Czarnecki, J.; Dabros, T. *Colloids Surf., A* **2010,** 372 (1-3), 15-21.

6. Czarnecki, J.; Tchoukov, P.; Dabros, T. *Energy & Fuels* **2012,** 26 (9), 5782-5786.

7. Tchoukov, P.; Yang, F.; Xu, Z.; Dabros, T.; Czarnecki, J.; Sjoblom, J. *Langmuir* **2014,** 30 (11), 3024-3033.

8. Yarranton, H. W.; Sztukowski, D. M.; Urrutia, P. *J. Colloid Interface Sci.* **2007,** 310 (1), 246-252.

9. Yan, Z.; Elliott, J. A. W.; Masliyah, J. H. *J. Colloid Interface Sci.* **1999,** 220 (2), 329-337.

10. Gao, S.; Moran, K.; Xu, Z.; Masliyah, J. *Energy & Fuels* **2009,** 23 (5), 2606-2612.

11. Feng, X.; Mussone, P.; Gao, S.; Wang, S.; Wu, S.-Y.; Masliyah, J. H.; Xu, Z. *Langmuir* **2010,** 26 (5), 3050-3057.

12. Wang, S.; Segin, N.; Wang, K.; Masliyah, J. H.; Xu, Z. *J. Phys. Chem. C* **2011,** 115 (21), 10576-10587.

13. Angle, C. W.; Dabros, T.; Hamza, H. A. *Energy & Fuels* **2007,** 21 (2), 912-919.

14. Hannisdal, A.; Ese, M.-H.; Hemmingsen, P. V.; Sjoblom, J. *Colloids Surf., A* **2006,** 276 (1-3), 45-58.

15. Pensini, E.; Harbottle, D.; Yang, F.; Tchoukov, P.; Li, Z.; Kailey, I.; Behles, J.; Masliyah, J.; Xu, Z. *Energy & Fuels* **2014,** 28 (11), 6760-6771.

16. Feng, X.; Xu, Z.; Masliyah, J. *Energy & Fuels* **2009,** 23 (1), 451-456.

17. Hou, J.; Feng, X.; Masliyah, J.; Xu, Z. *Energy & Fuels* **2012,** 26 (3), 1740-1745.

18. Erni, P. *Soft Matter* **2011,** 7 (17), 7586-7600.

19. Miller, R.; Ferri, J. K.; Javadi, A.; Kragel, J.; Mucic, N.; Wustneck, R. *Colloid. Polym. Sci.* **2010,** 288 (9), 937-950.

20. Harbottle, D.; Chen, Q.; Moorthy, K.; Wang, L.; Xu, S.; Liu, Q.; Sjoblom, J.; Xu, Z. *Langmuir* **2014,** 30 (23), 6730-6738.

21. Spiecker, P. M.; Kilpatrick, P. K. *Langmuir* **2004**, 20 (10), 4022-4032.

22. Verruto, V. J.; Le, R. K.; Kilpatrick, P. K. *J. Phys. Chem. B* **2009**, 113 (42), 13788-13799.

23. Gromer, A.; Penfold, R.; Gunning, A. P.; Kirby, A. R.; Morris, V. J. *Soft Matter* **2010,** 6 (16), 3957-3969.

24. Butt, H.-J.; Cappella, B.; Kappl, M. *Surf. Sci. Rep.* **2005,** 59 (1-6), 1-152.

25. Bonaccurso, E.; Kappl, M.; Butt, H.-J. *Curr. Opin. Colloid Interface Sci.* **2008,** 13 (3), 107-119.

26. Ducker, W. A.; Xu, Z.; Isrealachvili, J. N. *Langmuir* **1994,** 10 (9), 3279-3289.

27. Hartley, P. G.; Grieser, F.; Mulvaney, P.; Stevens, G. W. *Langmuir* **1999,** 15 (21), 7282-7289.

28. Aston, D. E.; Berg, J. C. *J. Colloid Interface Sci.* **2001,** 235 (1), 162-169.

29. Chan, D. Y. C.; Klaseboer, E.; Manica, R. *Soft Matter* **2011,** 7 (6), 2235-2264.

30. Filip, D.; Uricanu, V. I.; Duits, M. H. G.; Van, D. E.; Mellema, J.; Agterof, W. G. M.; Mugele, F. *Langmuir* **2006,** 22 (2), 560-574.

31. Krasowska, M.; Prestidge, C. A.; Beattie, D. A. Atomic force microscopy for determining surface interactions of relevance for food foams and emulsions. In *Food Texture Design and Optimization*, John Wiley & Sons, Ltd: **2014**; 402-422.

32. Tabor, R. F.; Chan, D. Y. C.; Grieser, F.; Dagastine, R. R. *J. Phys. Chem. Lett.* **2011,** 2 (5), 434-437.

33. Tabor, R. F.; Grieser, F.; Dagastine, R. R.; Chan, D. Y. C. *J. Colloid Interface Sci.* **2012,** 371 (1), 1-14.

34. Uricanu, V. I.; Duits, M. H. G.; Filip, D.; Nelissen, R. M. F.; Agterof, W. G. M. *J. Colloid Interface Sci.* **2006,** 298 (2), 920-934.

35. Chan, D. Y. C.; Dagastine, R. R.; White, L. R. *J. Colloid Interface Sci.* **2001,** 236 (1), 141-154.

36. Webber, G. B.; Edwards, S. A.; Stevens, G. W.; Grieser, F.; Dagastine, R. R.; Chan, D. Y. C. *Soft Matter* **2008,** 4 (6), 1270-1278.

37. Lockie, H.; Manica, R.; Tabor, R. F.; Stevens, G. W.; Grieser, F.; Chan, D. Y. C.; Dagastine, R. R. *Langmuir* **2012,** 28 (9), 4259-4266.

38. Manor, O.; Chau, T. T.; Stevens, G. W.; Chan, D. Y. C.; Grieser, F.; Dagastine, R. R. *Langmuir* **2012,** 28 (10), 4599-4604.

39. Tabor, R. F.; Lockie, H.; Mair, D.; Manica, R.; Chan, D. Y. C.; Grieser, F.; Dagastine, R. R. *J. Phys. Chem. Lett.* **2011,** 2 (9), 961-965.

40. Dagastine, R. R.; Manica, R.; Carnie, S. L.; Chan, D. Y. C.; Stevens, G. W.; Grieser, F. *Science* **2006,** 313 (5784), 210-213.

41. Shi, C.; Zhang, L.; Xie, L.; Lu, X.; Liu, Q.; Mantilla, C. A.; Van Den Berg, F. G. A.; Zeng, H. *Langmuir* **2016,** 32 (10), 2302-2310.

42. Vakarelski, I. U.; Li, E. Q.; Thoroddsen, S. T. *Colloids Surf., A* **2014,** 462, 259-263.

43. Woodward, N. C.; Gunning, A. P.; Maldonado-Valderrama, J.; Wilde, P. J.; Morris, V. J. *Langmuir* **2010,** 26 (15), 12560-12566.

44. Kuznicki, N. P.; Harbottle, D.; Masliyah, J. H.; Xu, Z. *Langmuir* **2016**, doi: 10.1021/acs.langmuir.6b02306.

45. Zhang, L. Y.; Lawrence, S.; Xu, Z.; Masliyah, J. H. *J. Colloid Interface Sci.* **2003,** 264 (1), 128-140.

46. Natarajan, A.; Kuznicki, N.; Harbottle, D.; Masliyah, J.; Zeng, H.; Xu, Z. *Langmuir* **2014,** 30 (31), 9370-9377.

47. Wang, S.; Liu, J.; Zhang, L.; Masliyah, J.; Xu, Z. *Langmuir* **2010,** 26 (1), 183-190.

48. Nguyen, A. V.; Evans, G. M.; Nalaskowski, J.; Miller, J. D. *Exp. Therm Fluid Sci.* **2004,** 28 (5), 387-394.

49. Manica, R.; Connor, J. N.; Dagastine, R. R.; Carnie, S. L.; Horn, R. G.; Chan, D. Y. C. *Phys. Fluids* **2008,** 20 (3).

50. Aston, D. E.; Berg, J. C. *Ind. Eng. Chem. Res.* **2002,** 41 (3), 389-396.

51. Wu, X. *Energy & Fuels* **2003,** 17 (1), 179-190.

52. Natarajan, A.; Xie, X.; Wang, S.; Liu, Q.; Masliyah, J.; Zeng, H.; Xu, Z. *J. Phys. Chem. C* **2011**, 115, 16043-16051.

53. Bos, M. A.; Van Vliet, T. *Adv. Colloid Interface Sci.* **2001,** 91 (3), 437-471.

54. Georgieva, D.; Schmitt, V.; Leal-Calderon, F.; Langevin, D. *Langmuir* **2009,** 25 (10), 5565-5573.

55.Gülseren, İ.; Corredig, M. *Food Colloids* **2014,** 34, 154-160.

56. Harbottle, D.; Liang, Y.; Xu, Z. Asphaltene-stabilized emulsions: an interfacial rheology study. Paper presented at IBEREO 2015: *Challenges in rheology and product development* September 9-11, **2015**, Coimbra, Portugal.

CHAPTER 6 CONCLUSIONS

6.1 CONCLUDING REMARKS

Emulsion stability for both "clean" and "contaminated" systems plays a significant role in our everyday life. Some processes require stable emulsions, such as manufacturing of facial creams and pharmaceuticals, while others require successful emulsion "breaking", as encountered in crude oil production.

The debate regarding charge at "clean" air-water and oil-water interfaces has been ongoing for the last 40 years, with different results obtained via experimental studies and numerical modelling. Since the effect of minute amounts of impurities as well as droplet deformation/coalescence on the experiment in clean systems can be significant, experimental studies using "clean" solvents are challenging. While using the thin liquid film technique, for example, film rupture is observed for clean interfaces and little information is obtained. Addition of non-ionic surfactants may be required to stabilize the interface, deviating from the studied system and compromising the validity of comparisons with pure interfaces. Cascade partial coalescence, where a droplet partially merges with the interface, leaving a stable smaller droplet behind, may be a useful tool to determine surface potential bounds for such clean systems, where variable zeta potential and electrophoretic mobility results were reported in open literature.

For significantly contaminated systems, partial coalescence is not likely to occur, since the thin film separating droplet and reservoir does not reach the critical thickness required for rupture. In the presence of steric forces for surfactant- and

polymer-coated droplet systems, a different approach is required to investigate the interfacial properties and emulsion stability. While coated surfaces, planar interfaces and "bulk" emulsion studies have been utilized to determine interfacial properties, quantification of dynamic forces at the interface remains a challenge.

Over the last two decades, AFM has been successfully employed to measure forces involving at least one deformable interface, such as bubbles and droplets both in surfactant-free solutions and with adsorbed interfacial materials. These studies are highly nontrivial due to the deformation of both the AFM cantilever and the droplet. However, they are more representative of interactions in "real" emulsion systems. The majority of reported work utilizes oil droplets in water; however a reverse system of water droplets in oil is of paramount importance to many industrial processes.

6.2 MAJOR CONTRIBUTIONS

In this work, the cascade partial coalescence process for clean interfaces was analyzed to predict the charge for a given oil-water system, while AFM was used to probe interfaces in "contaminated" systems. The results from these studies enhanced our understanding of emulsion stability in both "clean" and "contaminated" systems.

For clean system, a model was developed to predict zeta potential, based on the occurrence of a partial coalescence cascade at oil-water interfaces, resulting in a stable droplet at the interface. This was achieved by writing out the balance between the forces in the system, such as the van der Waals and electrostatic

double layer force. The effect of salt concentration on partial coalescence of toluene and heptane droplets in KCl solutions was investigated, showing a smaller size of the last stable droplet (and hence less negative charge at the interface) as salt concentration increased. While partial coalescence was observed for the majority of conditions, complete coalescence occurred at a high salt concentration of 1 M KCl, where the double layer is screened. This observation is consistent with the hypothesis that the droplets are stabilized by surface charges. The proposed model can be applied in reverse: a minimum droplet size can be calculated based on the charge of the interface, providing predictions on whether partial coalescence would slow down separation/mixing for a variety of processes.

For the "contaminated" water-in-crude oil emulsion system, AFM was successfully used to monitor the changes in droplet deformation and track force development at the interface. This study represents a unique approach for tracking the dynamic changes in interfacial network *in situ*. Over a short aging period (up to 15 min), interfacial deformation was well predicted by the augmented Stokes-Reynolds-Young-Laplace model, developed for viscous interfaces. However, upon further exposure to asphaltene solution, droplet deformation was over predicted by the model. By investigating the physical properties of this mechanical barrier over time, such as interfacial tension, dilatational rheology and interfacial "crumpling" upon droplet volume reduction as a function of time, a deviation from Laplacian behavior was observed. By introducing a viscoelasticity parameter to account for interfacial stiffening, we were able to predict droplet deformation of aged droplets under AFM cantilever compression using

experimentally-determined elasticity. This parameter was shown to be important for modelling non-Laplacian systems with significant viscoelastic contributions, important for systems involving biological cell membranes and polymer blends.

When demulsifier was added to the system, interfacial softening occurred immediately and the system reverted back to Laplacian. The adhesion force progressively decreased and the probe was ultimately engulfed into the droplet after 10 min, which corresponds to clay displacement from the interface and a less stable emulsion system. This study demonstrated the successful use of AFM to gauge effectiveness of various surface active species in stabilizing and displacing the protective films surrounding water droplets in oil.

The major contributions to science of this thesis are developing a novel model describing the stability of "clean" surfactant-free systems using cascade partial coalescence measurements, and quantifying the forces present in "contaminated" water-in-oil emulsion systems by AFM colloidal probe force measurements. Including a novel viscoelasticity parameter in the high force SRYL equation to account for surface elasticity makes the SRYL model more accurate and versatile for predicting droplet deformation in non-Laplacian systems.

6.3 RECOMMENDATIONS FOR FUTURE RESEARCH

For the "clean" system, further studies would be of great interest:

- Investigating a range of salts in the aqueous phase, such as KNO_3 and K_2SO_4, or by following Hoffmeister series, in order to accurately obtain the isoelectric point/ point of zero charge for clean systems and segregate

the effect of double layer compression versus "specific ion adsorption" and ion size.

- Preliminary work showed a different mechanism for droplets close to the isoelectric point/ point of zero charge (complete coalescence) versus those in high salt concentration solutions (1 M KCl; partial coalescence cascade versus a droplet undergoing complete coalescence). Comparing the vertical and horizontal rates of collapse for different solvents under these conditions could provide some fundamental knowledge on the process.

- The partial coalescence study setup could be further modified to investigate interactions between asphaltene-in-toluene droplets and aqueous/mica and aqueous/glass interface at various salt and asphaltene concentrations. Comparing these interactions (low *Re*) with AFM and micropipette experiments (high *Re*) would encompass the whole range of forces present in industrial emulsion systems.

For the "contaminated" crude oil system, the following studies would be of interest:

- Measuring interactions between the probe and water droplet in various asphaltene and bitumen concentrations/ solvents of different aromaticities using solution exchange or solvent washing. As solvent quality decreases, presence of aggregates and flocs interferes with the laser signal in AFM and interfacial tracking during dilatational rheology/interfacial tension measurements. This limitation, arising from asphaltenes/bitumen present in the continuous phase, could be overcome by exchanging bulk solution

with pure solvent of the same aromaticity upon different aging times. Since the molecules responsible for emulsion stability are irreversibly adsorbed at the interface, solvent exchange would allow for investigation of systems with a high shear contribution/ viscoelasticity.

- Investigating the hydrodynamic effect of probe approaching solid substrates versus droplets would allow for quantification of forces at the deformable interface, by including "surface viscosity" and evaluating the disjoining pressure term in the augmented SRYL model with and without adsorbed brushes.

- A study between two water droplets of known size, immobilized on the cantilever and substrate would improve our understanding of the challenges in the crude oil systems. As mentioned in the introduction, only a fraction of asphaltenes may be responsible for interfacial network formation. It would be interesting to measure the effectiveness of different asphaltene fractions using AFM along with dilatational and shear rheology to track the network development and emulsion stability *in situ*.

- Further studies using other demulsifiers could be done to gauge their effectiveness and track droplet "softening". A concentration profile for EC-4 and other demulsifiers could be obtained to predict optimal concentrations *in situ*, where droplets become deformable and particles could penetrate the interface.

BIBLIOGRAPHY

Andersen, S. I.; Del Rio, J. M.; Khvostitchenko, D.; Shakir, S.; Lira-Galeana, C. *Langmuir* **2001**, 17 (2), 307-313.

Angle, C. W.; Dabros, T.; Hamza, H. A. *Energy & Fuels* **2007**, 21 (2), 912-919.

Aston, D. E.; Berg, J. C. *Ind. Eng. Chem. Res.* **2002,** 41 (3), 389-396.

Aston, D. E.; Berg, J. C. *J. Colloid Interface Sci.* **2001,** 235 (1), 162-169.

Beattie, J. K.; Djerdjev, A. M.; Warr, G. G. *Faraday Discuss.* **2008**, 141, 31-39.

Bird, J. C.; Ristenpart, W. D.; Belmonte, A.; Stone, H. A. *Phys. Rev. Lett.* **2009**, 103, 164502.

Blanchette, F.; and Bigioni, T. P. *Nat. Phys.* **2006**, 2 (4), 254-257.

Blanchette, F.; Bigioni, T. P. *J. Fluid Mech.* **2009**, 620, 333-352.

Blanchette, F.; Messio, L.; Bush, J. W. M. *Phys. Fluids* **2009**, 21, 072107.

Borcia, R.; Bestehorn, M. *Langmuir* **2013**, 29 (14), 4426-4429.

Borkovec, M.; Behrens, S. H. *J. Phys. Chem. B* **2008**, 112, 10795–10799.

Bos, M. A.; Van Vliet, T. *Adv. Colloid Interface Sci.* **2001,** 91 (3), 437-471.

Bozzano, G.; Dente, M. *Comput.Chem.Eng.* **2011**, 35 (5), 901-906.

Bonaccurso, E.; Kappl, M.; Butt, H.-J. *Curr. Opin. Colloid Interface Sci.* **2008,** 13 (3), 107-119.

Browne, C.; Tabor, R. F.; Chan, D. Y. C.; Dagastine, R. R.; Ashokkumar, M.; Grieser, F. *Langmuir* **2011**, 27, 12025– 12032.

Butt, H. J.; Cappella, B.; Kappl, M. *Surf. Sci. Rep*. **2005**, 59, 1–152.

Butt, H.J. *J. Colloid Interface Sci.* **1994**, 166, 109-117.

Cammarata, R. C. *Prog. Surf. Sci.* **1994**, 46, 1-3.

Carnie, S. L.; Chan, D. Y. C. *J. Colloid Interface Sci.* **1993**, 161, 260–264.

Chan, D. Y. C.; Klaseboer, E.; Manica, R. *Soft Matter* **2011**, 7 (6), 2235-2264.

Chan, D. Y. C.; Dagastine, R. R.; White, L. R. *J. Colloid Interface Sci.* **2001**, 236, 141-154.

Charles, G. E.; Mason, S. G. *J. Colloid Sci.* **1960**, 15 (2), 105– 122.

Charles, G. E.; Mason, S. G. *J. Colloid Sci.* **1960**, 15 (3), 236-267.

Chen, L.; Heim, L.-O.; Golovko, D. S.; Bonaccurso, E. *Appl. Phys. Lett.* **2012**, 101, 031601.

Chen, X.; Mandre, S.; Feng, J. J. *Phys. Fluids* **2006**, 18 (9), 092103.

Chen, X.; Mandre, S.; Feng, J. *J. Phys. Fluids* **2006**, 18, 051705.

Ciunel, K.; Arm´elin, M.; Findenegg, G. H.; von Klitzing, R. *Langmuir* **2005**, 21, 4790–4793.

Connor, J. N.; Horn, R. G. *Faraday Discuss.* **2003**, 123, 193-206.

Creux, P.; Lachaise, J.; Graciaa, A.; Beattie, J. K.; Djerdjev, A. M. *J. Phys. Chem. B* **2009**, 113 (43), 14146-14150.

Creux, P.; Lachaise, J.; Graciaa, A.; Beattie, J. K. *J. Phys. Chem. C* **2007**, 111 (9), 3753-3755.

Czarnecki, J.; Tchoukov, P.; Dabros, T. *Energy & Fuels* **2012**, 26 (9), 5782-5786.

Czarnecki, J.; Moran, K.; Yang, X. *Can. J. Chem. Eng.* **2007**, 85 (5), 748-755.

Dabros, T.; Yeung, A.; Masliyah, J.; Czarnecki, J. *J. Colloid Interface Sci.* **1999**, 210 (1), 222-224.

Dagastine, R. R.; Manica, R.; Carnie, S. L.; Chan, D. Y. C.; Stevens, G. W.; Grieser, F. *Science* **2006,** 313 (5784), 210-213.

de Gennes, P. G. *Adv. Colloid Interface Sci.* **1987**, 27, 189-209.

Derjaguin, B. V.; Churaev N. V.; Muller, V. M. *Surface Forces,* Consultants Bureau, New York, **1987**.

dos Santos, A. P.; Levin, Y. *Faraday Discuss.* **2013**, 160, 75-87.

dos Santos, A. P.; Levin, Y. *Langmuir* **2012**, 28 (2), 1304-1308.

dos Santos, A. P.; Levin, Y. *J. Chem. Phys.* **2010**, 133, 154107.

Dreher, T. M.; Glass, J.; O'Connor, A. J.; Stevens, G. W. *AIChE J.* **1999**, 45 (6), 1182-1190.

Ducker, W. A.; Xu, Z.; Israelachvili, J. N. *Langmuir* **1994**, 10, 3279-3289.

Eggers, J. *Rev. Mod. Phys.* **1997**, 69 (3), 865-929.

Eow, J. S.; Ghadiri, M.; Sharif, A. *Colloids Surf. A Physicochem. Eng. Asp.* **2003**, 225 (1-3), 193-210.

Erni, P.; Jerri, H. A.; Wong, K.; Parker, A. *Soft Matter* **2012**, 8, 6958-6967.

Erni, P. *Soft Matter* **2011**, 7, 7586-760.

Erni, P.; Windhab, E. J.; Gunde, R.; Graber, M.; Pfister, B.; Parker, A.; Fischer, P. *Biomacromolecules* **2007,** 8 (11), 3458-3466.

Feng, X.; Mussone, P.; Gao, S.; Wang, S.; Wu, S.; Masliyah, J. H.; Xu, Z. *Langmuir* **2010,** 26 (5), 3050-3057.

Feng, X.; Xu, Z.; Masliyah, *J. Energy & Fuels* **2009**, 23 (1), 451-456.

Filip, D.; Uricanu, V. I.; Duits, M. H. G.; Agterof, W. G. M., Mellema, J. *Langmuir* **2005**, 21, 115-126.

Forth, J.; French, D. J.; Gromov, A. V.; King, S.; Titmuss, S.; Lord, K. M.; Ridout, M. J.; Wilde, P. J.; Clegg, P. S. *Langmuir* **2015**, 31 (34), 9312-9324.

Freer, E. M.; Radke, C. J. *J. Adhes.* **2004**, 80, 481-496.

Gafonova, O. V.; Yarranton, H. W. *J. Colloid Interface Sci.* **2001**, 241 (2), 469-478.

Gao, S.; Moran, K.; Xu, Z.; Masliyah, J. *J. Phys. Chem. B* **2010**, 114 (23), 7710-7718.

Gao, S.; Moran, K.; Xu, Z.; Masliyah, J. *Energy & Fuels* **2009**, 23 (5), 2606-2612.

Georgieva, D.; Schmitt, V.; Leal-Calderon, F.; Langevin, D. *Langmuir* **2009,** 25 (10), 5565-5573.

Gilet, T.; Bush, J. W. M. *Phys. Fluids* **2012**, 24, 122103.

Gilet, T.; Mulleners, K.; Lecomte, J. P.; Vandewalle. N.; Dorbolo, S. *Phys. Rev. E: Stat., Nonlinear, Soft Matter Phys.* **2007**, 75, 036303.

Gillies, G.; Prestidge, C. A. *Langmuir* **2005**, 21, 12342-12347.

Gillies, G.; Prestidge, C. A.; Attard, P. *Langmuir* **2002**, 18, 1674-1679.

Gray-Weale, A.; Beattie, J. K. *Phys. Chem. Chem. Phys.* **2009**, 11 (46), 10994-11005.

Gromer, A.; Penfold, R.; Gunning, A. P.; Kirby, A. R.; Morris, V. J. *Soft Matter* **2010**, 6, 3957-3969.

Gu, G.; Zhang, L.; Xu, Z.; Masliyah, J. *Energy & Fuels* **2007**, 21 (6), 3462-3468.

Gunning, A. P.; Kirby, A. R.; Wilde, P. J.; Penfold, R.; Woodward, N. C.; Morris, V. J. *Soft Matter* **2013**, 9 (48), 11473-11479.

Gülseren, İ.; Corredig, M. *Food Colloids* **2014,** *34*, 154-160.

Hartley, P. G.; Grieser, F.; Mulvaney, P.; Stevens, G. W. *Langmuir* **1999,** 15 (21), 7282-7289.

Hamlin, B. S.; Creasey, J. C.; Ristenpart, W. D. *Phys. Rev. Lett.* **2012**, 109, 094501.

Hänni-Ciunel, K.; Schelero, N.; von Klitzing, R. *Faraday Discuss.* **2009**, 141, 41–53.

Hannisdal, A.; Ese, M.; Hemmingsen, P. V.; Sjoblom, *J. Colloids Surf. A: Physicochem. Eng. Aspects* **2006**, 276 (1-3), 45-58.

Harbottle, D.; Liang, Y.; Xu, Z. Asphaltene-stabilized emulsions: an interfacial rheology study. Paper presented at IBEREO 2015: *Challenges in rheology and product development* September 9-11, **2015**, Coimbra, Portugal.

Harbottle, D.; Chen, Q.; Moorthy, K.; Wang, L.; Xu, S.; Liu, Q.; Sjoblom, J.; Xu, Z. *Langm*uir, **2014**, 30, 6730-6738.

Harbottle, D.; Bueno, P.; Isaksson, R.; Kretzschmar, I. *J. Colloid Interface Sci.* **2011**, 362 (1), 235-241.

Hodgson, T. D.; Lee, J. C. *J. Colloid Interface Sci.* **1969**, 30 (1), 94-108.

Hodgson, T. D.; Woods, D. R. *J. Colloid Interface Sci.* **1969**, 30 (4), 429-446.

Honey, E. M.; Kavehpour, H. P. *Phys. Rev. E Stat. Nonlin. Soft Matter Phys.* **2006**, 73 (2), 1-4.

Hou, J.; Feng, X.; Masliyah, J.; Xu, Z. *Energy & Fuels* **2012**, 26 (3), 1740-1745.

Jestin, J.; Simon, S.; Zupancic, L.; Barré,L. *Langmuir* **2007**, 23, 10471-10478.

Jungwirth P.; Winter, B. *Annu. Rev. Phys. Chem.* **2008**, 59, 343–346.

Kavehpour, H. P. *Ann. Rev. Fluid Mech.* **2015**, 47, 245-268.

Kilpatrick, P. K. *J. Am. Chem. Soc.* **2012**, 4017-4026.

Kiran, S. K.; Acosta, E. J.; Moran, K. *Energy & Fuels* **2009**, 23 (6), 3139-3149.

Kiran, S. K.; Acosta, E. J.; Moran, K. *J. Colloid Interface Sci.* **2009**, 336 (1), 304-313.

Knecht, V.; Levine, Z. A.; Vernier, P. T. *J. Colloid Interface Sci.* **2010**, 352 (2), 223-231.

Kosmulski, M. *J. Colloid Interface Sci.* **2011**, 353 (1), 1-15.

Krasowska, M.; Prestidge, C. A.; Beattie, D. A. *Atomic force microscopy for determining surface interactions of relevance for food foams and emulsions.* In: Dar, Y. L.; Light, J. M. (Eds.). *Food Texture Design and Optimization* **2014**, 402-422. doi: 10.1002/9781118765616.ch16.

Krasowska, M.; Carnie, S. L.; Fornasiero, D.; Ralston, J. *J. Phys. Chem. C* **2011**, 115, 11065-11076.

Kuznicki, N. P.; Harbottle, D.; Masliyah, J. H.; Xu, Z. *Langmuir* **2016**, DOI: 10.1021/acs.langmuir.6b02306.

Kuznicki, N. P.; Krasowska, M.; Sellaperumage, P. M. F.; Xu, Z.; Masliyah, J.; Ralston, J.; Popescu, M. N. *Soft Matter* **2013**, 9, 4516-4523.

Langevin, D. *Adv. Colloid Interface Sci.* **2000**, 88, 209-222.

Langevin, D.; Argillier, J-F. *Adv Colloid Interface Sci* **2015**, DOI: http://dx.doi.org/10.1016/j.cis.2015.10.005.

Li, E. Q.; Al-Otaibi, S.; Vakarelski, I. U.; Thoroddsen, S. T. *J. Fluid Mech.* **2014**, 744 (1), R1-R14.

Liggieri, L.; Santini, E.; Guzmán, E.; Maestro, A.; Ravera, F. *Soft Matter* **2011**, 7, 7699-7709.

Lockie, H.; Manica, R.; Tabor, R. F.; Stevens, G. W.; Grieser, F.; Chan, D. Y. C.; Dagastine, R. R. *Langmuir* **2012,** 28 (9), 4259-4266.

Long, J.; Xu, Z.; Masliyah, J. H. *Energy & Fuels* **2005**, 19 (4), 1440-1446.

Lu, J.; Corvalan, C. M. *Chem. Eng. Sci*. **2012**, 78, 9-13.

Maldonado-Valderrama, J.; Rodríguez Patino, J. M. *Curr. Opin. Colloid Interface Sci.* **2010**, 15, 271-282.

Manga, M.; Stone, H. A. *J. Fluid Mech.* **1995**, 287, 279–298.

Manica, R.; Connor, J. N.; Dagastine, R. R.; Carnie, S. L.; Horn, R. G.; Chan, D. Y. C. *Phys. Fluids* **2008,** 20 (3).

Manor, O.; Chau, T. T.; Stevens, G. W.; Chan, D. Y. C.; Grieser, F.; Dagastine, R. R *Langmuir* **2012**, 28, 4599-4604.

Manor, O.; Vakarelski, I. U.; Stevens, G. W.; Grieser, F.; Dagastine, R. R.; Chan, D. Y. C. *Langmuir* **2008**, 24, 11533–11543.

Marinova, K. G.; Alargova, R. G.; Denkov, N. D.; Velev, O. D.; Petsev, D. N.; Ivanov, I. B.; Borwankar, R. P. *Langmuir* **1996**, 12, 2045–2051.

Martin, D. W.; Blanchette, F. *Phys. Fluids* **2015**, 27, 012103.

Masliyah, J. H. J.; Czarnecki, J.; Xu, Z. *Handbook on Theory and Practice of Bitumen Recovery from Athabasca Oil Sands*, Theoretical aspects, Kingsley Publishing Services, Cochrane (Canada), **2011**, vol.1.

Masliyah, J.; Zhou, Z.; Xu, Z.; Czarnecki, J.; Hamza, H. *Can. J. Chem. Eng.* **2004**, 82 (4), 628-654.

McLean, J. D.; Kilpatrick, P. K. *J. Colloid Interface Sci.* **1997**, 196 (1), 23-34.

Miller, R.; Ferri, J. K.; Javardi, A.; Krägel, J.; Mucic, N.; Wüstneck, R. *Colloid Polym. Sci.* **2010**, 288, 937-950.

Mohammed, R. A.; Bailey, A. I.; Luckham, P. F.; Taylor, S. E. *Colloids Surf. Physicochem. Eng. Aspects* **1993**, 80 (2-3), 223-235.

Mohammed, R. A.; Bailey, A. I.; Luckham, P. F.; Taylor, S. E. *Colloids Surf. Physicochem. Eng. Aspects* **1993**, 80 (2-3), 237-242.

Mousavichoubeh, M.; Shariaty-Niassar, M.; Ghadiri, M. *Chem. Eng. Sci.* **2011**, 66 (21), 5330-5337.

Mousavichouhbeh, M.; Ghadiri, M.; Shariaty-Niassar, M. *Chem. Eng. Process.* **2011**, 50, 338–344.

Munz, M.; Mills, T. *Langmuir* **2014**, 30, 4243-4252.

Natarajan, A.; Kuznicki, N.; Harbottle, D.; Masliyah, J.; Zeng, H.; Xu, Z. *Langmuir* **2014**, 30, 9370-9377.

Natarajan, A.; Xie, J.; Wang, S.; Masliyah, J.; Zeng, H.; Xu, Z. *J. Phys. Chem. C* **2011**, 115 (32), 16043-16051.

Nguyen, A. V.; Evans, G. M.; Nalaskowski, J.; Miller, J. D. *Exp. Therm. Fluid Sci.* **2004**, 5, 387-394.

Parsegian, V. A. *Van der Waals Forces: a Handbook for Biologists, Chemists, Engineers, and Physicists*, Cambridge University Press, New York, **2006**.

Pauchard, V.; Rane, J. P.; Banerjee, S. *Langmuir* **2014**, 30 (43), 12795-12803.

Pensini, E.; Harbottle, D.; Yang, F.; Tchoukov, P.; Li, Z.; Kailey, I.; Behles, J.; Masliyah, J.; Xu, Z. *Energy & Fuels* **2014**, 28 (11), 6760-6771.

Petersen, P. B.; Saykally, R. J. *Chem. Phys. Lett.* **2008**, 458, 255–261.

Petersen, P. B.; Saykally, R. J. *Annu. Rev. Phys. Chem.* **2006**, 57, 333-364.

Petersen, P. B.; Saykally, R. J. *J. Phys. Chem. B* **2005,** 109 (16), 7976-7980.

Petersen, P. B.; Saykally, R. J.; Mucha, M.; Jungwirth, P. *J. Phys. Chem. B* **2005**, 109, 10915–10921.

Pincus. P. A.; Safran, S. A. *Europhys. Lett.* **1998**, 42, 103–108.

Pucci, G.; Harris, D. M.; Bush, J. W. M. *Phys. Fluids* **2015**, 27, 061704.

Rane, J.P.; Pauchard, V.; Couzis, A.; Banerjee, S. *Langmuir* **2013**, 29, 4750-4759.

Ravera, F.; Loglio, G.; Kovalchuk, V. I. *Curr. Opin. Colloid Interface Sci.* **2012**, 15, 217-228.

Ray, B.; Biswas, G.; Sharma, A. *J. Fluid Mech.* **2010**, 655, 72-104.

Ristenpart, W. D.; Bird, J. C.; Belmonte, A.; Dollar, F.; Stone, H. A. *Nature* **2009**, 461, 377–380.

Saadatmand, M.; Yarranton, H. W.; Moran, K. *Ind. Eng. Chem. Res.* **2008**, 47 (22), 8828-8839.

Shi, C.; Zhang, L.; Xie, L.; Lu, X.; Liu, Q.; Mantilla, C. A.; van den Berg, F. G. A.; Zeng, H. *Langmuir* **2016**, 32 (10), 2302-2310.

Shi, C.; Chan, D. Y. C.; Liu, Q.; Zeng, H. *J. Phys. Chem. C* **2014**, 118, 25000-25008.

Shuttleworth, R. *Proc. Phys. Soc.* **1950**, A63, 444-457.

Sonnefeld, J. *Colloids Surf. A Physicochem. Eng. Asp.* **2001**, 190(1-2), 179-183.

Spiecker, P. M.; Kilpatrick, P. K. *Langmuir* **2004**, 20 (10), 4022-4032.

Tabor, R. F.; Grieser, F.; Dagastine, R. R.; Chan, D. Y. C. *J. Colloid Interface Sci.* **2012**, 371, 1–14.

Tabor, R. F.; Lockie, H.; Mair, D.; Manica, R.; Chan, D. Y. C.; Grieser, F.; Dagastine, R. R. *J. Phys. Chem. Lett.* **2011,** 2 (9), 961-965.

Takahashi, M. *J. Phys. Chem. B* **2005**, 109 (46), 21858-21864.

Taylor, S.D.; Czarnecki, J.; Masliyah, J. *J. Colloid Interface Sci.* **2002**, 252, 149-160.

Tchoukov, P.; Yang, F.; Xu, Z.; Dabros, T.; Czarnecki, J.; Sjoblom, J. *Langmuir* **2014**, 30 (11), 3024-3033.

Tchoukov, P.; Czarnecki, J.; Dabros, T. *Colloids Surf., A* **2010,** 372 (1-3), 15-21.

Thoroddsen, S. T.; Etoh, T. G.; Takehara, K. *Annu. Rev. Fluid Mech.* **2008**, 40, 257-285.

Thoroddsen, S. T.; Takehara, K. *Phys. Fluids* **2000,** 12 (6), 1265-1267.

Vakarelski, I. U.; Li, E. Q.; Thoroddsen, S. T. *Colloids Surf. A* **2014**, 462, 259-263.

Vakarelski, I. U.; Manica, R.; Tang, X.; O'Shea, S. J.; Stevens, G. W.; Grieser, F.; Dagastine, R. R.; Chan, D. Y. C. *Proc. Natl. Acad. Sci. U. S. A.* **2010**, 107, 11177–11182.

Vandewalle, N.; Terwagne, D.; Mulleners, K.; Gilet, T.; Dorbolo, S. *Phys. Fluids* **2006**, 18, 091106.

Varadaraj, R.; Brons, C. *Energy & Fuels* **2007**, 21 (1), 195-198.

Varadaraj, R.; Brons, C. *Energy & Fuels* **2007**, 21 (1), 199-204.

Varadaraj, R.; Brons, C. *Energy & Fuels* **2007**, 21 (3), 1617-1621.

Verruto, V. J.; Le, R. K.; Kilpatrick, P. K. *J. Phys. Chem. B* **2009**, 113 (42), 13788-13799.

Wang, S.; Segin, N.; Wang, K.; Masliyah, J. H.; Xu, Z. *J. Phys. Chem. C* **2011**, 115 (21), 10576-10587.

Wang, S.; Liu, J.; Zhang, L.; Masliyah, J.; Xu, Z. *Langmuir* **2010**, 26 (1), 183-190.

Webber, G. B.; Manica, R.; Edwards, S. A.; Carnie, S. L.; Stevens, G. W.; Grieser, F.; Dagastine, R. R.; Chan, D. Y. C. *J. Phys. Chem. C* **2008**, 112, 567-574.

Wilde, P. J. *Curr. Opin. Colloid Interface Sci.* **2000**, 5, 176-181.

Woodward, N. C.; Gunning, A. P.; Maldonado-Valderrama, J.; Wilde, P. J.; Morris, V. J. *Langmuir* **2010**, 26 (15), 12560-12566.

Wu, X. *Energy & Fuels* **2003,** 17 (1), 179-190.

Xu, J. H.; Li, S. W.; Tan. J.; Luo, G. S. *Microfluid. Nanofluid.* **2008**, 5, 711–717.

Xu, Y.; Dabros, T.; Hamza, H.; Shefantook, W. *Petrol. Sci. Technol.* **1999,** 17 (9), 1051-1070.

Yan, Y.; Masliyah, J. H. *Colloids Surf. A Physicochem. Eng. Aspects* **1993**, 75, 123-132.

Yan, Z.; Elliott, J. A. W.; Masliyah, J. H. *J. Colloid Interface Sci.* **1999**, 220 (2), 329-337.

Yang, F.; Tchoukov, P.; Dettman, H.; Teklebrhan, R. B.; Liu, L.; Dabros, T.; Czarnecki, J.; Masliyah, J.; Xu, Z. *Energy & Fuels* **2015**, 29 (8), 4783-4794.

Yang, F.; Tchoukov, P.; Pensini, E.; Dabros, T.; Czarnecki, J.; Masliyah, J.; Xu, Z. *Energy & Fuels* **2014**, 28 (11), 6897-6904.

Yarranton, H. W.; Sztukowski, D. M.; Urrutia, P. *J. Colloid Interface Sci.* **2007**, 310 (1), 246-252.

Yarranton, H. W.; Sztukowski, D. M.; Urrutia, R. *J. Colloid Interface Sci.* **2007**, 310, 253-259.

Yeung, A.; Dabros, T.; Masliyah, J.; Czarnecki, *J. Colloids Surf. Physicochem. Eng. Aspects* **2000**, 174 (1-2), 169-181.

Yeung, A.; Dabros, T.; Masliyah, J. *Langmuir* **1997**, 13, 6597-6606.

Yue, P.; Zhou, C.; Feng, J. *J. Phys. Fluids* **2006**, 18, 102102.

Zhang, L. Y.; Lawrence, S.; Xu, Z.; Masliyah, J. H. *J. Colloid Interface Sci.* **2003**, 264 (1), 128-140.

Zhang, L. Y.; Xu, Z.; Masliyah, J. H. *Langmuir* **2003**, 19 (23), 9730-9741.

Zhao, H.; Brunsvold, A.; Munkejord, S. T. *Int. J. Multiph. Flow* **2011**, 37 (9), 1109-1119.

Zou, J.; Wang, P. F.; Zhang, T. R.; Ruan, X. *Phys. Fluids* **2011**, 23, 044101.

APPENDIX A

Additional figures for Chapter 3.

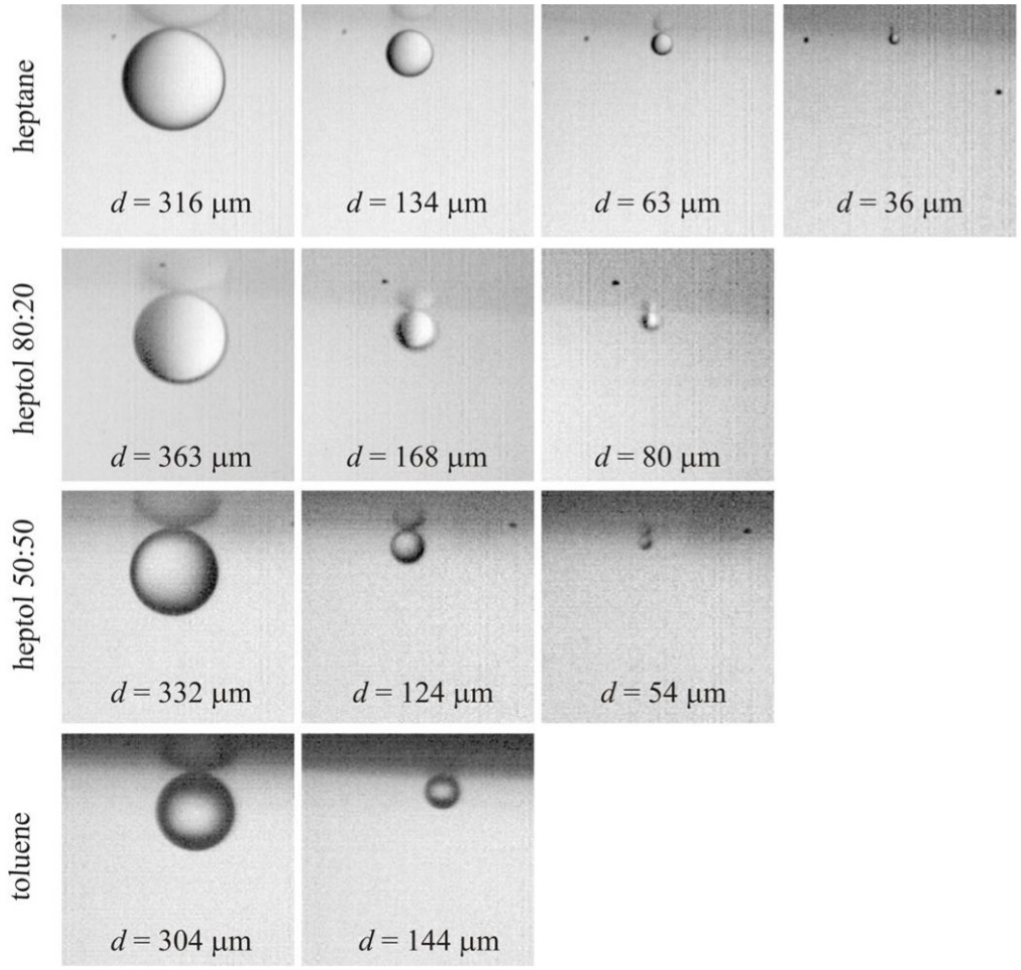

Figure A-1 The sequence of droplets undergoing partial-coalescence events, up to the final stable droplet, at various heptol - water interfaces; *d* denotes the diameter of the corresponding droplet.

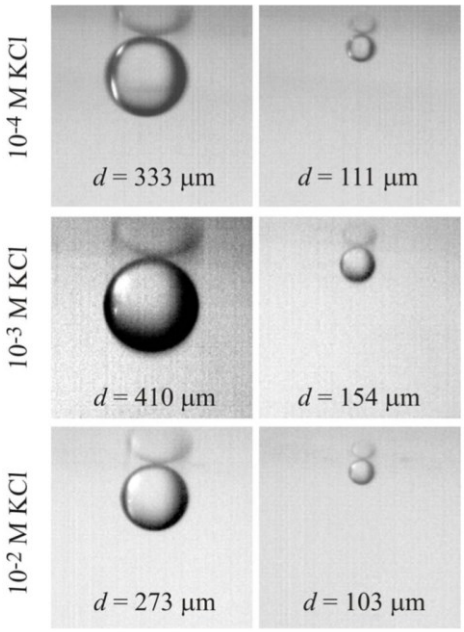

Figure A-2 The sequence of droplet undergoing partial-coalescence events, up to the final stable droplet, at various toluene - salt solution interfaces.

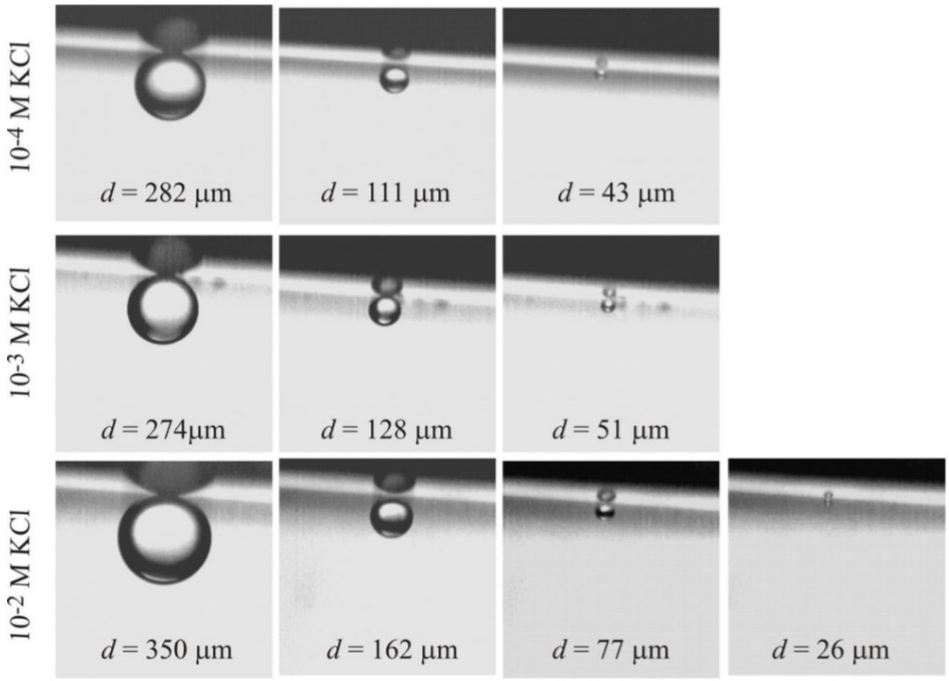

Figure A-3 The sequence of droplets undergoing partial-coalescence events, up to the final stable droplet, at various *n*-heptane - salt solution interfaces.

Table A-1 Average toluene droplet diameters and the "daughter/mother" droplet size ratios in aqueous solutions at pH=3.

Sequence	Mili Q water	10^{-3} M KCl	10^{-2} M KCl
Droplet 1	379 (0.49)	368 (0.46)	433 (0.44)
Droplet 2	187 (0.44)	170 (0.47)	190 (0.43)
Droplet 3	83 (0.41)	80 (0.43)	82 (0.34)
Droplet 4	34	34	28

Table A-2 Average toluene droplet diameters and the "daughter/mother" droplet size ratios in aqueous solutions at pH=4.

Sequence	Mili Q water	10^{-3} M KCl	10^{-2} M KCl
Droplet 1	391 (0.43)	348 (0.43)	338 (0.41)
Droplet 2	169 (0.46)	151	140 (0.41)
Droplet 3	77	-	58 (0.34)
Droplet 4	-	-	20

Table A-3 Average toluene droplet diameters and the "daughter/mother" droplet size ratios in aqueous solutions at pH=5.

Sequence	10^{-4} M KCl	10^{-3} M KCl	10^{-2} M KCl
Droplet 1	348 (0.47)	356 (0.45)	333 (0.38)
Droplet 2	165	159	128

Table A-4 Average toluene droplet diameters and the "daughter/mother" droplet size ratios in aqueous solutions at pH=7.

Sequence	10^{-4} M KCl	10^{-3} M KCl	10^{-2} M KCl
Droplet 1	394 (0.47)	353 (0.45)	337 (0.39)
Droplet 2	186	159	133 (0.41)
Droplet 3	-	-	55

Table A-5 Average toluene droplet diameters and the "daughter/mother" droplet size ratios in aqueous solutions at pH=8.

Sequence	10^{-4} M KCl	10^{-3} M KCl	10^{-2} M KCl
Droplet 1	394 (0.47)	384 (0.44)	337 (0.40)
Droplet 2	186	170	136 (0.40)
Droplet 3	-	-	54

Table A-6 Average heptane droplet diameters and the "daughter/mother" droplet size ratios in aqueous solutions at pH=3.

Sequence	Mili Q water	10^{-2} M KCl
Droplet 1	347 (0.41)	344 (0.44)
Droplet 2	141 (0.38)	153 (0.42)
Droplet 3	54	64 (0.34)
Droplet 4	-	22 (0.41)
Droplet 5	-	9

Table A-7 Average heptane droplet diameters and the "daughter/mother" droplet size ratios in aqueous solutions at pH=4.

Sequence	Mili Q water	10^{-3} M KCl	10^{-2} M KCl
Droplet 1	341 (0.33)	361 (0.44)	331 (0.44)
Droplet 2	114 (0.38)	159 (0.42)	147 (0.42)
Droplet 3	43	66 (0.28)	61 (0.31)
Droplet 4	-	18	19

Table A-8 Average heptane droplet diameters and the "daughter/mother" droplet size ratios in aqueous solutions at pH=5.

Sequence	10^{-4} M KCl	10^{-3} M KCl	10^{-2} M KCl
Droplet 1	339 (0.43)	340 (0.38)	366 (0.44)
Droplet 2	144 (0.43)	128 (0.34)	162 (0.44)
Droplet 3	62 (0.35)	43	71 (0.34)
Droplet 4	22	-	24

Table A-9 Average heptane droplet diameters and the "daughter/mother" droplet size ratios in aqueous solutions at pH=7.

Sequence	10^{-4} M KCl	10^{-3} M KCl	10^{-2} M KCl
Droplet 1	342 (0.44)	344 (0.34)	355 (0.42)
Droplet 2	152 (0.38)	119	149 (0.41)
Droplet 3	57	-	61

Table A-10 Average heptane droplet diameters and the "daughter/mother" droplet size ratios in aqueous solutions at pH=8.

Sequence	**10^{-4} M KCl**	**10^{-3} M KCl**	**10^{-2} M KCl**
Droplet 1	355 (0.44)	348 (0.37)	343 (0.39)
Droplet 2	156 (0.42)	128	135 (0.40)
Droplet 3	65	-	54

It's interesting to note that in the Tables listed above, A-1 – A-10, the number of events and final droplet size varies based on the solvent used (toluene or heptane), salt concentration and pH, while the Bond and Ohnesorge numbers described in Chapter 3 are virtually constant for all of the different conditions, as shown in Figure A-4 (below). As discussed in Chapter 3, *Bo* indicates the tendency of gravity to inhibit partial coalescence, while *Oh* signifies tendency of viscosity in both phases to dampen capillary waves and suppress partial coalescence.

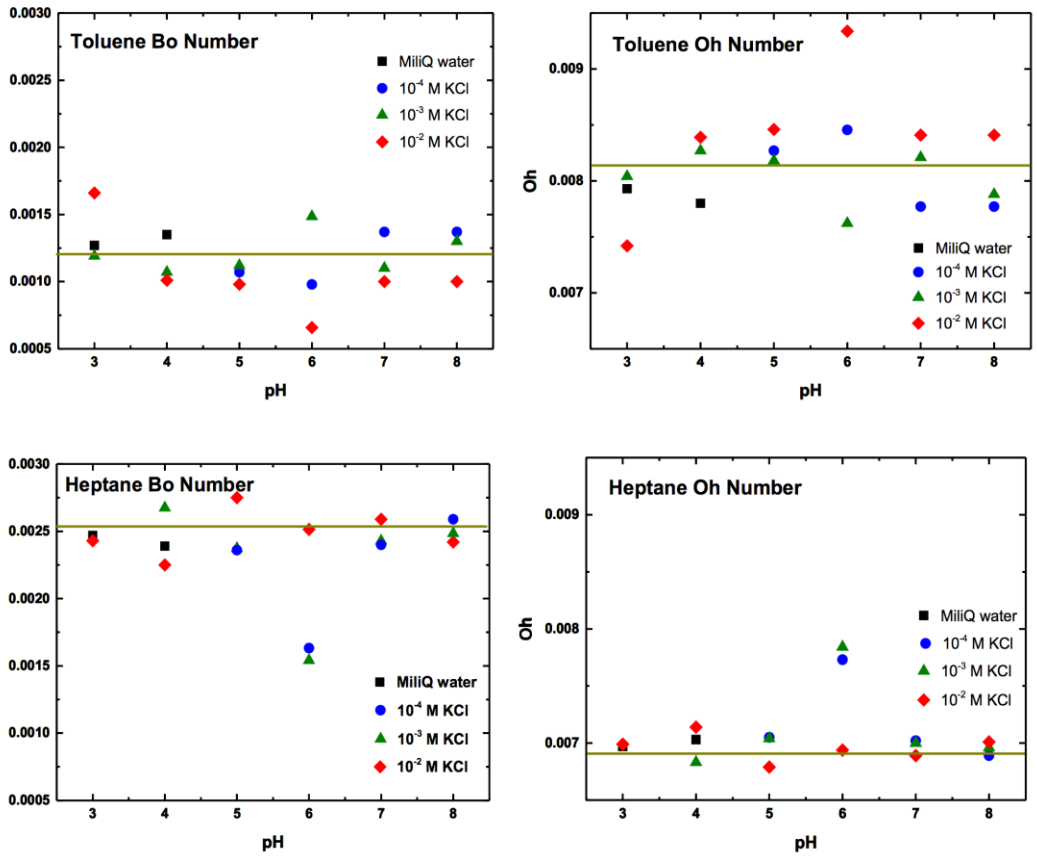

Figure A-4 Toluene and Heptane *Bo* and *Oh* numbers for the various conditions described in Tables A-1- A-10.

APPENDIX B

Additional figures for Chapter 4.

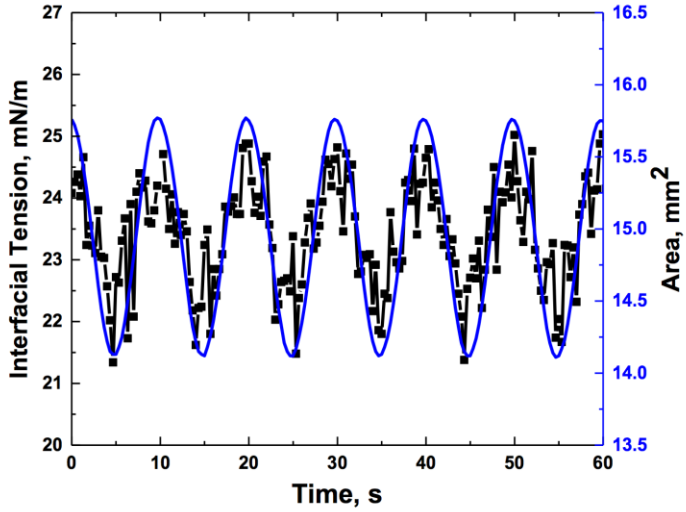

Figure B-1 Changes in droplet area (blue line) and interfacial tension (black squares) as a function of droplet aging time.

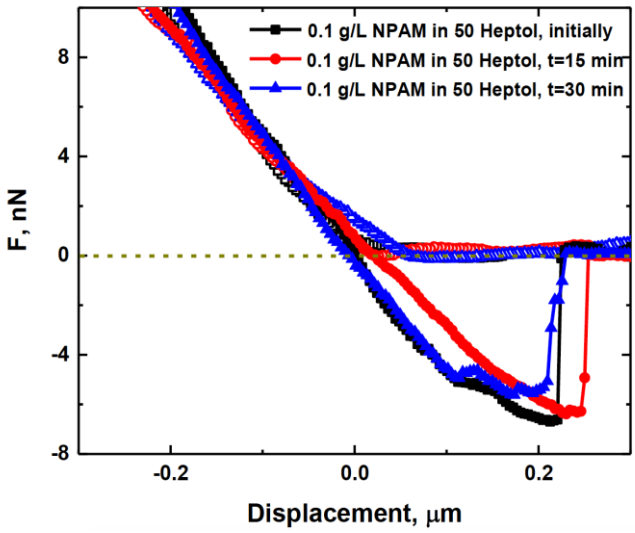

Figure B-2 Interactions between silica probe (D ≈ 8 μm) and water droplet (D ≈ 70 μm) in 0.1 g/L NPAM (asphaltene)-in-50 heptol solution upon cantilever approach (open symbols) and retract (filled symbols), over time.

The slope and adhesion force magnitude remain virtually unchanged, implying that the majority of the "interfacial stiffening" of the droplet occurs during cantilever alignment and approach to the interface, which takes 5-7 min. These findings are consistent with the development of a high dilatational elasticity (Figure 4.6) and in-plane shear (crumpling ratio, Figure 4.5) within the first couple of minutes of droplet aging time. Therefore, only the 15 min aging time AFM force curve was included and analyzed in the manuscript. It should be noted that NPAMs (asphaltenes) are close to their precipitation point in 50 heptol, with nanoaggregates causing additional laser scattering and leading to the "waviness" in the force curves.

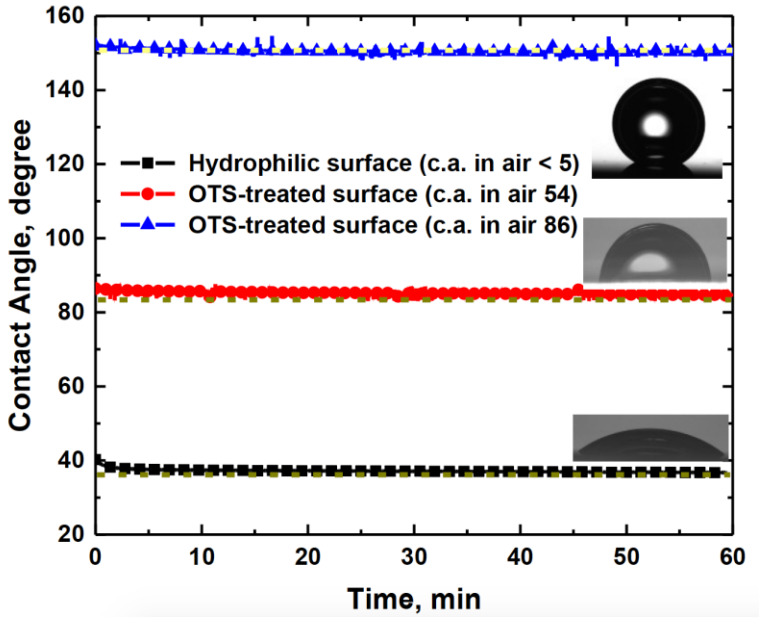

Figure B-3 Water droplet contact angles on hydrophilic and OTS-treated silica substrates in 0.1 g/L NPAM (asphaltene)-in-toluene solution. The dashed lines represent the water droplet contact angle in NPAM-free toluene, and the symbols represent water droplet contact angles in the presence of NPAM.

Hydrophilic substrates (c.a. in air < 5°) resulted in low contact angle ~ 39°, with droplets spreading and coalescing to form a uniform liquid layer on the substrate. For strongly hydrophobic surfaces (c.a. in air ~ 86°), water droplets in toluene solution (c.a. ~ 150°) were observed to be unstable and readily detached from the substrate. However, the most stable and reproducible results were obtained using surfaces of intermediate hydrophobicity (c.a. in air ~ 54°), i.e. c.a. ~ 86° in toluene solution. All substrates used in the current study were treated with OTS to exhibit the intermediate hydrophobicity. The contact angle of the corresponding substrate in 0.1 g/L NPAM in 50 heptol also remained unchanged for 1 hr at ~ 76° (c.a. ~ 74° in "clean" 50 heptol solution).

AFM Imaging:

An Agilent 5500 AFM was used under AAC mode in air to obtain topographical images of sample surfaces. Silicon nitride cantilevers (model NCHV-AW) with a nominal resonance frequency of 300-350 kHz were used to image silica substrates soaked in the NPAM solutions. The amplitude setpoint (A_S) was set to 98% of the free amplitude (A_0) to avoid surface damage. Silica wafers (1x1 cm) were soaked in 0.1 g/L NPAM-in-toluene solutions for varying periods of time. All surfaces were rinsed with copious amounts of toluene and gently blow-dried with nitrogen before imaging the substrate in air.

Figure B-4 (below) shows that NPAMs adsorb on the surface in the first 15 min and further soaking time (or NPAM concentration) did not show any effect on the substrate topography and surface features.

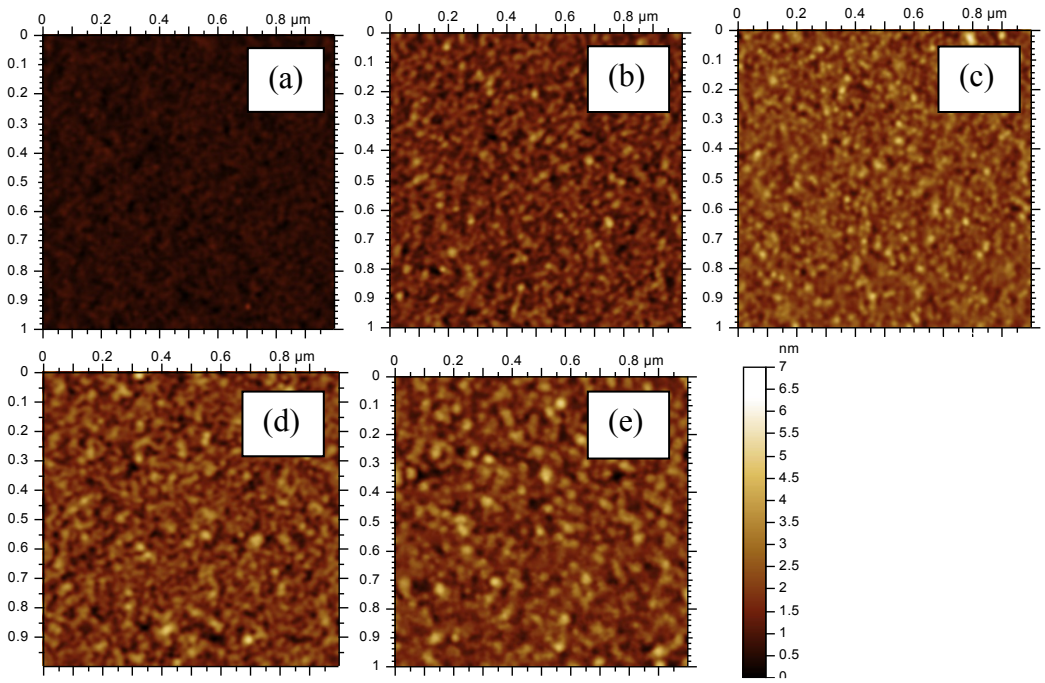

Figure B-4 AFM scans (1 × 1 µm) of hydrophilic silica wafers (a) after piranha solution cleaning and soaked in 0.1 g/L NPAM-in-toluene solution for (b) 15 min, (c) 30 min and (d) 1 hr. Silica wafer was also soaked in (e) 1 g/L NPAM-in-toluene solution for 2 hr.

Table B-1 Image properties obtained from a 1 × 1 μm image scan (Figure S4). The contact angle reported relate to a water droplet on the NPAM-coated silica substrate in air.

	RMS (nm)	**Max. height (nm)**	**Mean height (nm)**	**Contact angle (°)**
Bare silica	0.15	1.16	0.12	<10
Silica exposed to 0.1 g/L NPAM-in-toluene soln. for 15 min	0.51	4.51	0.40	79
Silica exposed to 0.1 g/L NPAM-in-toluene soln. for 30 min	0.54	5.71	0.42	79
Silica exposed to 0.1 g/L NPAM-in-toluene soln. for 1 hr	0.59	5.16	0.46	80
Silica exposed to 1 g/L NPAM-in-toluene soln. for 2 hrs	0.64	5.12	0.50	82

Detailed analysis reveals that surface roughness and aggregate height of NPAMs did not change significantly after the first 15 min of aging. The apparent steady state behavior of the surface morphology is confirmed by measuring the water droplet contact angle in air on the NPAM-coated substrates. At t = 0 the contact angle is less than 10°, confirming the highly hydrophilic nature of the clean substrate. Following immersion in the NPAM solution, the water droplet contact angle increased to ~ 80° after 15 min and showed minimal variation with further aging.

SEM Imaging:

The colloidal probe cantilevers were imaged before and after AFM force measurements using the SEM feature of the Automated Mineral Analyzer, MLA 250 (Bruker, Camarillo, CA). The MLA 250 uses an SEM equipped with a high-speed energy dispersive X-ray spectrometer (EDS) to automatically acquire images. In this study, a 35° EDS take off angle was used.

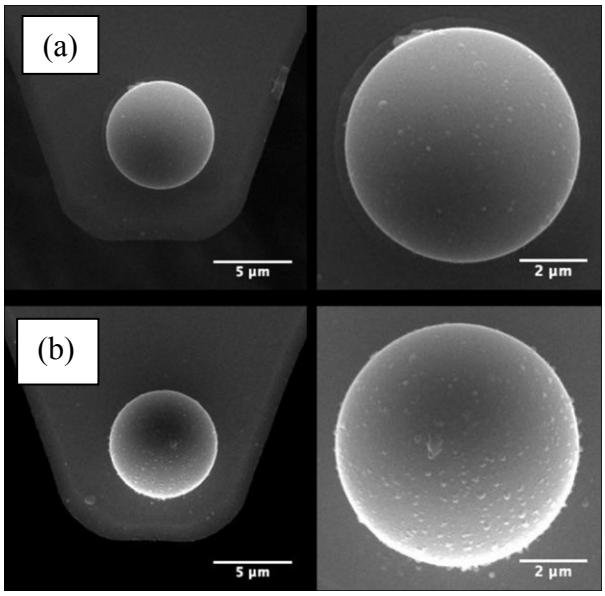

Figure B-5 SEM images of carbon coated modified AFM probe: (a) clean silica microsphere (D ≈ 7 µm) used for AFM force measurements, top row, and (b) the microsphere after exposure to 0.1 g/L NPAM-in-toluene solution for 1 hr (D ≈ 6.9 µm), bottom row. The contact area of the silica sphere does not change significantly during force measurements.

Stokes-Reynolds-Young-Laplace Model

As discussed in Chapter 4, the Stokes-Reynolds-Young-Laplace (SRYL) model has been extensively used to predict droplet deformations and system forces, as well as calculate the film thickness and predict the droplet profile for a variety of bubble and droplet systems with Laplacian interfaces. The key elements included in this model are: (i) a description of how droplets/bubbles deform under the influence of stresses arising from the balance of surface forces (disjoining pressure), hydrodynamic flow and Laplace pressure, (ii) a description of the flow of the intervening fluid film (Stokes flow for AFM experiments) and (iii) a consideration of surface forces, which depend on separation between the surfaces.

A simplified analytical solution of the SRYL model, valid for quasi-steady interactions and high forces, was used in this thesis in order to compare experimental AFM data for a system exhibiting viscoelasticity (an *in-plane* shear contribution) versus droplet deformations predicted with SRYL (see Eqn. 4 in Chapter 4). This equation only predicts the high force "constant compliance" region for probe (spherical particle)-droplet experiments, however, in order to predict the complete force profile, the full equations (given below) have to be solved numerically. For interactions between a spherical particle and a drop in AFM experiments, one has to numerically solve the Stokes-Reynolds equation, assuming for example a tangentially immobile interface, together with the augmented Young-Laplace equation in combination with the initial and boundary conditions, such as symmetry at the center and an outer asymptotic solution.

These equations are taken from two recent reviews by Derek Chan, Evert Klaseboer and Rogerio Manica: *Soft Matter* **2011**, 7 (6), 2235-2264.[1]

Adv. Colloid Interface Sci. **2011**, 165, 70-90.[2]

The film thickness parameters are defined in Figure B-6 (below):[2]

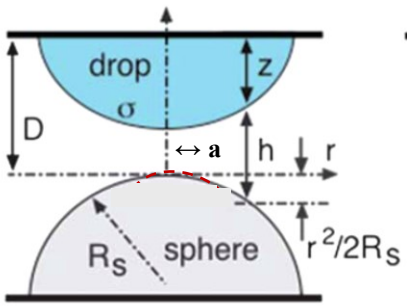

Figure B-6 Parameters for the interactions between a droplet and a solid sphere.[2]

Using the assumption of lubrication and immobile boundary condition, the Stokes Reynolds equation for evolution of the film *h(r,t)* can be derived:

$$\frac{\partial h}{\partial t} = \frac{1}{12\mu r}\frac{\partial}{\partial r}\left(rh^3\frac{\partial p}{\partial r}\right) \tag{1}$$

where μ is the viscosity.

The pressure is obtained from the augmented Young-Laplace equation:

$$\frac{\sigma}{r}\frac{\partial}{\partial r}\left(r\frac{\partial h}{\partial r}\right) = \frac{2\sigma}{R_{ds}} - \Pi - p \tag{2}$$

where $R_{ds} \equiv \frac{1}{\left[\frac{1}{R_O}+\frac{1}{R_S}\right]}$, R_s is the radius of the spherical particle and R_D is the radius of the unperturbed droplet.

Surface force interactions are specified by the Laplace pressure, disjoining pressure, $\Pi(h)$ (which would include van der Waals, electrical double layer interactions and steric effects), and hydrodynamic pressure p.

Eqns. (1) and (2) are referred to as the Stokes-Reynolds-Young-Laplace equations. These equations can be solved by the method of lines, and the dynamic force (F) can be calculated by Eqn. (3):[1]

$$F = 2\pi \int_0^\infty [p(r,t) + \Pi(h(r,t))] r dr \tag{3}$$

For probe-droplet AFM experiments with low cantilever velocity (negligible effect of hydrodynamics), the shape of the droplet is given by the inner equation and asymptotic solution of Eqn. (2): [2]

$$h(r,t) \rightarrow h(0,t) + \frac{r^2}{2R_{ds}} - \frac{F(t)}{2\pi\sigma_o} \log\left(\frac{r}{2R_{dso}}\right) + H(R_{dso},t), r > a \tag{4}$$

The outer asymptotic solution, applicable when the extent of droplet deformations arising from interactions is small on the scale of droplet size is given by:

$$z(r,t) \rightarrow R_o(1 - \cos\theta_o) - \frac{r^2}{2R_L} + \frac{F(t)}{2\pi\sigma_o}\left\{ \log\left(\frac{r}{2R_o}\right) + B(\theta_o)\right\}, \; r \rightarrow a \tag{5}$$

$$B(\theta) = \begin{cases} 1 + \frac{1}{2}\log\left(\frac{1+\cos\theta}{1-\cos\theta}\right) & \text{pinned } r_1 \\ 1 + \frac{1}{2}\log\left(\frac{1+\cos\theta}{1-\cos\theta}\right) - \left(\frac{1}{2+\cos\theta}\right) & \text{constant } \theta_o \end{cases} \tag{6}$$

The high force equation used in this thesis arises from evaluating Eqn. (4) at r=a:[1]

$$\begin{aligned} \Delta D(t) &\equiv D(t) - R_o(1 - \cos\theta_o) - h(a,t) \\ &\cong \frac{F(t)}{4\pi\sigma}\left\{\log\left(\frac{F(t)R_{ds}}{8\pi\sigma R_o^2}\right) + 2B(\theta_o) - 1\right\} \end{aligned} \tag{7}$$

APPENDIX C

Additional figures for Chapter 5.

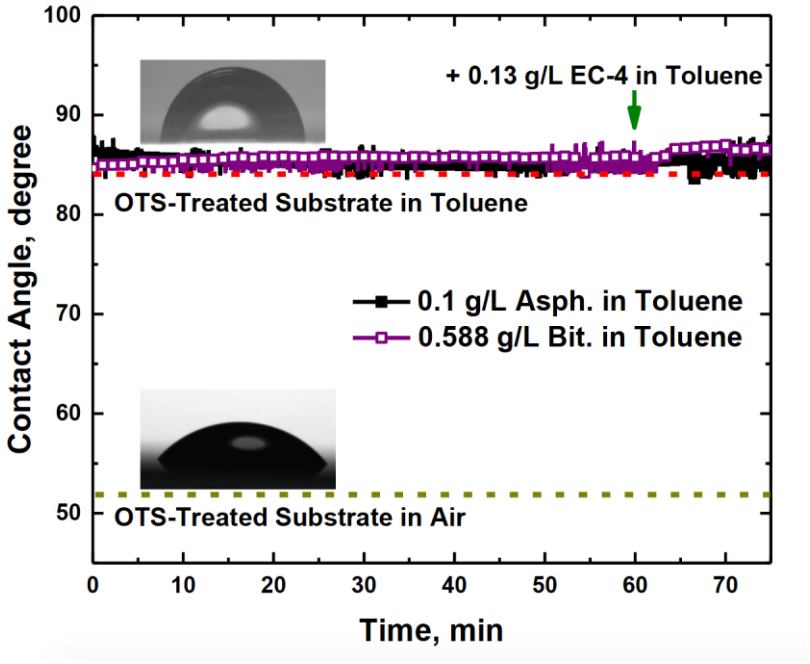

Figure C-1 Contact angle of a water droplet on OTS-treated substrate in corresponding asphaltene and bitumen solutions in toluene up to 1 hr, after which EC-4 was added to the solution.

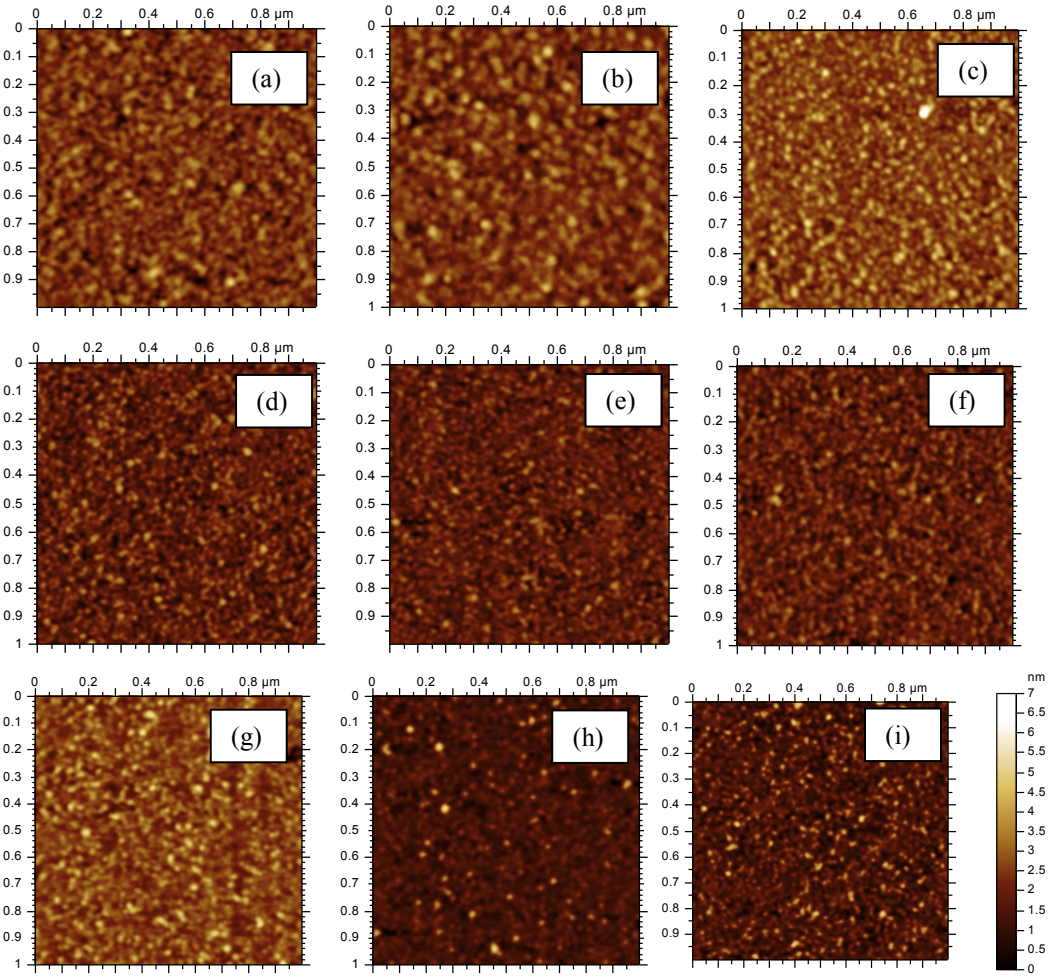

Figure C-2 AFM scans (1x1 µm) of hydrophilic silica wafers exposed to (a) 0.1 g/L asphaltene in toluene solution for 1 hr, (b) 1 g/L asphaltene in toluene solution for 1 hr, (c) 0.1 g/L asphaltene in toluene solution for 1 hr + 0.13 g/L EC-4 for 15 min; (d) 0.294 g/L (e) 0.588 g/L and (f) 1.1174 g/L bitumen-in-toluene for 1 hr. The images below them correspond to the surfaces exposed to the respective bitumen-in-toluene solutions for 1 hr + 0.13 g/L EC-4 for 15 min.

Table C-1 Image properties obtained from a 1x1 μm image scan (Figure C-2) and contact angle in air.

	RMS (nm)	**Max height (nm)**	**Mean height (nm)**	**C.A.**
Bare silica	0.15	1.16	0.12	<10
Silica exposed to 0.1 g/L asphaltenes in toluene for 1 hr	0.59	5.16	0.46	80
Silica exposed to 1 g/L asphaltenes in toluene for 2 hrs	0.64	5.12	0.50	82
Silica exposed to 0.1 g/L asphaltenes in toluene for 1 hr + 0.13 g/L EC-4 for 15 min	0.68	8.38	0.53	72
Silica exposed to 0.294 g/L bitumen-in-toluene for 1 hr (d)	0.48	4.3	0.36	77
Silica exposed to 0.588 g/L bitumen-in-toluene for 1 hr (e)	0.42	4.4	0.32	77
Silica exposed to 1.1174 g/L bitumen-in-toluene for 1 hr (f)	0.46	4.3	0.36	78
(d) + 0.13 g/L EC-4 for 15 min	0.63	10.5	0.46	70
(e) + 0.13 g/L EC-4 for 15 min	0.42	5.3	0.30	71
(f) + 0.13 g/L EC-4 for 15 min	0.62	7	0.46	72

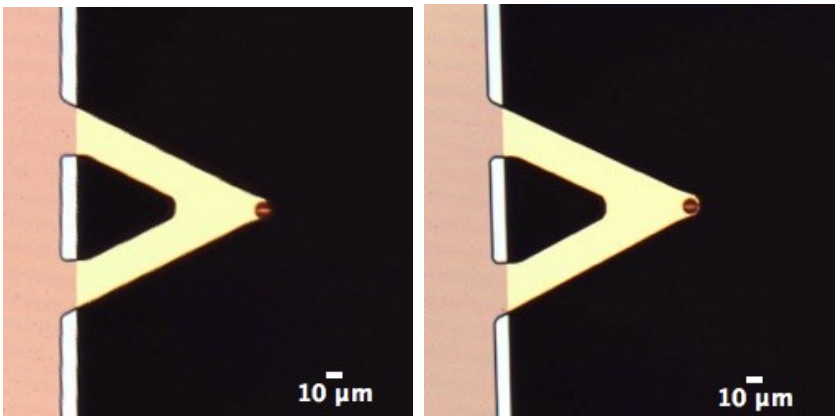

Figure C-3 AFM modified cantilevers, with glass spheres attached to a tipless probe (a) before the measurement (D=8.6 µm) and (b) after exposure to 0.1 g/L asphaltene in toluene solution for 1 hr (D=9.1 µm).

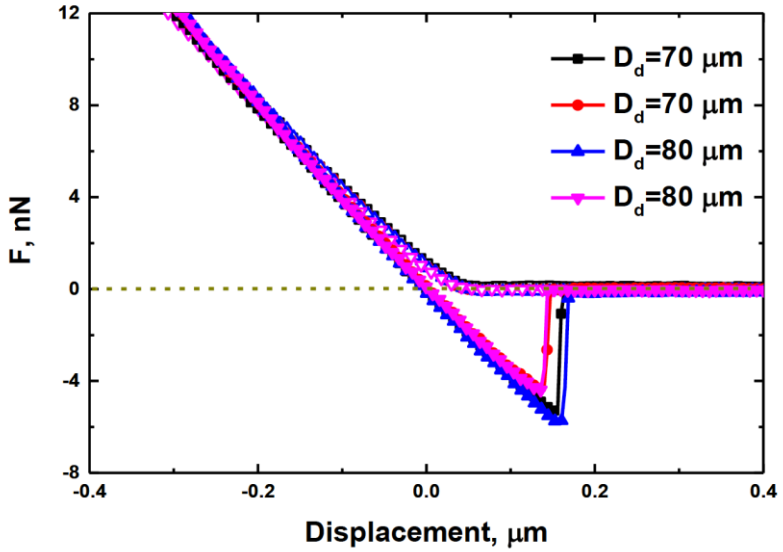

Figure C-4 Force measurements between a silica sphere (D≈ 8 µm) and two different water droplets after 1 hr aging in 0.1 g/L asphaltene in toluene solution upon approach (open symbols) and retract (filled symbols). The adhesion force magnitude for both of the droplets varied between 4.46 and 5.50 nN, contributing to an error bar of 9.8 %.

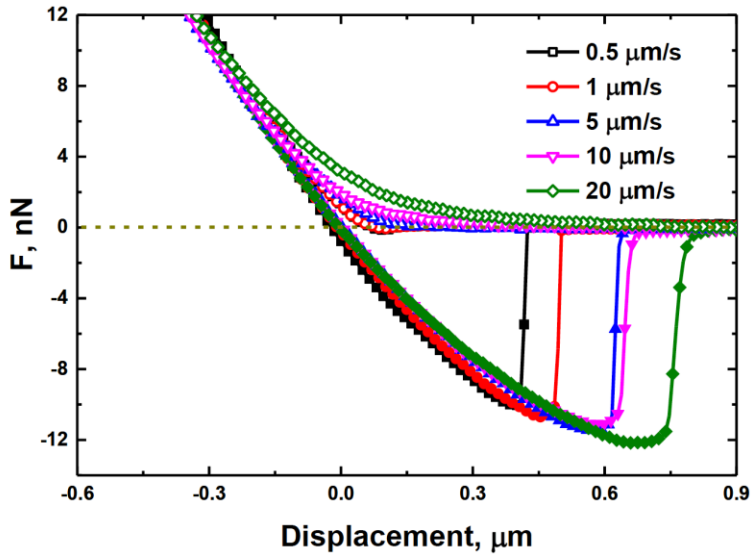

Figure C-5 Force measurements between a water droplet (D≈ 85 µm), attached to a cantilever, and substrate in 0.1 g/L asphaltene in toluene solution after 15 min stabilization time, as a function of cantilever drive velocity. Open symbols represent approach and filled symbols - the retract branch of the force curve.

Effect of Solvent Aromaticity on Water Droplet Behavior in Asphaltene and Bitumen Systems:

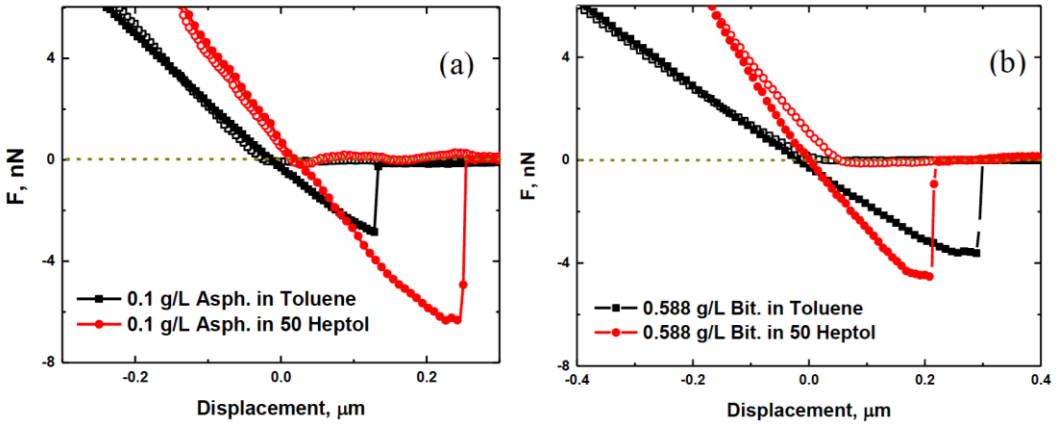

Figure C-6 Interactions between silica probe (D ≈ 8 µm) and water droplet in (a) 0.1 g/L asphaltene ($D_{droplet}$ ≈ 70 µm) and (b) corresponding 0.588 g/L bitumen

solution ($D_{droplet} \approx 85$ µm) in toluene and 50 heptol after 15 min aging. Open symbols denote cantilever approach, while filled symbols-retract. Since 50 heptol is a "poor" solvent for asphaltenes, the presence of nanoaggregates caused laser scattering and the "waviness" of the force curves. This was not observed for the corresponding bitumen solution, since indigenous species such as resins and napthenic acids could keep asphaltenes "dissolved".

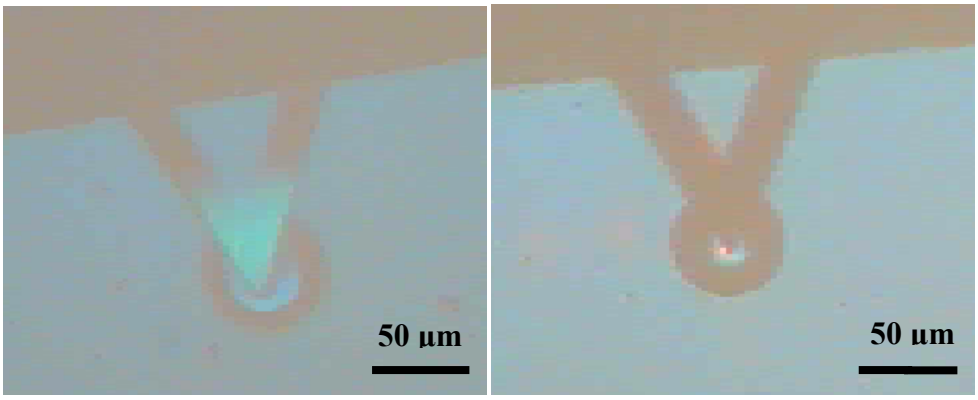

Figure C-7 Water droplet in 0.588 g/L bitumen in 50 heptol solution at t=15 min. The cantilever is manually stopped while pushing on the interface. The image next to it is water droplet in 0.588 g/L bitumen in toluene at an equivalent time. If we were to push the cantilever further, it would be engulfed in the droplet.

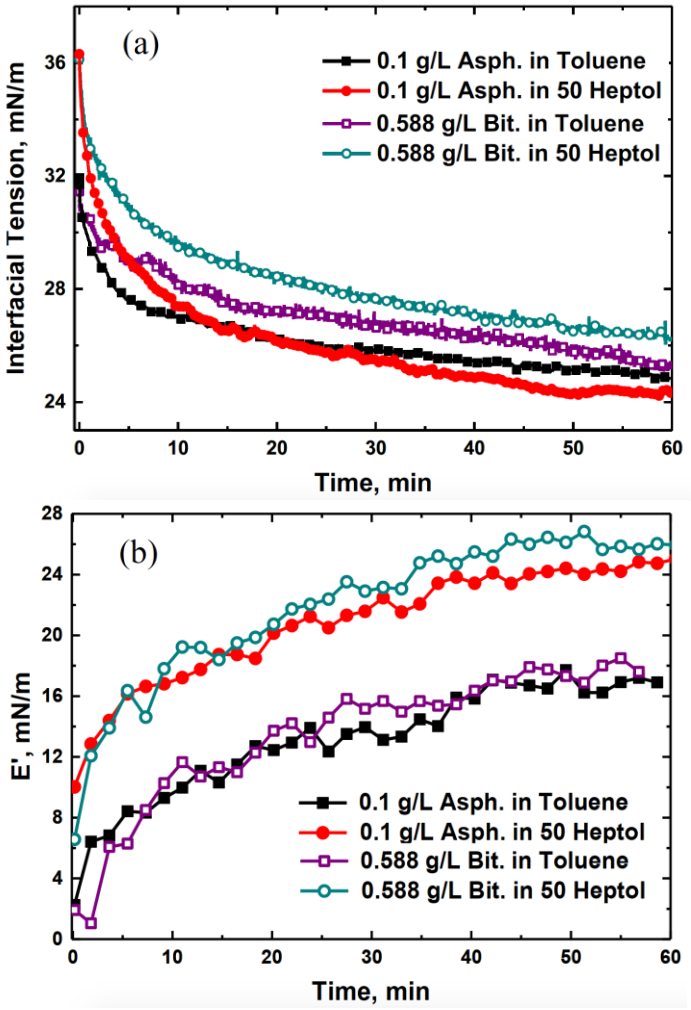

Figure C-8 (a) Interfacial tension and (b) elasticity of a water droplet in corresponding asphaltene (filled symbols) and bitumen (open symbols) in toluene and 50 heptol solutions.

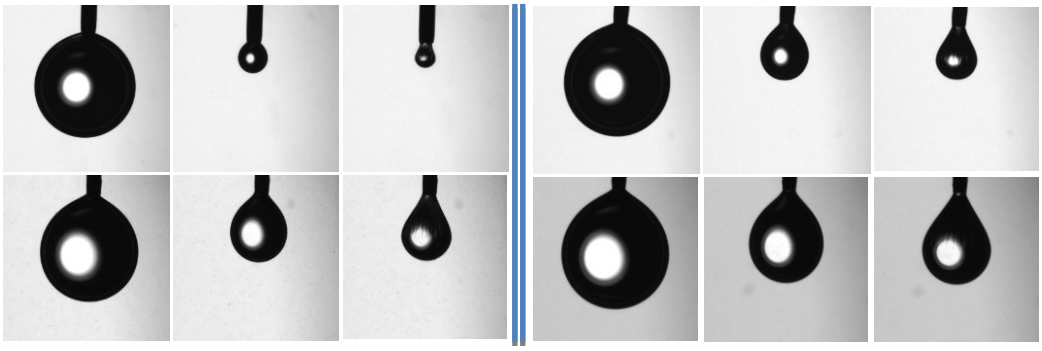

Figure C-9 Crumping "skins" upon volume reduction observed for the water

droplet in 0.1 g/L asphaltene (right) and equivalent 0.588 g/L bitumen (left) solutions after 60 min aging time. The top sequence showcases water droplet shapes in toluene, while the bottom one corresponds to those in 50 heptol.

Table C-2 Crumpling ratios following 1 hr aging for equivalent asphaltene and bitumen solutions.

	0.1 g/L Asphaltene Soln.	**0.588 g/L Bitumen Soln.**
Toluene	0.11	0.24
50 Heptol	0.37	0.49

Shear Rheology Measurements

Rheology measurements of asphaltene and bitumen solution/ water interfaces were obtained using an AR-G2 rheometer (New Castle, USA). Storage and loss moduli were recorded over 12 hrs using the Double Wall Ring (DWR) geometry. For these experiments, 19.2 mL of Milli-Q water and 15 mL of the oil solution were added to the Delrin trough. The DWR ring geometry was positioned at the interface and oscillated at 0.5 Hz and 0.8 % strain. All measurements were completed at room temperature (24 °C).

Following the time-dependent study the yield strength of the formed interfacial layer was measured using an oscillation strain sweep with the strain varying between 0.01% and 100% at constant oscillation frequency (0.5 Hz).

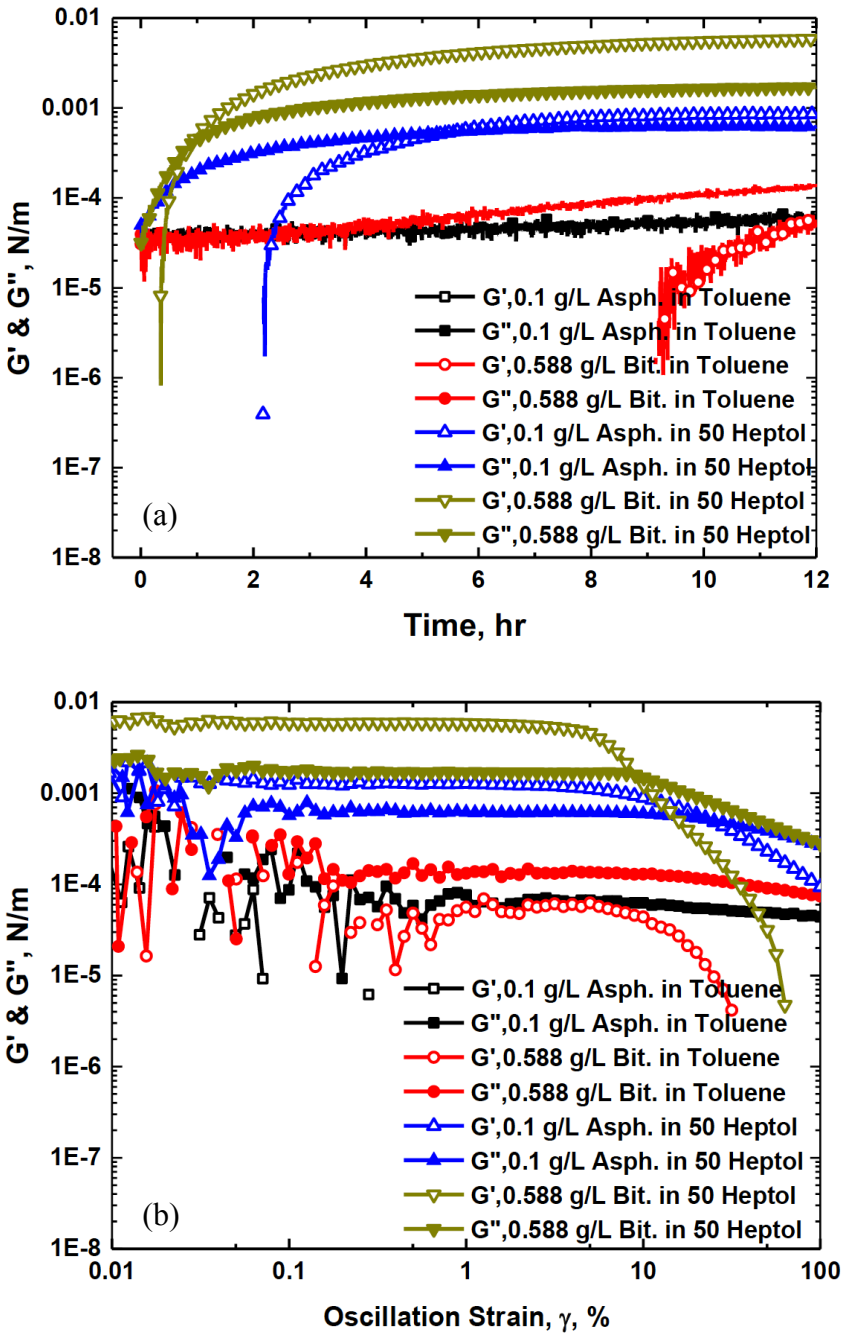

Figure C-10 (a) Storage (G') and loss (G'') modulus of various solutions and (b) amplitude sweep of asphaltene and bitumen solutions after 12 hrs aging.